Dissertation
submitted to the
Combined Faculties for the Natural Sciences
and for Mathemathics
of the
Ruperto-Carola University of Heidelberg, Germany
for the degree of
Doctor of Natural Sciences

presented by

Diplom-Physiker:	Michael Doran
born in:	Achern, Germany
Oral examination:	02.07.2002

Theory and phenomenology of quintessence

Referees: Prof. Dr. Christof Wetterich
Prof. Dr. Michael G. Schmidt

Zusammenfassung

Wir untersuchen kosmologische Quintessenz-Modelle. Quintessenz ist eine hypothetische, fast homogen im Universum verteilte Energieform. Wir führen die kosmologische Störungsrechnung und die Berechnung der Anisotropien der Hintergrundstrahlung eichinvariant durch. Für viele Modelle folgen dabei Quintessenzfluktuationen zu frühen Zeiten einfachen Potenzgesetzen. Die Auswirkungen von Quintessenz auf die Kosmische Hintergrundstrahlung und das Alter des Universums werden durch drei intuitive Parameter beschrieben. Wir quantifizieren die Relation der Peaks im Spektrum der Hintergrundstrahlung zur sogenannten akustischen Skala und zeigen, dass sich die akustische Skala aus Experimenten ablesen lässt. Damit und mittels der Strukturentstehung schränken wir zwei bedeutende Modelle ein. Quantenkorrekturen zu den klassischen Quintessenzpotentialen werden berechnet, wodurch Modelle mit Kopplungen zu dunkler Materie unwahrscheinlich scheinen. Schliesslich stellen wir CMBEASY, ein Programm zur Berechnung der Kosmischen Hintergrundstrahlung vor.

Abstract

We investigate cosmological models containing quintessence. Quintessence is a hypothetical form of energy distributed almost homogeneously throughout the Universe. We calculate cosmological perturbations and cosmic microwave background anisotropies using gauge-invariant variables. For many models, quintessence fluctuations follow simple power laws at early times. The implications of quintessence on the cosmic microwave background and the age of the universe are described via three intuitive parameters. We quantify the relation between the peaks in the multipole spectrum of the cosmic microwave background to the so called acoustic scale. We show that this acoustic scale is extractable from experimental data. Using this and constraints from structure formation, we considerably restrict two frequently used quintessence models. Quantum loop corrections to the classical quintessence potentials are calculated. From this, models with a coupling to dark matter become unlikely. Finally, we present CMBEASY, a computer code for calculating the cosmic microwave background anisotropies

Contents

1

Introduction

According to the *Hitchhiker's guide to the Galaxy*, 'space is ... mind-bogglingly big' [1]. And, one should add, it is getting bigger. This is no surprise, for most of the galaxies are moving away from each other. Intuitively, gravitation should slow down this expansion. For years, scientists asked the question whether this deceleration would bring the expansion to a halt and lead to a crunch. It was a surprise when in 1998 distance measurements using supernovae (exploding stars) indicated that the expansion of the universe may on the contrary be accelerated [2]. According to Einstein's theory of relativity (applied to cosmology), an accelerated expansion necessitates a form of energy with so-called negative pressure. While the universe expands, the negative pressure of this energy means that it becomes more and more important with respect to ordinary matter. Figure 1.1 depicts the scaling of different components with the overall expansion of the universe. The two dark energy models plotted are seen to catch up and overtake the density of matter at the present time.

Combining different observational tests one is led to conclude that this (unknown) energy constitutes more than half of the energy density within the universe. It surpasses the mass of baryons (making up stars and galaxies) by about a factor of 10 and it also 'weighs' about twice as much as cold dark matter. Cold dark matter, in turn, is some form of matter that gravitationally behaves like ordinary baryonic matter, yet non-interacting with baryons. Naturally, the mysterious energy has been given the name 'dark energy'. For those among us that spontaneously associate 'Star Wars' with dark energy, a more noble name has been proposed: quintessence [3]. Yet, years before the mysterious energy was christened, cosmological models involving a light scalar field have been investigated [4–8]. Today, these light scalar field models are the prototype of quintessence. The motivation for proposing these light scalar fields comes from more fundamental theories, like string theories which feature such fields. In addition, the field models may solve the cosmological constant problem [6]. The cosmological constant is associated with the vacuum energy of the universe. From naive quantum field theory calculations one is lead to conclude [9,10] that its observed value and the value most naturally expected differ by 120 decimal places (more of this in section 7). Having no under-

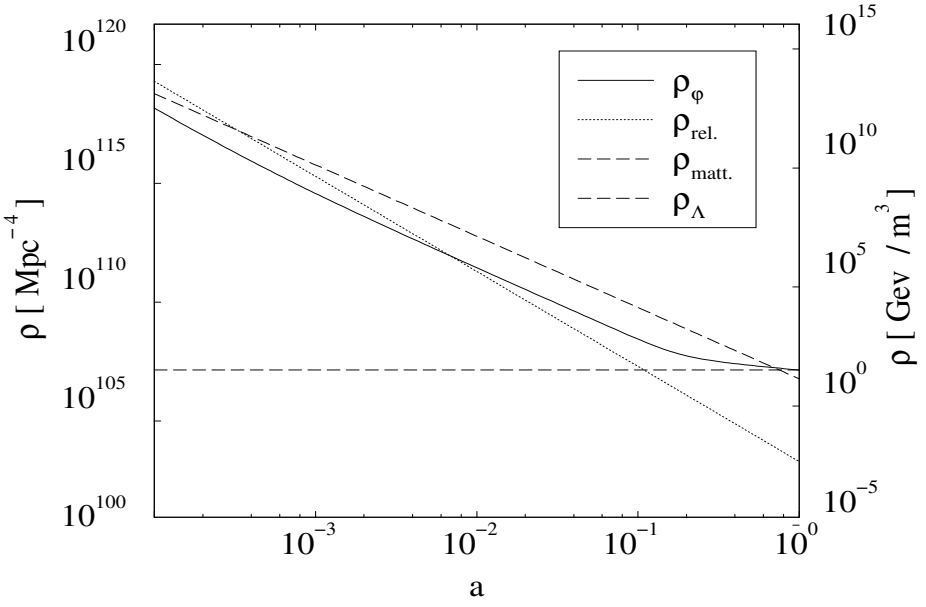

Figure 1.1: Energy density of radiation, matter, leaping kinetic term quintessence and vacuum energy (cosmological constant). The energy densities are plotted as a function of the scale factor a. The scale factor is related to the redshift via $z = a^{-1} - 1$ and today one has $a = 1$. The densities of radiation and matter scale like a^{-4} and a^{-3} respectively. At about $a \approx 10^{-4}$, matter becomes more important than radiation. The contribution from the cosmological constant (vacuum energy) is negligible throughout most of the history of the universe. The densities of matter and vacuum energy would only recently be of the same order of magnitude. This involves fine-tuning of the cosmological constant. More natural seems the behaviour of the (leaping kinetic term) quintessence model, denoted by ρ_φ. It scales like the dominant species throughout the early history of the universe, contributing at the percent level towards the total energy density. In this phenomenological model, some event at $a \approx 0.1$ leads to a change in the quintessence behaviour. From then on, it becomes more and more important with respect to matter. Even though the parameters of the model still need to be adjusted, the tuning is on the level of $1 : 1000$, as opposed to the 120 decimal places of the cosmological constant.

standing of how this mysterious cancellation should happen, theoreticians prefer a vanishing cosmological constant. As life is rarely fair, present cosmological data is very well compatible with dark energy being a cosmological constant. In contrast to the severe fine-tuning for a cosmological constant, scalar field quintessence models very often have attractor solutions [11–13]. Over an impressing broad range of initial conditions the field moves swiftly towards its attractor (see Figure 1.2). This is a much desired feature, because many scientists believe that our universe should in some way be generic. Sure, the universe could be very special indeed, however, historically mankind has moved from the center of the world to the outer region

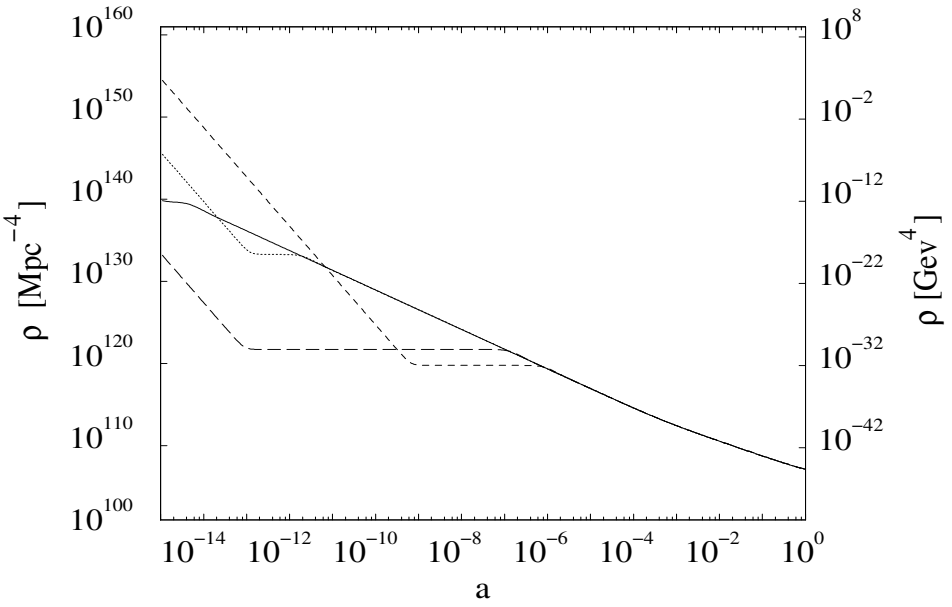

Figure 1.2: Convergence of different initial conditions (dotted, dashed and long-dashed line) towards the attractor solution (solid line). Shown is the energy density of the quintessence field as a function of the scale factor a. The present time corresponds to $a = 1$ and Electron-proton recombination occurred at $a_{\rm ls} \approx 10^{-3}$. The quintessence model used is an inverse power law with power $\alpha = -3$ (see section 2.3 for details).

of a typical galaxy. From this, it is only a small step to assume that also our universe should not be too dependent on fine-tuned initial conditions. Exactly to what extent one is accepting a tuning of initial conditions remains personal taste. For many people, the tuning still needed to yield for example the right amount of dark energy today is too much to accept scalar quintessence models. One should remark here that the models on the market are phenomenological models. There could well be a mechanism (e.g. fluctuations changing the effective potential) that leads generically to a behaviour of the scalar field that presently may look fine-tuned.

Maybe even more mind-bogglingly than the vast size of the universe is the fact that within the framework of 'standard' physics[1], one is capable of understanding many phenomena in the history of the universe, back to when it has been younger than a fraction of a second. A very nice example of this is the theory (and observation) of the Cosmic Microwave Background (CMB) radiation. The radiation is made up of photons that once were part of a hot, spatially almost uniform plasma filling the universe. About 300'000 years after the big-bang, the universe was cool enough for the electrons and protons in the plasma to recombine and form neutral hydrogen. The photons that before and during this process scattered off free elec-

[1] Well, some of it is not *so* standard, actually.

trons suddenly were able to travel freely. About $10'000'000'000$ years later, some of these photons (redshifted by the expansion of the universe that also stretches their wavelength) hit the detectors of balloon and satellite borne experiments. As it turns out, the radiation looks almost the same in all directions on the sky: it is the thermal radiation of a black body with temperature 2.7 K. Yet, when applying Einstein's theory of general relativity to small density fluctuations within the primeval plasma, one finds that depending on the scale, fluctuations should behave differently. It is a remarkable success story that several experiments in the late 1990's and early 2000's have measured these scale-dependent fluctuations. Independently of supernovae measurements, the CMB data also favours some form of dark energy contributing about 70% towards the present energy content of the universe [14,15].

The stage is thus set. If the experiments and our understanding of them is to be trusted, then one needs to devise tests to differentiate between various forms of dark energy. As scalar field quintessence is usually time-dependent, tests at different epochs may reveal its nature. Our aim is not to restrict a particular model as good as possible, but to describe effects of quintessence on some of the observations in an model-independent way. With very few intuitive parameters, such as the average fractional energy density before recombination, we will be able to accurately quantify main implications of quintessence on the CMB, SNe Ia and the age of the universe.

Yet with today's precision experiments, analytic estimates need to be supplemented by numerical simulations. A very useful tool for this is the publicly available CMBFAST package [16]. During this work, we have substantially modified this code (see Chapter 8). With the kind permission of the authors of CMBFAST, U. Seljak and M. Zaldarriaga, this modified package has been presented to the public during the XXXVII. Rencontres de Moriond [17]. The new code has been designed to facilitate modifications. As it also features a graphical user interface, it goes under the name of CMBEASY.

The scalar quintessence field is usually treated at the classical level. Even though it might be motivated by more fundamental theories, this does a-priori not mean that quantum fluctuations are included. In principle, and for as long as one does not view the potentials as already effective, fluctuations below the scale of the more fundamental theory need to be taken into account. We will turn to this important issue in Chapter 7.

We have tried to make this thesis as self contained as possible. However, once in a while abbreviations and conventions cosmologists are familiar with may have slipped into the text without further explanation. If so, we would like to apologize for any inconvenience caused. Our conventions and tables summarizing frequently used symbols as well as conversion factors of mega Parsec to other units can be found in Appendix D.

This thesis is organized as follows: in Chapter 2, we review the expansion history of universes containing dark energy. After this, several quintessence models frequently used in the literature are briefly introduced. The scaling of various quint-

essence related quantities with conformal time is also presented in this chapter for models with attractor solutions. Chapter 3 treats cosmological perturbation theory including scalar quintessence. The perturbations are mostly expressed in gauge-invariant variables, however some results are additionally stated in synchronous gauge. In Chapter 4, we start by reviewing intuitive concepts in the theory of cosmic microwave background anisotropies. Afterwards, the derivation of the main formulae needed to calculate CMB anisotropies is presented along the lines of [18]. The line of sight strategy [16] implemented in CMBFAST and CMBEASY together with the appropriate gauge invariant formulae used in CMBEASY are (re-)derived at the end of Chapter 4. The initial conditions for all perturbation variables are calculated in Chapter 5. In addition, an analytic solution to the equation of motion of the scalar field fluctuation is found. This solution holds generally whenever the field is in its attractor. Chapter 6 deals with observational tests for quintessence. After discussing the effects on the multipole spectrum of the CMB, we present fitting formulae for the so-called shifts of the peaks in this spectrum. We will show that the shift of the third peak is particularly insensitive to different cosmological models. Using this result, we extract the so-called acoustic scale from CMB data. Comparing values for the acoustic scale predicted by specific models to this experimental value, and combining with cluster abundance constraints we restrict two types of quintessence models in more detail. The end of Chapter 6 deals with quintessence implications on the recent expansion history and hence on SNe Ia-experiments. In Chapter 7, quantum loop corrections to the scalar field potentials are calculated. Finally, the object oriented design of the CMBEASY package is presented in Chapter 8.

— 2 —

Quintessence in the homogenous Universe

In general relativity, Einstein's equations relate the geometry of the universe locally to the energy momentum content. The geometry is expressed via the metric $g_{\mu\nu}$ and subsequently through the Ricci Tensor $R_{\mu\nu}$ and the curvature scalar R, while the energy momentum tensor is commonly denoted by $T_{\mu\nu}$. Using the reduced Plank mass $\mathrm{M_P} \equiv (8\pi G)^{-1/2}$, Einstein's equations read[1]

$$T_{\mu\nu} = \mathrm{M_P^2}\left(R_{\mu\nu} - \frac{1}{2}g_{\mu\nu}R\right). \tag{2.1}$$

In order to solve these in general very complicated coupled differential equations analytically, one needs to guess the geometry of the space and hence the metric. The most general metric that is isotropic and homogenous on constant time hyper-surfaces is the Robertson Walker metric. This metric comes in three 'flavours', for the cases of negative, positive or vanishing 3-curvature in the constant time hyper-surfaces. A vanishing of this 3-curvature means a spatially flat universe (we will sloppily call this just a 'flat universe'). Now, there is strong theoretical prejudice for a flat universe. Firstly, the theory of inflation predicts it. Secondly and maybe more convincingly: A Friedmann Robertson Walker universe starting with a small deviation from spatial flatness will get more and more curved as time goes on [20]. Experimentally, the universe is found to be at least very nearly flat [14,21]. So *if* the Universe would have a small but detectable curvature, then it must have departed from being undetectable close to flat just recently. This is not very natural to assume. We will thus usually limit our discussion to flat universes, as this simplifies the discussion (and presentation) greatly. Having said this, we take the Robertson Walker metric of the form

$$ds^2 \equiv g_{\mu\nu}\mathrm{d}x^\mu \mathrm{d}x^\nu = a^2(\tau)\left(-\mathrm{d}\tau^2 + \delta_{ij}\mathrm{d}x^i\mathrm{d}x^j\right), \tag{2.2}$$

[1] An eventual cosmological constant is assumed to be part of the energy momentum tensor.

where the conformal time τ is related to the usual time t by $\mathrm{d}\tau = a^{-1}\mathrm{d}t$. The expression 'conformal time' is well chosen, for the metric (2.2) is conformally related to the usual Minkowski metric $\eta_{\mu\nu} = \mathrm{diag}(-1, 1, 1, 1)$ by the conformal factor $a(\tau)$. We normalize $a(\tau)$ such that today, we have

$$a_0 \equiv a(\tau_0) = 1, \tag{2.3}$$

where here and in the following a subscript 0 will denote quantities as measured today. As $a(\tau)$ determines the stretching of *physical* length scales,

$$l^2_{\mathrm{physical}}(\tau) = g_{ij} l^i l^j = a^2(\tau)\delta_{ij} l^i l^j = a^2(\tau)\boldsymbol{l}^2, \tag{2.4}$$

it is commonly called the *scale factor*. Please note that 3-vectors are in bold, spatial components are denoted by Latin indices and the 3-vector scalar product is the usual one: $\boldsymbol{x}\,\boldsymbol{y} = \delta_{ij} x^i x^j$.

It is common practice to describe the matter content of the universe by fluids. Even in cases where this description is no longer valid and one needs to think in terms of distribution functions, we will still *identify* certain parts of these distributions with fluid terminology. For a start, let us briefly forget about cases where the fluid description breaks down and note that the energy momentum tensor for a *perfect* fluid is [22] (see also Section 3.2)

$$\bar{T}^{\mu}_{\ \nu} = \mathrm{diag}(-\bar{\rho}, \bar{p}, \bar{p}, \bar{p}), \tag{2.5}$$

where $\bar{\rho}(\tau)$ is the (unperturbed[2]) energy density and $\bar{p}(\tau)$ is the pressure. The relation between $\bar{\rho}$ and $\bar{p}$ is expressed in the equation of state

$$\bar{p}(\tau) = w(\tau)\bar{\rho}(\tau). \tag{2.6}$$

For non-relativistic matter, the pressure vanishes, whereas photons and massless neutrinos have $w = 1/3$. From the $0-0$ part of Einstein's Equation (2.1), we we get the Friedmann equation

$$3\mathrm{M}_{\mathrm{P}}^2 H^2 = \rho(\tau). \tag{2.7}$$

Here, the Hubble parameter H is related to the scale factor $a(\tau)$ by

$$H \equiv a^{-1}\frac{\mathrm{d}a}{\mathrm{d}t} = a^{-1}\frac{\mathrm{d}a}{\mathrm{d}\tau}\frac{\mathrm{d}\tau}{\mathrm{d}t} \equiv a^{-2}\dot{a}, \tag{2.8}$$

where a dot denotes a derivative with respect to conformal time τ throughout this work. Conservation of the zero component of the energy momentum tensor, $\nabla_\mu \bar{T}^{\mu}_{\ 0} = 0$, yields the useful relation

$$\frac{\dot{\bar{\rho}}}{\bar{\rho}} = -3(1+w)\frac{\dot{a}}{a}. \tag{2.9}$$

[2] Anticipating perturbation theory, we denote background quantities by a bar.

Finally, by combining Friedmann's equation (2.7) with the $i-i$ part of Einstein's equation one obtains

$$\sum_{\text{all species}} \left(\bar{\rho} \left[\frac{1}{3} + w \right] \right) = -2\mathrm{M}_{\mathrm{P}}^2 \, a^{-1} \, \frac{\mathrm{d}^2 a}{\mathrm{d}t^2}. \tag{2.10}$$

2.1 Constituents of the Universe

We know very little about the *precise* content of the universe. Big Bang Nucleosynthesis (BBN), the Cosmic Microwave Background (CMB) as well as the counting of luminous matter tells us that only a few percent of the content of the universe can be baryons: summing up their energy contribution is just not enough to fulfill the (flat) Friedmann equation (2.7) given the observed value of the Hubble constant. We will denote the fraction of baryon energy to the total energy density as Ω^{b}, where

$$\Omega^{\mathrm{x}} \equiv \frac{\rho_{\mathrm{x}}}{\rho_{\mathrm{crit}}} = \frac{\rho_{\mathrm{x}}}{3\mathrm{M}_{\mathrm{P}}^2 H^2}, \tag{2.11}$$

for any species X, and we have defined $\rho_{\mathrm{crit}} \equiv 3\mathrm{M}_{\mathrm{P}}^2 H^2$. It is clear from the definition of Ω^{x}, that in a flat universe, the sum of all Ω^{x}, Ω^{tot} needs to be unity. If not baryons, what else is out there? In principle, there are many possibilities and candidates e.g. from particle physics to black holes are considered. Funny enough, the simplest candidate behaving like ordinary pressureless matter and yet non-interacting with baryons is very successfully describing many aspects of our Universe. Having no clue what exactly could be this candidate, one calls it *cold dark matter*. As we will soon see, CMB, SNe Ia and structure formation all point in the direction of $\Omega_0^{\mathrm{c}} \approx 0.3$.

Yet, this still does not add up to unity and again both CMB and SNe Ia experiments favour some form of *dark energy* that at least in the recent universe $z \lessapprox 1$ should have a negative equation of state

$$w^{\varphi}(\tau) = \frac{\bar{p}_{\varphi}}{\bar{\rho}_{\varphi}}. \tag{2.12}$$

We will denote all kinds of dark energy - including the possibility of a cosmological constant (where $w^{\Lambda} \equiv w^{\varphi} = -1$) by the index φ.

Under the assumption that today only cold dark matter and dark energy play a major role, one obtains from Equation (2.10) that a universe with

$$w_0^{\varphi} \, \Omega_0^{\varphi} < -\frac{1}{3}, \tag{2.13}$$

is expanding in an accelerated way.

2.2 Scalar Quintessence Action and Equation of Motion

The action for a scalar field minimally coupled to gravity is

$$S = -\int \mathrm{d}^4x\,\sqrt{-g}\left[\frac{1}{2}\partial_\mu\varphi\,\partial^\mu\varphi + V(\varphi)\right], \tag{2.14}$$

where $g \equiv g_{\mu\nu}$. Using $\delta\sqrt{-g} = -\frac{1}{2}\sqrt{-g}g_{\mu\nu}\delta g^{\mu\nu}$, we get for the energy momentum tensor [23]

$$T^\mu_{\ \nu} \equiv -\frac{2}{\sqrt{-g}}\frac{\delta S}{\delta g^{\alpha\nu}}\,g^{\alpha\mu} \tag{2.15}$$

$$= \varphi^{,\mu}\varphi_{,\nu} - \delta^\mu_\nu\left(\frac{1}{2}\varphi^{,\alpha}\varphi_{,\alpha} + V\right). \tag{2.16}$$

For the homogenous background value $\bar{\varphi}(\tau)$ of $\varphi(x)$, the spatial derivatives vanish and we are left with an energy momentum tensor of the perfect fluid form (2.5), where

$$\bar{\rho}_\varphi = \frac{1}{2}a^{-2}\dot{\bar{\varphi}}^2 + V \qquad \text{and} \quad \bar{p}_\varphi = \frac{1}{2}a^{-2}\dot{\bar{\varphi}}^2 - V. \tag{2.17}$$

We can thus simply use Equation (2.9) to obtain the equation of motion

$$\ddot{\bar{\varphi}} + 2\frac{\dot{a}}{a}\dot{\bar{\varphi}} + a^2\frac{\partial V}{\partial\bar{\varphi}} = 0. \tag{2.18}$$

2.3 Popular Quintessence Models

Since the early work of [4–8], many potentials for the scalar field have been proposed. Also, a coupling [11,30,31] to dark matter has been investigated. We will briefly introduce some of the more popular models on the market, starting with one of the oldest ones, the exponential potential.

Exponential Potential

The exponential potential (EP)

$$V^{\mathrm{EP}} = \mathrm{M}_\mathrm{P}^4\exp(-\lambda\varphi/\mathrm{M}_\mathrm{P}), \tag{2.19}$$

is motivated by higher dimensional theories [6]. It exhibits an attractor solution where Ω_0^φ is determined by $\Omega_0^\varphi = 3/\lambda^2$ and the equation of state follows that of radiation (matter) in the RD (MD) era. Hence, its equation of state vanishes today [11] and therefore it cannot lead to an accelerated expansion. In Section 7, we will see that it is stable under quantum fluctuations.

Leaping Kinetic Term

While keeping the exponential potential, one can modify the kinetic term in the action (2.14). Multiplying it with a field dependent factor, one gets [32]

$$\mathcal{L} = k(\varphi)\partial_\mu\varphi\,\partial^\mu\varphi - \mathrm{M_P^4}\exp(\varphi/\mathrm{M_P}). \tag{2.20}$$

By means of the transformation $\varphi \to K(\varphi)$, where $k(\varphi) = \frac{\partial K(\varphi)}{\partial\varphi}$, one can translate these models back to canonical kinetic terms with non-exponential potential. It is very convenient to choose a leaping kinetic term (LKT)

$$k(\varphi) = k_{\min} + \tanh\left[\sigma\left(\varphi - \varphi_1\right)/\mathrm{M_P}\right] + 1, \tag{2.21}$$

where the constant $k_{\min}$ determines the amount of quintessence in the early universe and $\sigma \approx \mathcal{O}(1)$ specifies the steepness of the transition between $k = k_{\min}$ and $k = 2 + k_{\min}$ which occurs at the field value $\varphi = \varphi_1$. Using this kinetic factor, one can independently specify the amount of dark energy in the early universe (via $\Omega^\varphi_{\text{early}} = 3[1 + w_{\text{backg.}}]k^2_{\min}$), as well as w_0^φ and Ω_0^φ (via φ_1 and σ). Because it is so versatile, we will use it frequently.

Modified Exponentials

Multiplying the exponential potential by a polynomial $V_p(\varphi)$, we arrive at the modified exponential potentials (AS) [33]

$$V^{\text{AS}} = V_p(\varphi)\exp(-\lambda\varphi/\mathrm{M_P}). \tag{2.22}$$

Novel features appear if the polynomial leads to a local minimum in the potential in which the field can be trapped.

Inverse Power Laws

Inverse power law (IPL) potentials

$$V^{\text{IPL}} = A\left(\frac{\varphi}{\mathrm{M_P}}\right)^{-\alpha}, \tag{2.23}$$

have been investigated thoroughly in the literature [5,12,34–37]. Here, the pre-factor A needs to be tuned in order to give the right amount of quintessence today. As IPL models feature attractor solutions, the equation of state today is determined solely by $w_0^\varphi = -2/(\alpha + 2)$. As it takes on negative values, it can lead to an accelerated expansion. Unfortunately the power α is phenomenologically restricted to values $\alpha \lessapprox 2$ [35,36]. This leads to more and more fine tuning of A, because as $\alpha \to 0$, IPL models behave more and more like a genuine cosmological constant. For phenomenologically acceptable values of α, A is of the order $10^{-30}\mathrm{M_P}$. Depending on one's taste (and interpretation of the pre-factor), this may or may not look fine tuned.

SUGRA Inspired Models

A mixture of the exponential and the inverse power law potential

$$V^{\mathrm{SUGRA}} = A \left(\frac{\varphi}{\mathrm{M_P}}\right)^{-\alpha} \exp\left(\frac{1}{2}[\varphi/\mathrm{M_P}]^2\right), \tag{2.24}$$

may arise from supergravity [38]. It features an accelerated expansion and is thus an interesting model. SUGRA inspired models have been investigated thoroughly for instance in [39].

Cooking it all up

In [40] a unifying expression

$$V^{\mathrm{UNI}} = A \left(\frac{\varphi}{\mathrm{M_P}}\right)^{-\alpha} \exp(-\lambda[\varphi/\mathrm{M_P}]^{\gamma}) \tag{2.25}$$

for mixing up EP, IPL and SUGRA potentials has been proposed. This form facilitates the discussion of such models as they become just limiting cases of one potential. We will use it briefly in Chapter 7.

2.3.1 Tracking and Attractor Solutions

Many quintessence models feature attractor solutions [5,6,12]. For a wide range of initial conditions, the field is drawn towards this solution in which it may stay forever (EP and IPL). In some models (like LKT), an event kicks it out of the attractor. In both cases, the equation of state w^{φ} during the early stages of cosmological evolution remains frozen. The Friedmann Equation (2.7) and the equation of motion (2.18) combine in the case of $\dot{w}^{\varphi} = 0$ to [12]

$$\sigma \frac{V'}{V} = \sqrt{3(1+w^{\varphi})}\mathrm{M_P^{-1}} \left(\Omega^{\varphi}\right)^{-\frac{1}{2}}, \tag{2.26}$$

where $\sigma = \mathrm{sign}(V')$. This is a very valuable result, because it will enable us to discuss the time dependence of V, V', V'' and φ as a function of w^{φ} solely. As the expression for D_g^{φ} contains a term $V'/\bar{\rho}_{\varphi}$, we note that

$$\frac{V'}{\bar{\rho}_{\varphi}} = \frac{V'}{T+V} = (1+w^{\varphi})\frac{V'}{2V}. \tag{2.27}$$

A relation to $\dot{\bar{\varphi}}$ can be found by considering

$$a^{-2}\dot{\bar{\varphi}}^2 = 2T = (1+w^{\varphi})\rho_{\varphi} = 3(1+w^{\varphi})\mathrm{M_P^2}a^{-2}\left(\frac{\dot{a}}{a}\right)^2 \Omega^{\varphi}, \tag{2.28}$$

and therefore

$$\dot{\bar{\varphi}} = \mathrm{M_P}\frac{\dot{a}}{a}\left[3(1+w^{\varphi})\Omega^{\varphi}\right]^{\frac{1}{2}}. \tag{2.29}$$

Combining this and Equation (2.26) yields

$$\sigma \frac{V'}{V} = 3(1 + w^{\varphi}) \frac{\dot{a}}{a} \dot{\bar{\varphi}}^{-1}. \tag{2.30}$$

Using the relations (2.26-2.30) above, we can now infer the scaling of various quintessence quantities with τ. As we will primarily need these for early times, we assume that during the early universe, the dominating energy contribution scales like radiation, i.e $\bar{\rho} \propto \tau^{-4}$. This is certainly valid if quintessence is subdominant and also in cases where exponential potentials are involved. Hence,

$$\Omega^{\varphi} = \frac{\bar{\rho}_{\varphi}}{\bar{\rho}_{\text{rel.}}} \propto \tau^{1-3w^{\varphi}}, \tag{2.31}$$

and therefore from Equation (2.29)

$$\dot{\bar{\varphi}} \propto \tau^{-\frac{1}{2}(1+3w^{\varphi})}, \tag{2.32}$$

and similarly from Equation (2.26)

$$\frac{V'}{V} \propto \tau^{\frac{1}{2}(3w^{\varphi}-1)}. \tag{2.33}$$

As $V \propto T$ in the tracking regime, we further have

$$V \propto \tau^{-2} \dot{\bar{\varphi}}^2 \propto \tau^{-3(1+w^{\varphi})} \tag{2.34}$$

and combining the two relations above

$$V' \propto \tau^{-\frac{1}{2}(7+3w^{\varphi})}. \tag{2.35}$$

Finally, the chain rule yields

$$V'' = \frac{\mathrm{d}V'}{\mathrm{d}\tau} \frac{\mathrm{d}\tau}{\mathrm{d}\phi} \propto \tau^{-4}, \tag{2.36}$$

independent of the equation of state.

2.4 Expansion History

Quintessence influences the expansion history of the universe. As we will see, it can for instance lead to a larger age of the universe. It could also alter the size of the so called sound horizon (see section 4). The imprints of this will then be seen in the cosmic microwave background. This section briefly reviews the properties of the different species, stressing the impact of quintessence.

From the Friedmann Equation (2.7), we see that the expansion of the universe is determined solely by the energy density. In this work, we consider contributions

Species	w
Photons	$1/3$
Massless neutrinos	$1/3$
Massive neutrinos	$0 < w < 1/3$
Baryons	0
Cold dark matter	0
Cosmological constant	-1
Quintessence[2]	$-1 < w < 1/3$

Table 2.1: Scaling behaviour of various species, expressed by the equation of state parameter $w = \bar{p}/\bar{\rho}$.

towards this energy density from baryons, cold dark matter, photons, massless neutrinos, quintessence and in principle massive neutrinos.

With the ansatz $\rho(\tau) \propto a(\tau)^{\gamma(\tau)}$, one immediately finds from Equation (2.9) that

$$\gamma + a\frac{\dot{\gamma}}{\dot{a}} \ln a = -3(1+w). \tag{2.37}$$

For slowly varying γ (additionally suppressed by $a \ln a$), this leads to

$$\bar{\rho}_{\mathrm{x}} \propto a^{-3(1+w_x)}. \tag{2.38}$$

We summarize the different scaling behaviour of the species in Table 2.1. Inserting $w = -1$ for a cosmological constant in Equation (2.38) and using Equation (2.7), we get

$$3\mathrm{M}_{\mathrm{P}}^2 H^2 = const, \tag{2.39}$$

and hence $a \propto \exp(H\,t)$ - the universe is undergoing inflation. Scales that were before in causal contact are pressed out of the *horizon*. With horizon, we mean the distance, a light signal with a *meaningful*[3] wavelength can travel from the big bang until some time t. Now, if at some earlier time with scale factor a_{e}, a photon travels a distance we would today call a lightyear, this distance will have grown due to the expansion by a factor of a_0/a_{e} until today. Hence, the horizon coincides with the conformal time

$$\text{Horizon} = \int_0^t \frac{\mathrm{d}t'}{a} = \int_0^{\tau(t)} \mathrm{d}\tau' = \tau. \tag{2.40}$$

The horizon size above is the size of the horizon as seen today. To find its physical size as seen at the time τ, one needs to scale the horizon by $a(\tau)$.

[3] Inflation stretches wavelengths in an extreme way. A wave with wavelength larger than the horizon will be undetectable and does not carry *useful* information.

[2] In principle, the range depends on the model and more extreme cases are possible (however, not for scalar quintessence models).

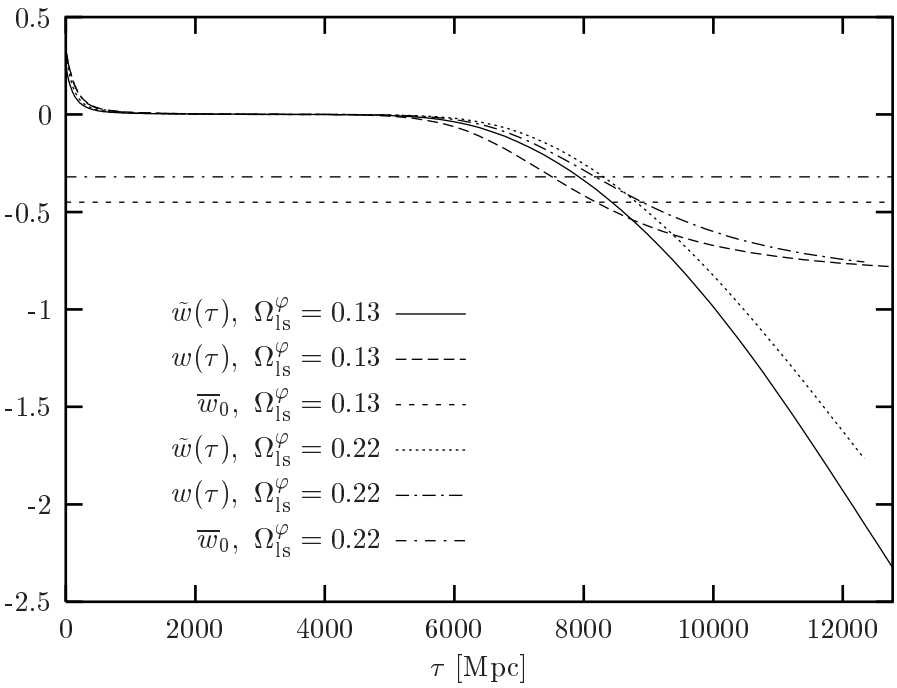

Figure 2.1: Equation of state $w(\tau)$, $\tilde{w}(\tau) \equiv \Omega^{\varphi}(\tau)w(\tau)\tau_0 / \int_0^{\tau_0} \Omega^{\varphi}(\tau')\mathrm{d}\tau'$ and averaged equation of state $\overline{w}_0$ for a leaping kinetic term model (see section 2.3) with $\bar{\Omega}^{\varphi}_{\mathrm{ls}} = 0.13$ and $\bar{\Omega}^{\varphi}_{\mathrm{ls}} = 0.22$.

As photons and massless neutrinos scale differently than baryons and cold dark matter, there is a scale factor

$$a_{\mathrm{eq}} = \frac{\Omega_0^{\mathrm{rel}}}{\Omega_0^{\mathrm{b}} + \Omega_0^{\mathrm{c}}} \approx 10^{-4}, \tag{2.41}$$

at which the relativistic and the pressureless matter energy density have been equal. Before a_{eq}, the universe has been dominated by radiation. In this case, the Friedmann equation (2.7) gives

$$a \propto \tau, \tag{2.42}$$

whereas in a matter dominated universe,

$$a \propto \tau^2. \tag{2.43}$$

Adding quintessence to this picture, things become more complicated. For the pure exponential potential, the expansion history both in the radiation and matter era remains unchanged, because w^{φ} follows the equation of state of the dominant species [11]. In general, however, this is not true anymore and one has to integrate the Friedmann equation numerically.

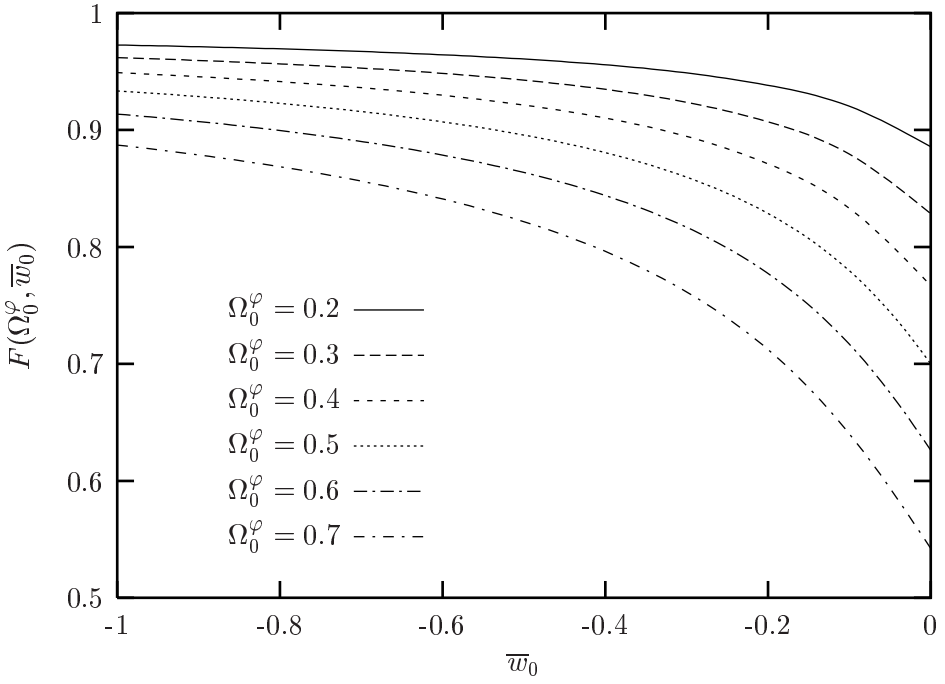

Figure 2.2: $F(\Omega_0^\varphi, \overline{w}_0)$ as a function of $\overline{w}_0$ of the dark energy component, for Ω_0^φ between 0.2 and 0.7. Between the limiting cases of $\overline{w}_0 = -1$ (cosmological constant) and $\overline{w}_0 = 0$ (corresponding to pressureless dust), the age of the Universe varies considerably.

Yet, we can make considerable progress, if we describe generic features of quintessence by suitably defined averages. For the equation of state, we use

$$\overline{w}_0 \equiv \int_0^{\tau_0} \Omega^\varphi(\tau) w^\varphi(\tau) \mathrm{d}\tau \times \left(\int_0^{\tau_0} \Omega^\varphi(\tau) \mathrm{d}\tau \right)^{-1}. \tag{2.44}$$

It is Ω^φ-weighted, reflecting the fact that the equation of state of the dark energy component is more significant if the dark energy constitutes a higher proportion of the total energy of the Universe (see Figure 2.1). In the limiting case that the equation of state did not change during the recent history of the Universe, the average is of course equal to w today. Nevertheless, the difference between the average $\overline{w}_0$ and today's value w_0 can be substantial for certain models, as can be seen from Table 6.2.

The Friedmann equation (2.7) for relativistic species together with baryonic and cold dark matter and a quintessence component reads

$$\begin{aligned} 3\mathrm{M}_\mathrm{P}^2 \dot{a}^2 a^{-4} &= \rho^\mathrm{m} + \rho^\mathrm{rel} + \rho^\varphi & (2.45) \\ &= \rho_0^\mathrm{m} a^{-3} + \rho_0^\mathrm{rel} a^{-4} + \rho_0^\varphi a^{-3(1+\overline{w}_0)}. & (2.46) \end{aligned}$$

Hence, using $3\mathrm{M}_\mathrm{P}^2 H_0^2 = \rho_0^{crit.}$, we have

$$\left(\frac{\mathrm{d}a}{\mathrm{d}\tau}\right)^2 = H_0^2 \left\{(1 - \Omega_0^\varphi - \Omega_0^\mathrm{r})a(\tau) + \Omega_0^\varphi a^{(1-3\overline{w}_0)} + \Omega_0^\mathrm{r}\right\}. \tag{2.47}$$

Upon integrating this, the conformal time today becomes

$$\tau_0 = 2H_0^{-1}(1 - \Omega_0^\varphi)^{-\frac{1}{2}} F(\Omega_0^\varphi, \overline{w}_0), \tag{2.48}$$

with F given by

$$F(\Omega_0^\varphi, \overline{w}_0) = \frac{1}{2}\int_0^1 \mathrm{d}a \left(a + \frac{\Omega_0^\varphi}{1 - \Omega_0^\varphi}\, a^{(1-3\overline{w}_0)} + \frac{\Omega_0^\mathrm{r}(1-a)}{1 - \Omega_0^\varphi}\right)^{-1/2}. \tag{2.49}$$

The integral F can be solved analytically for special values of $\overline{w}_0$, e.g.

$$F(\Omega_0^\varphi, \overline{w}_0 = 0) = \sqrt{1 - \Omega_0^\varphi}\left(1 - \sqrt{\Omega_0^\mathrm{r}}\right) + O(\Omega_0^\mathrm{r}). \tag{2.50}$$

Since (2.49) is dominated by a close to one (typically $\overline{w}_0 \leq 0$) only the present epoch matters, consistent with the averaging procedure (2.44). From this we regain on inserting (2.50) in Equation (2.48) the trivial result that the age of the Universe is the same for a cold dark matter and a pressureless dark energy universe. We plot $F(\Omega_0^\varphi, \overline{w}_0)$ for various values of Ω_0^φ in Figure 2.2.

3

Fluctuations in Linear Theory

In the previous chapter, we have seen that using the Robertson-Walker metric, we can solve Einstein's equation. The result is almost miraculously simple. However, the universe is not completely homogenous. On the contrary: it is quite clumpy on the scales of the solar system or even galaxies. Yet, the larger the scale one looks at, the more homogenous it becomes. In addition, the inhomogeneities usually grow due to gravitational infall. Hence, in the early universe, we may expect only small departures from homogeneity. This is where linear perturbation theory enters the stage. Starting from the homogenous FRW universe, one perturbs the metric and the energy momentum tensor. It is convenient to expand these perturbations in (generalized) Fourier modes and to classify physical quantities in the 3-dimensional constant time hyper-surfaces by their transformation properties [24–26,18]. Eigenfunctions of the 3-dimensional Laplace operator

$$\Delta Q_{\boldsymbol{k}}(\boldsymbol{x}) = -k^2 Q_{\boldsymbol{k}}(\boldsymbol{x}) \tag{3.1}$$

are used to decompose the metric and energy momentum perturbations into scalar, vector and tensor parts (called *modes*). The benefit of this classification is that different modes do not mix in first order perturbation theory [26]: the perturbation equations decouple. Furthermore, a coupling between perturbations of different *Fourier* modes $\boldsymbol{k}$ and $\boldsymbol{k}'$ involves products of perturbations. These would be of second order and are thus neglected. Hence, also modes with different $\boldsymbol{k}$ decouple and it is not necessary to display the wave vector $\boldsymbol{k}$ of the eigenfunctions Q explicitly. For the same reason, it is not necessary to keep the integration over the Fourier modes explicitly in the equations. One should however keep in mind that for instance the energy density is

$$\rho(\tau, \boldsymbol{x}) = \bar{\rho} + \int \frac{\mathrm{d}^3 k}{(2\pi)^3}\, \delta\rho(\tau, \boldsymbol{k})\, Q_{\boldsymbol{k}}(\boldsymbol{x}), \tag{3.2}$$

and it is only the decoupling of different $\boldsymbol{k}$ modes that will enable us to compare the *integrands* directly.

If the 3-space is flat (the case we are primarily interested in), then $Q = \exp(i\boldsymbol{k}\boldsymbol{x})$ is the solution of the Laplace equation (3.1). Now, take for instance some vector V_i. One can decompose it into a gradient and a (divergence-less) rotation part:

$$\boldsymbol{V} = \mathrm{grad}\phi + \mathrm{rot}\boldsymbol{B} \tag{3.3}$$

The function ϕ is a scalar, yet it contributes to a vector. In general, we can construct the scalar basis functions by deriving Q. Let us define[1]

$$Q_i \equiv -k^{-1}Q_{,i} \tag{3.4}$$

$$Q_{ij} \equiv k^{-2}Q_{,ij} + \frac{1}{3}\delta_{ij}, \tag{3.5}$$

where Q_{ij} is traceless by construction and gives the scalar contribution towards a symmetric tensor. In general, the contributions to a vector field $\boldsymbol{B}$ by some scalar function B can thus be written as:

$$B_i = BQ_i \tag{3.6}$$

and for a tensor field, we have

$$H_{ij} = H_L Q\delta_{ij} + H_T Q_{ij} \tag{3.7}$$

In exactly the same manner, basis functions for vector and tensor type perturbations can be derived. For instance, the divergence-less part of a vector field is expressed [25] via $Q_i^{(V)}(\boldsymbol{x})$ solving the vector Helmholtz equation

$$Q_{i,j}^{(V),j} + k^2 Q_i^{(V)} = 0, \tag{3.8}$$

and being divergence-less: $Q_{,i}^{(V)i} = 0$. As we assume that the quintessence field is a scalar under general coordinate transformations, it has to be a scalar under spatial transformations also. We will therefore restrict ourselves to the discussion of scalar perturbations. The most general line element for a perturbed Robertson Walker metric is [25]

$$ds^2 = a(\tau)^2\left[-(1+2A)d\tau^2 - B_i d\tau dx^i + (\delta_{ij} + 2H_{ij})dx^i dx^j\right] \tag{3.9}$$

Where in the scalar case B_i and H_{ij} are given by Equations (3.6) and (3.7).

3.1 The Gauge Problem

General coordinate transformations are a main ingredient of general relativity. Unfortunately, the freedom to choose a coordinate system needs to be used with care in

[1] We follow [25], but restrict ourselves to flat universes. Hence the covariant 3-derivative $Q_{|i}$ can be replaced by the partial derivative $Q_{,i}$.

cosmology. Let us see, how this comes about. Consider an infinitesimal coordinate transformation

$$x^\mu \to \tilde{x}^\mu = x^\mu + \epsilon^\mu(\tau, \boldsymbol{x}), \tag{3.10}$$

where the derivative of ϵ^μ is also assumed to be at most of the order ϵ. We know that some tensor expressed in the new coordinate system will be

$$\tilde{T}^{\mu\cdots}_{\nu\ldots}(\tilde{x}) = \left(\frac{\partial \tilde{x}^\mu}{\partial x^\alpha}\right)\left(\frac{\partial x^\beta}{\partial \tilde{x}^\nu}\right)\ldots T^{\alpha\cdots}_{\beta\ldots}(x), \tag{3.11}$$

where the transformation matrices are

$$\begin{aligned}
\left(\frac{\partial \tilde{x}^\mu}{\partial x^\nu}\right) &= \delta^\mu_\nu + \frac{\partial \epsilon^\mu(\tau, \boldsymbol{x})}{\partial x^\nu} && (3.12)\\
\left(\frac{\partial x^\mu}{\partial \tilde{x}^\nu}\right) &= \delta^\mu_\nu - \frac{\partial \epsilon^\mu(\tau, \boldsymbol{x})}{\partial \tilde{x}^\nu} && (3.13)\\
&= \delta^\mu_\nu - \frac{\partial \epsilon^\mu(\tau, \boldsymbol{x})}{\partial x^\alpha}\frac{\partial x^\alpha}{\partial \tilde{x}^\nu} && (3.14)\\
&= \delta^\mu_\nu - \frac{\partial \epsilon^\mu(\tau, \boldsymbol{x})}{\partial x^\nu} + \mathcal{O}(\epsilon^2). && (3.15)
\end{aligned}$$

The last equation in the above holds, because we have assumed that the derivative of ϵ is also of the order ϵ. Thus, working to order ϵ, the tensor transformation (3.11) becomes

$$\tilde{T}^{\mu\cdots}_{\nu\ldots}(\tilde{x}) = T^{\mu\cdots}_{\nu\ldots}(x) + \bar{T}^{\alpha\cdots}_{\nu\ldots}(x)\frac{\partial \epsilon^\mu(\tau, \boldsymbol{x})}{\partial x^\alpha} + \cdots - \bar{T}^{\mu\cdots}_{\alpha\ldots}(x)\frac{\partial \epsilon^\alpha(\tau, \boldsymbol{x})}{\partial x^\nu} - \cdots \tag{3.16}$$

If we were willing to give up the nice FRW background universe, we could happily use the transformation Equation (3.16). However, we would like to make the coordinate transformation (3.10), but *without* paying the price of changing the *background* physics. The reason why we would like to keep the background physics the same regardless of our coordinate transformations is that we would like the background to maintain its Robertson-Walker metric, for we have seen that it is the Robertson-Walker metric that leads to the convenient Friedmann equation. So, in order to stick to the old coordinates for the background, we have to go back from $\tilde{x}$ to x in the argument of $\tilde{T}$:

$$\begin{aligned}
\tilde{T}^{\mu\cdots}_{\nu\ldots}(\tilde{x}) &= \tilde{T}^{\mu\cdots}_{\nu\ldots}(x+\epsilon)\\
&= \tilde{T}^{\mu\cdots}_{\nu\ldots}(x) + \epsilon^\alpha\left(\frac{\partial \tilde{T}^{\mu\cdots}_{\nu\ldots}(\xi)}{\partial \xi^\alpha}\right)_{|\xi=x}\\
&= \tilde{T}^{\mu\cdots}_{\nu\ldots}(x) + \epsilon^\alpha\left(\frac{\partial T^{\mu\cdots}_{\nu\ldots}(\xi)}{\partial \xi^\alpha}\right)_{|\xi=x} + \mathcal{O}(\epsilon^2). && (3.17)
\end{aligned}$$

Here, we have used the transformation Equation (3.16). Putting Equations (3.16) and (3.17) together, we get the final gauge transformation law

$$\tilde{T}^{\mu\ldots}_{\nu\ldots}(x) = T^{\mu\ldots}_{\nu\ldots}(x) - \bar{T}^{\mu\ldots}_{\nu\ldots\,,\alpha}(\tau)\epsilon^{\alpha} + \bar{T}^{\alpha\ldots}_{\nu\ldots}(\tau)\epsilon^{\mu}_{,\alpha} + \cdots - \bar{T}^{\mu\ldots}_{\alpha\ldots}(\tau)\epsilon^{\alpha}_{,\nu} - \cdots . \quad (3.18)$$

The derivatives above combine to give the Lie derivative $L_\epsilon \bar{T}$ and we can rewrite Equation (3.18) rather elegant as

$$\tilde{T}(x) = T(x) - L_\epsilon \bar{T}. \quad (3.19)$$

Having derived the transformation equation, let us see what this means for the metric. Using Equation (3.18), we get

$$\tilde{g}_{\mu\nu}(x) = g_{\mu\nu}(x) - \bar{g}_{\alpha\nu}\epsilon^{\alpha}_{,\mu} - \bar{g}_{\mu\alpha}\epsilon^{\alpha}_{,\nu} - \epsilon^{\alpha}\,\bar{g}_{\mu\nu,\,\alpha}. \quad (3.20)$$

It is the last term in the above equation that would quantify the change in the background, if we allowed one. However, as we stick to the same background, we will interpret this term as a contribution to the change of the perturbation variables due to the coordinate transformation. This is the conceptional difference between the *coordinate* transformation (changing the background, the coordinates and the fluctuations) and the *gauge* transformation (changing only the fluctuations, keeping the old coordinates and background quantities). The transformation four vector ϵ can be decomposed into scalar and vector parts. Following [25], we set

$$\begin{aligned} \tilde{\tau} &= \tau + T(\tau)Q(\boldsymbol{x}) \\ \tilde{x}^i &= x^i + L(\tau)Q^i(\boldsymbol{x}) + L^{(V)}(\tau)Q^{(V)\,i}(\boldsymbol{x}). \end{aligned} \quad (3.21)$$

The vector contribution will not affect scalar perturbations, just like scalar, vector and tensor perturbations decouple in linear approximation. Using the above tranformation (3.21) in (3.20), we can calculate for instance the change in the metric perturbation B:

$$\begin{aligned} \tilde{g}_{0i}(x) &= g_{0i}(x) - \bar{g}_{\alpha i}(\tau)\epsilon^{\alpha}_{,0} - \bar{g}_{0\alpha}(\tau)\epsilon^{\alpha}_{,i} - \epsilon^{\alpha}\,\bar{g}_{0i,\,\alpha} \\ &= g_{0i}(x) - \bar{g}_{ji}(\tau)\dot{L}Q^j - \bar{g}_{00}(\tau)TQ_{,i} \\ &= -a^2(\tau)\left(B + \dot{L} + kT\right)Q_i \\ &\equiv -a^2(\tau)\,\tilde{B}\,Q_i \end{aligned} \quad (3.22)$$

Similar calculations yield the transformation properties of all the metric perturbation variables:

$$\begin{aligned} \tilde{A}(\tau) &= A(\tau) - \frac{\dot{a}}{a}T(\tau) - \dot{T}(\tau) \\ \tilde{B}(\tau) &= B(\tau) + \dot{L} + kT(\tau) \\ \tilde{H}_L(\tau) &= H_L(\tau) - \frac{\dot{a}}{a}T - \frac{k}{3}L(\tau) \\ \tilde{H}_T(\tau) &= H_T(\tau) + kL(\tau) \end{aligned} \quad (3.23)$$

From the transformation properties (3.23) of the scalar metric fluctuations, it is clear that one can choose the functions $T(\tau)$ and $L(\tau)$ such, that two of the perturbation variables vanish. Popular choices are the synchronous gauge defined by $A = 0,\ B = 0$ and the longitudinal gauge with $H_T = B = 0$.

Having the transformation law (3.23) at hand, one can construct gauge-invariant combinations, the so called *Bardeen* potentials

$$\Psi \equiv A - \frac{\dot{a}}{a}k^{-1}\sigma - k^{-1}\dot{\sigma} \tag{3.24}$$

$$\Phi \equiv H_L + \frac{1}{3}H_T - \frac{\dot{a}}{a}k^{-1}\sigma, \tag{3.25}$$

where $\sigma \equiv k^{-1}\dot{H}_T - B$ vanishes in the longitudinal gauge. Hence, the line element in the longitudinal gauge takes on the particularly convenient form

$$ds^2 = a(\tau)^2\left[-(1+2\Psi)d\tau^2 + (\delta_{ij}+2\Phi)dx^i dx^j\right], \tag{3.26}$$

where we have restricted ourselves to scalar contributions. One expects that in general, the fluctuations in the energy momentum tensor will also be gauge dependent. This is the true *gauge-problem*. Due to the different metric in different gauges, comoving observers in different gauges will measure different energy perturbations.

3.2 The Energy Momentum Tensor

Having defined the metric, we will now specify the energy momentum tensor for matter and radiation. Even though photons during recombination (and neutrinos) need to be described by a distribution function, it is still convenient to identify certain moments of these distributions as *fluid* perturbations. Here, we are going to derive the perturbation equations for one single species.[2] After deriving the perturbation equations in the fluid description, we will turn to quintessence perturbations.

The imperfect fluid

Let us start by defining the energy momentum tensor of a (possibly imperfect) fluid:

$$T^{\mu}_{\ \nu} = p\delta^{\mu}_{\ \nu} + (p+\rho)u^{\mu}u_{\nu} + \pi^{\mu}_{\ \nu} \tag{3.27}$$

Here, the 4-velocity u is the velocity of the matter rest frame with respect to the coordinate frame. Usually, one assumes that the spatial components u^i are first order perturbations. With this in mind, we get from

$$u^{\mu}u^{\nu}g_{\mu\nu} = -1 \tag{3.28}$$

[2] In Appendix C (see also Chapter 5) we give the full equations (including momentum transfer between baryons and photons) used to calculate the CMB anisotropies.

the time component

$$u^0 = a(\tau)^{-1}(1 - A(\tau)). \tag{3.29}$$

Next, we set for the spatial part

$$u^i = a^{-1} v(\tau) Q^i, \tag{3.30}$$

defining v. Lowering the index, we find for the covariant velocity

$$u_0 = -a(1 + A) \qquad u_i = a(v - B)Q_i. \tag{3.31}$$

Using the same conventions as [26,18], let us set

$$\rho \equiv \bar{\rho}(\tau)\,[1 + \delta(\tau)Q], \tag{3.32}$$

and the spatial trace

$$p\,\delta^i{}_j \equiv \bar{p}(\tau)\,[1 + \pi_{\rm L}(\tau)Q]\,\delta^i{}_j, \tag{3.33}$$

while for the traceless part

$$\pi^i{}_j \equiv \bar{p}\,\Pi\,Q^i_j. \tag{3.34}$$

This *defines* the perturbations Π and $\pi_{\rm L}$ and δ. Working to first order one gets from these definitions

$$\begin{aligned}
T^0{}_0 &= -\bar{\rho}(1 + \delta\, Q) \\
T^0{}_i &= (\bar{\rho} + \bar{p})\,(v - B)\,Q_i \\
T^i{}_0 &= -(\bar{\rho} + \bar{p})\,v\,Q^i && (3.35)\\
T^i{}_j &= \bar{p}\left[(1 + \pi_{\rm L}\,Q)\delta^i_j + \Pi Q^i_j\right]. && (3.36)
\end{aligned}$$

Gauging the Energy

We will now investigate the gauge dependence of the energy momentum perturbations. From Equations (3.18), (3.21) and (2.9), we get

$$\begin{aligned}
\tilde{T}^0{}_0(x) &= T^0{}_0(x) + \bar{T}^0{}_0\epsilon^0_{,0} - \bar{T}^0{}_0\epsilon^0_{,0} - \bar{T}^0{}_{0,0}\epsilon^0 && (3.37)\\
&= -\bar{\rho}\left(1 + \left[\delta - \frac{\dot{\bar{\rho}}}{\bar{\rho}}T\right] Q\right) \\
&= -\bar{\rho}\left(1 + \left[\delta + 3(1 + w)\frac{\dot{a}}{a}T\right] Q\right). && (3.38)
\end{aligned}$$

Hence,

$$\tilde{\delta} = \delta + 3(1 + w)\frac{\dot{a}}{a}T. \tag{3.39}$$

The velocity perturbation transforms as

$$\tilde{v} = v + \dot{L}, \tag{3.40}$$

which can be seen by either calculating $d\tilde{x}^i/d\tilde{\tau}$ or by transforming $T^i{}_0$. Finally, we get from a calculation similar to the one for δ, that $\pi_{\rm L}$, transforms as

$$\tilde{\pi}_{\rm L} = \pi_{\rm L} - \frac{\dot{\bar{p}}}{\bar{p}}T = \pi_{\rm L} + 3(1+w)\frac{c_s^2}{w}\frac{\dot{a}}{a}T, \tag{3.41}$$

where the sound speed is given by

$$c_s^2 \equiv \frac{\dot{\bar{p}}}{\dot{\bar{\rho}}}. \tag{3.42}$$

The vanishing of the off diagonal elements $\bar{T}^i{}_j$ ensures that Π is gauge invariant from the start.

3.3 Gauge Invariant Energy-Momentum Perturbations

There are many ways to combine one of the energy-momentum perturbations with the metric fluctuations (or another energy-momentum perturbation) to form gauge-invariant quantities. Following [18], we will use

$$\begin{aligned}
V &\equiv v - \frac{1}{k}\dot{H}_T = v^{(longit)} && (3.43)\\
D_g &\equiv \delta + 3(1+w)\left(H_L + \frac{1}{3}H_T\right) = \delta^{(longit)} + 3(1+w)\Phi && (3.44)\\
D &\equiv \delta^{(longit)} + 3(1+w)\frac{\dot{a}}{a}\frac{V}{k} && (3.45)\\
\Gamma &\equiv \pi_{\rm L} - \frac{c_s^2}{w}\delta, && (3.46)
\end{aligned}$$

where $(longit)$ labels perturbations in the longitudinal gauge, and Γ can be viewed as entropy production rate. This is due to the fact that for *adiabatic* perturbations $\delta p/\delta\rho = \dot{\bar{p}}/\dot{\bar{\rho}}$ and therefore[3]

$$\Gamma^{(adiab)} = \frac{\delta p}{\bar{p}} - \frac{\delta p/\delta\rho}{w}\frac{\delta\rho}{\bar{\rho}} = 0. \tag{3.47}$$

Perturbed Einstein's and Conservation Equation

Having defined the metric and the energy momentum tensor, we are now in the position to use Einstein's equation to relate the metric perturbations to the matter

[3] To avoid confusion of the δ's in this line: $\delta\rho$ is the absolute perturbation $\bar{\rho}\times\delta$.

perturbations. We will first derive the equations with $\delta,\ v\ldots$ in the longitudinal gauge and in a second step move to the gauge invariant variables. The perturbed part of Einstein's equations yields

$$a^2\,\bar{\rho}\,\delta = 2\mathrm{M}_\mathrm{P}^2\left\{k^2\Phi + 3\frac{\dot{a}}{a}\left(\dot{\Phi} - \frac{\dot{a}}{a}\Psi\right)\right\} \qquad \text{from } G^0{}_0, \tag{3.48}$$

$$a^2\,v\,(\bar{\rho}+\bar{p}) = 2\mathrm{M}_\mathrm{P}^2\,k\left(\frac{\dot{a}}{a}\Psi - \dot{\Phi}\right) \qquad \text{from } G^0{}_i, \tag{3.49}$$

$$a^2\bar{p}\,\Pi = = -\mathrm{M}_\mathrm{P}^2\,k^2(\Phi+\Psi) \qquad \text{from } G^i{}_j. \tag{3.50}$$

Conservation of the energy component $T^{\mu}_{0;\mu} = 0$, gives

$$-\dot{\delta} = \left(\frac{\dot{\bar{\rho}}}{\bar{\rho}} + 3\frac{\dot{a}}{a}\right)\delta + (1+w)(vk + 3\dot{\Phi}) + 3\frac{\dot{a}}{a}w\pi_\mathrm{L}, \tag{3.51}$$

whereas the momentum part $T^{\mu}_{i;\mu} = 0$ yields

$$-\dot{v} = 4\frac{\dot{a}}{a}\bar{\rho}\,v + v\,\frac{\dot{\bar{\rho}}}{\bar{\rho}}\frac{1+c_s^2}{1+w} - k\Psi + \frac{w\,k}{1+w}\left(\frac{2}{3}\Pi - \pi_\mathrm{L}\right). \tag{3.52}$$

Please note that in principle, the equation of state w and the speed of sound c_s could be time dependent. Moving to the gauge-invariant perturbations and using Equation (2.9) we can rewrite equations (3.48-3.50) as

$$a^2\bar{\rho}D = 2\,\mathrm{M}_\mathrm{P}^2\,k^2\Phi \tag{3.53}$$

$$a^2(\bar{\rho}+\bar{p})V = 2\,\mathrm{M}_\mathrm{P}^2\,k\left(\frac{\dot{a}}{a}\Psi - \dot{\Phi}\right) \tag{3.54}$$

$$a^2\bar{p}\,\Pi = -\mathrm{M}_\mathrm{P}^2\,k^2(\Phi+\Psi), \tag{3.55}$$

where we have simplified (3.53) using the expression for v from Equation (3.49). The dynamics of the the matter perturbations is governed by Equations (3.51) and (3.52) expressed in gauge invariant variables. Using

$$\dot{w} = \frac{\dot{\bar{\rho}}}{\bar{\rho}}\left(c_s^2 - w\right) \tag{3.56}$$

and Equation (2.9), we obtain

$$\dot{D}_g + 3\left(c_s^2 - w\right)\frac{\dot{a}}{a}D_g + k\,V(1+w) + 3\frac{\dot{a}}{a}\,w\,\Gamma = 0, \tag{3.57}$$

and

$$\begin{aligned}\dot{V} = {} & \frac{\dot{a}}{a}(3c_s^2-1)V + k\left[\Psi - 3c_s^2\Phi\right] \\ & + \frac{c_s^2 k}{1+w}D_g + \frac{wk}{1+w}\left[\Gamma - \frac{2}{3}\Pi\right]\end{aligned} \tag{3.58}$$

3.4 Perturbed Quintessence Energy Momentum Tensor

The energy perturbation δ is defined relative to $\bar{\rho}$. For the quintessence field, it will be advantageous to consider the absolute perturbation of a scalar quantity. From (3.18), we see that any scalar $\varphi = \bar{\varphi} + \chi$ transforms as $\tilde{\varphi} = \varphi - \dot{\bar{\varphi}}T$. Hence, the perturbation χ transforms like $\tilde{\chi} = \chi - \dot{\bar{\varphi}}T$ and the combination

$$X \equiv \chi - \dot{\bar{\varphi}}\, k^{-1}\, \sigma \tag{3.59}$$

is gauge invariant. Due to the vanishing of σ in the longitudinal gauge, we simply have $\chi^{(longit.)} = X$. For the quintessence field we write

$$\varphi(\tau, \boldsymbol{x}) = \bar{\varphi}(\tau) + \chi(\tau), \tag{3.60}$$

where we as usual suppressed the $\boldsymbol{k}$ integration and the $\boldsymbol{k}$ dependence of χ. We now use the above expression for X (3.59) to define the gauge invariant field fluctuation and write gauge-invariantly $\varphi = \bar{\varphi}(\tau) + X(\tau)$.

The perturbed energy momentum tensor follows from inserting the fluctuating $\varphi(\tau, \boldsymbol{x})$ and the perturbed metric into Equation (2.15). In *longitudinal gauge* (where $\chi = X$), it is given by

$$\begin{aligned}
\delta T^{0}_{\ 0}{}^{(longit)} &= \left[a^{-2}\left(\dot{\bar{\varphi}}^2\,\Psi - \dot{X}\dot{\bar{\varphi}}\right) - V'(\varphi)X\right]\, Q && (3.61)\\
\delta T^{i}_{\ j}{}^{(longit)} &= -\left[a^{-2}\left(\dot{\bar{\varphi}}^2\,\Psi - \dot{X}\dot{\bar{\varphi}}\right) + V'(\varphi)X\right]\, Q\,\delta^i_j && (3.62)\\
\delta T^{0}_{\ i}{}^{(longit)} &= a^{-2}\, k\,\dot{\bar{\varphi}}\, X\, Q_i && (3.63)\\
\delta T^{i}_{\ 0}{}^{(longit)} &= -a^{-2}\, k\,\dot{\bar{\varphi}}\, X\, Q^i. && (3.64)
\end{aligned}$$

Here, the potential $V(\varphi)$ should not be confused with the gauge invariant velocity perturbation V, which for quintessence will be denoted by V_φ. Despite the fact that only gauge invariant variables appear in Equations (3.61 - 3.64), none of them is gauge invariant. For instance $\delta T^0_{\ 0}$ transforms as a scalar.[4] As spatial off diagonal elements vanish, we immediately get

$$\Pi_\varphi = 0. \tag{3.67}$$

[4] We can easily see this from Equation (3.37), where $\delta\tilde{T}^{0}_{\ 0} = \delta T^0_{\ 0} - \dot{\bar{T}}^0_{\ 0}\,\epsilon^0$. Hence, the quantity $\mathcal{T} \equiv \delta T^0_{\ 0} - k^{-1}\sigma\dot{\bar{T}}^0_{\ 0}$ is gauge invariant and $\mathcal{T} = \delta T^{0}_{\ 0}{}^{(longit)}$. Thus, the perturbation in the synchronous gauge follows from

$$\begin{aligned}
\delta T^{0}_{\ 0}{}^{(sync)} &= \mathcal{T} + k^{-1}\sigma^{(sync)}\,\dot{\bar{T}}^0_{\ 0} = \delta T^{0}_{\ 0}{}^{(longit)} + k^{-1}\,\sigma^{(sync)}\dot{\bar{T}}^0_{\ 0} && (3.65)\\
&= -a^{-2}\,\dot{\bar{\varphi}}\,\dot{\chi}^{(sync)} - V'\chi^{(sync)}, && (3.66)
\end{aligned}$$

in agreement with the direct calculation using Equation (2.15) in the synchronous gauge.

To solve Equations (3.53) and (3.54), an expression for D_φ and V is needed. Comparing Equation (3.35) with Equation (3.64) in longitudinal gauge, yields

$$a^{-2}k\,\dot{\bar{\varphi}}\,X = (\bar{\rho}_\varphi + \bar{p}_\varphi)V_\varphi. \tag{3.68}$$

Using $\bar{\rho}_\varphi + \bar{p}_\varphi = a^{-2}\dot{\bar{\varphi}}^2$ from Equation (2.17), we find the *gauge invariant* expression

$$V_\varphi = k\,\dot{\bar{\varphi}}^{-1}\,X. \tag{3.69}$$

An expression for the density perturbation D_g is obtained by inserting Equation (3.61) in Equation (3.44)

$$\begin{aligned} D_g^\varphi &= \bar{\rho}_\varphi^{-1}\left[-\delta T^0_{\ 0}{}^{(longit)} + 3(\bar{\rho}_\varphi + \bar{p}_\varphi)\Phi\right] && (3.70)\\ &= \bar{\rho}_\varphi^{-1}\left[a^{-2}\dot{\bar{\varphi}}\left(\dot{X} + \dot{\bar{\varphi}}\{3\Phi - \Psi\}\right) + V'(\varphi)X\right] && (3.71)\\ &= (1+w^\varphi)\left[3\Phi - \Psi\ + \dot{X}\,\dot{\bar{\varphi}}^{-1}\right] + X\,V'(\varphi)\,\bar{\rho}_\varphi^{-1} && (3.72) \end{aligned}$$

where we have once again used $\bar{\rho}_\varphi + \bar{p}_\varphi = a^{-2}\dot{\bar{\varphi}}^2$. The perturbation D_φ then follows from D_g^φ using Equations (3.45) and (3.69).

Equation of Motion of the Quintessence Field Perturbation

Energy conservation, $T^\mu_{0;\mu} = 0$ (or alternatively the Klein-Gordon equation), yields the gauge invariant equation of motion

$$\ddot{X} = \dot{\bar{\varphi}}\left(\dot{\Psi} - 3\dot{\Phi}\right) - 2a^2V'(\varphi)\Psi - \left[a^2\,V''(\varphi) + k^2\right]X - 2\frac{\dot{a}}{a}\dot{X}, \tag{3.73}$$

for the field perturbation X. That this equation is truly gauge invariant follows from the equation of motion

$$\ddot{\chi} = -2Aa^2V'(\varphi) + \dot{\bar{\varphi}}(\dot{A} - kB - 3\dot{H}_L) - \left[a^2\,V''(\varphi) + k^2\right]\chi - 2\frac{\dot{a}}{a}\dot{\chi}, \tag{3.74}$$

derived without gauge fixing and a subsequent gauge transformation of all perturbation variables. To see the invariance, the τ-derivative of Equation (2.18) leading to $\frac{\mathrm{d}^3}{\mathrm{d}\tau^3}\bar{\varphi} + \left[2\frac{\ddot{a}}{a} - 6\left(\frac{\dot{a}}{a}\right)^2 + a^2V''\right]\dot{\bar{\varphi}} = 0$ is useful.

3.5 Synchronous Gauge Quintessence Field

Most of the existing literature uses synchronous gauge. In addition, the widely used CMBFAST computer code which integrates the perturbation equations is implemented in this gauge. In terms of the perturbation variables defined in [27], the equations for the quintessence field have been derived for instance in [28,29]. Here,

we will re-derive them using the gauge invariant equations of the previous section. The perturbation H_{ij} of Equation (3.9) is defined in [27] as

$$2H_{ij} = \hat{k}_i\hat{k}_j\, h\, Q + 6\eta\left(\hat{k}_i\hat{k}_j - \frac{1}{3}\delta_{ij}\right)Q \tag{3.75}$$

$$= \frac{1}{3}h\delta_{ij}Q - (h+6\eta)Q_{ij}, \tag{3.76}$$

in other words, H_T contains terms both from h and η,

$$H_L = \frac{1}{6}h, \qquad H_T = -\frac{1}{2}(h+6\eta). \tag{3.77}$$

Even though we will not need them here, we note that using h and η, the Bardeen potentials become

$$\Psi = \frac{1}{2k^2}\left[\frac{\dot{a}}{a}\left(\dot{h}+6\dot{\eta}\right) + \left(\ddot{h}+6\ddot{\eta}\right)\right] \tag{3.78}$$

$$\Phi = \frac{4}{3}h - \eta + \frac{1}{2k^2}\frac{\dot{a}}{a}\left(\dot{h}+6\dot{\eta}\right). \tag{3.79}$$

Turning to the perturbation evolution, a short manipulation of Equation (3.69), using the expression for V_φ and X in the synchronous gauge yields

$$v_\varphi^{(sync)} = k\,\dot{\bar{\varphi}}^{-1}\,\chi^{(sync)}. \tag{3.80}$$

In the notation of [27], one uses $\theta \equiv ik^j v_j Q^{-1}$. Now, $v_j = vQ_j = -k^{-1}vQ_{,j} = -ik^{-1}k_j vQ$ and hence

$$\theta_\varphi^{(sync)} = -i^2 k^j k_j k^{-1}\, v_\varphi^{(sync)}$$

$$= k\, v_\varphi^{(sync)} \tag{3.81}$$

$$= k^2\,\dot{\bar{\varphi}}^{-1}\,\chi^{(sync)}. \tag{3.82}$$

In the Footnote on page 27, we have already derived

$$\delta_\varphi^{(sync)}\bar{\rho}_\varphi = -a^{-2}\,\dot{\bar{\varphi}}\,\dot{\chi}^{(sync)} - V'\chi^{(sync)}. \tag{3.83}$$

Alternatively, in synchronous gauge $\delta T^0_{\ 0} = -\delta\rho$ holds, giving the same result. Finally, the perturbation $\chi^{(sync)}$ obeys the equation of motion

$$\ddot{\chi}^{(sync)} + 2\frac{\dot{a}}{a}\dot{\chi} + k^2\chi^{(sync)} + a^2V''(\varphi)\chi^{(sync)} + \frac{1}{2}\dot{h}\dot{\bar{\varphi}} = 0, \tag{3.84}$$

which can be derived using the non-gauge-fixed equation of motion (3.74) and Equation (3.77).

3.6 Solutions for Perfect Fluids

In order to get some intuition for the perturbation variables, we briefly summarize their behaviour in simple settings. Chapter 5 will generalize these ideas in great detail to early time perturbations.

The perturbation equations (3.53) - (3.58) simplify considerably for a shear free fluid ($\Pi = 0$) with vanishing entropy production ($\Gamma = 0$). The easily obtained analytic solution for pressureless dust ($w = c_s^2 = \Gamma = \Pi = 0$), is [18]

$$\begin{aligned} V &= V_0(k\tau) \\ D_g &= -V_0\left[15 + \frac{1}{2}(k\tau)^2\right] \\ \Psi &= 3V_0, \end{aligned} \tag{3.85}$$

where V_0 is an integration constant. We see, that the gravitational potential $\Psi = -\Phi$ is constant in a matter dominated universe. Turning to the relativistic fluid with $w = c_s^2 = 1/3$, $\Gamma = \Pi = 0$, the solution on super horizon scales ($k\tau \ll 1$) becomes [18]

$$\begin{aligned} V &= V_0(k\tau) \\ D_g &= -12V_0 - \frac{2}{3}V_0(k\tau)^2 \\ \Psi &= 2V_0, \end{aligned} \tag{3.86}$$

where again V_0 is an arbitrary constant. Hence, also in a radiation dominated universe, Ψ remains constant. Finally, the solution on sub horizon scales ($k\tau \gg 1$) is

$$\begin{aligned} V &= V_2 \sin\left(k\tau/\sqrt{3}\right) \\ D_g &= \frac{4}{\sqrt{3}}V_2 \cos\left(k\tau/\sqrt{3}\right) \\ \Psi &= -\frac{3}{2}(k\tau)^{-2}D_g\,. \end{aligned} \tag{3.87}$$

Interestingly, the perturbation variables oscillate within the horizon in a radiation dominated universe. As the photons in the cosmic microwave background are emitted from such a radiation fluid, one suspects to see oscillation patterns depending on the scale k. This is quite true, even though the details are a bit more complicated. We will pick up the oscillatory solution again in Chapter 4, but before that a look at quintessence perturbations is in order.

For modes that are well inside the horizon, we neglect gravitational feedback.[5] The equation of motion (3.73) for X becomes

$$\ddot{X} + 2\frac{\dot{a}}{a}\dot{X} + \left[a^2\, V''(\varphi) + k^2\right] X = 0. \tag{3.88}$$

[5] This assumption is by no means correct in the case of super-horizon perturbations.

On sub-horizon scales, $k^2 \gg a^2 V''(\varphi)$. In addition, $\dot{a}/a = 1/\tau$ during radiation domination and $\dot{a}/a = 2/\tau$ in a matter dominated universe. Thus, sub-horizon wise, we get

$$\ddot{X} + \frac{2s}{\tau}\dot{X} + k^2 X = 0, \tag{3.89}$$

with $s = 1, 2$ for RD and MD respectively. In both cases, the solution to Equation (3.89) is

$$X(\tau) = \tau^{1-s}\sqrt{k}\left[c_1 j_{s-1}(k\tau) + c_2 n_{s-1}(k\tau)\right], \tag{3.90}$$

where $c_1,\ c_2$ are constants and $j_l,\ n_l$ are spherical Bessel and Neumann functions. Figures 5.2 and 5.1 nicely show the oscillatory behaviour of X as soon as the mode is well inside the horizon. Super-horizon modes will be discussed in section 5.2. There, we will show that X usually follows a power law in τ.

4

The Cosmic Microwave Background

The cosmic microwave background has been accidently discovered by Penzias & Wilson in 1965 [42]. It is formed by a sea of photons that arrive almost isotropically from all directions in the sky. Before we review the main features of the CMB anisotropy calculation (starting with Section 4.2), we would like to gain some results from intuition that hold also in the detailed calculation.

4.1 Intuition

Let us start by the observation, that a thermal photon gas has occupation numbers

$$\begin{aligned} N &= \left(\exp(\hbar\omega/k_{\mathrm{b}}\bar{T}) - 1\right)^{-1} \\ &= \left(\exp(hc/k_{\mathrm{b}}\bar{T}\lambda) - 1\right)^{-1}, \end{aligned} \tag{4.1}$$

where k_{b} is the Boltzmann constant, c is the speed of light and λ is the wave length of a photon determining its energy. Now, the frequency of a microwave (with say $\lambda = 10\,\mathrm{cm}$) is $f = 3 \times 10^9\mathrm{Hz}$, whereas the Hubble parameter is

$$H_0 \approx 100\,\mathrm{km}\,s^{-1}\mathrm{Mpc}^{-1} \approx 2 \times 10^{-18}\mathrm{Hz}. \tag{4.2}$$

Thus, the microwave frequency is much higher than the relative expansion rate of the universe. Hence, for the photon gas, the universe expands *adiabatically* and from quantum mechanics, we know that the occupation number should be conserved. Along with the physical scales, the wavelength stretches with the expansion $\lambda \propto a$. In order to conserve the occupation number, we thus find

$$\bar{T} \propto a^{-1}. \tag{4.3}$$

Alternatively, the energy density of a photon gas $\rho_\gamma \propto \bar{T}^4$, and as $\rho_\gamma \propto a^{-4}$, we see that $\bar{T} \propto a^{-1}$ as above.

Within the photon-baryon plasma, sound waves propagate at the huge speed of [45]

$$c_s^2 = \frac{\mathrm{d}\bar{p}}{\mathrm{d}\bar{\rho}} = \frac{1}{3}\frac{\mathrm{d}\bar{\rho}_\gamma}{\mathrm{d}\left(\bar{\rho}_\gamma + \bar{\rho}_b\right)}, \tag{4.4}$$

which is $\approx 1/3$ until recombination destroys the plasma. The *sound horizon* is the distance, a sound wave can at most travel since $\tau = 0$. It is given by

$$s(\tau) = \int_0^\tau \mathrm{d}\tau' c_s(\tau'), \tag{4.5}$$

and owing to the fact that $c_s^2 \approx 1/3$ during most of the time until decoupling, one simply has $s(\tau) \approx \tau\sqrt{1/3}$. Now, the plasma is opaque to photons. Just at the end of recombination, the universe is transparent enough for photons to travel almost freely. Therefore, most of the CMB photons seen today scattered for the last time at around the epoch of decoupling. Naturally, this epoch is also called last scattering. Using the Saha equation [43], one finds that the redshift of last scattering is $z_{\mathrm{ls}} \approx 1100$. This corresponds to $\tau \approx 300\mathrm{Mpc}$ and therefore a sound horizon of $s \approx 170\mathrm{Mpc}$. As far as sound-waves are concerned, the only (large) scale present at last scattering is this sound horizon. We have already seen in Section 3.6 that within the horizon, photon perturbations start to oscillate. Thus, one expects 'resonances' [45] of the form

$$\cos(k \times s_{\mathrm{ls}} + \varphi), \tag{4.6}$$

where φ accounts for a possible overall phase shift.[1]

In adiabatic models, this shift is $\varphi \approx 0.2$. We will later find more detailed formulae for the shifts of the peaks. However, for a first estimate, it is enough to consider $\varphi = 0$ and hence, one expects peaks in Fourier space at

$$k = \frac{m\,\pi}{s} \approx m \times 0.018\mathrm{Mpc}^{-1}, \tag{4.7}$$

where m is an integer.

The CMB experiments do not measure temperature anisotropies in Fourier space directly, but angular correlations on the sky today. Therefore, it is natural to quote the results in terms of coefficients C_l of a Legendre series (see Section 4.2 below). The photons last scattered at z_{ls} stream freely as a plane wave towards us. In terms of Legendre polynomials a plane wave is expanded with spherical Bessel functions j_l as coefficients. As the 'distance' the plane wave travels is $\tau_0 - \tau_{\mathrm{ls}} \approx \tau_0$, the wave is given today by $\exp(ik\tau_0)$. It turns out that the Bessel functions in the Legendre expansion of $\exp(ik\tau_0)$ take on the argument $j_l(k\tau_0)$ (see Section 4.5.1). Now, spherical Bessel functions are peaked when the argument equals the multipole l. Therefore, a feature present in Fourier space at last scattering translates into a

[1] Unfortunately, there are many quantities that are commonly denoted by the Greek letter ϕ. However, the reader should have no problem to keep the peak shift φ and the field φ apart, as the peak shift is occurring only here and in the section about peak shifts and in both cases, the quintessence field φ is not present.

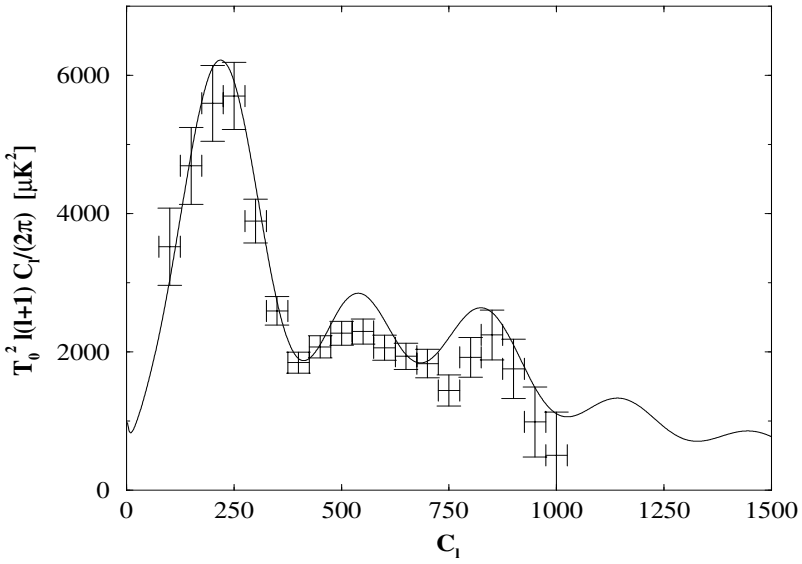

Figure 4.1: Boomerang 2001 data and the spectrum for a LKT model with $h = 0.65$, $\Omega_0^\varphi = 0.7$, $\Omega_0^{\rm b} h^2 = 0.022$, $n = 0.97$. In this model, the horizons at last scattering and today are $\tau_{\rm ls} = 280\,{\rm Mpc}$, $\tau_0 = 14400\,{\rm Mpc}$. The roughly estimated peak positions are $l = 260, 520, 780 \ldots$.

feature in the multipole decomposition today at

$$l \approx k\tau_0. \tag{4.8}$$

For the k-values of (4.7), one gets (using $\tau_0 \approx 14400\,{\rm Mpc}$ of the model depicted in Figure 4.1) $l_{\rm peak} \approx 260, 520, 780 \ldots$. Figure 4.1, showing experimental data as well as theoretical predictions for the C_l spectrum nicely demonstrates that the estimate of peak positions[2] is fairly adequate. The occurrence of peaks spaced by roughly the same $\Delta l \approx 200 - 300$ in the multipole spectrum leads to the definition of the *acoustic scale* [44,45]

$$l_{\rm A} = \pi \frac{\tau_0 - \tau_{\rm ls}}{s} = \pi \frac{\tau_0 - \tau_{\rm ls}}{\bar{c}_s \tau_{\rm ls}}, \tag{4.9}$$

where $\bar{c}_s = \tau_{\rm ls}^{-1} \int_0^{\tau_{\rm ls}} {\rm d}\tau c_s(\tau)$ is the average sound speed until last scattering. In terms of l_A, our estimate of peak positions, (4.8) is just $l_m = m\, l_A$.

4.2 The Multipole Spectrum

The temperature anisotropies are usually quoted in terms of coefficients C_l of 2-point correlations. Suppose, we knew the temperature anisotropy $\Delta(\boldsymbol{n})$ today on

[2] Or rather inter-peak spacing, as we didn't include the shift.

planet earth pointing in direction $\boldsymbol{n}$ in the sky.[3] We can expand this in terms of spherical harmonics [4]

$$\Delta(\boldsymbol{n}) \equiv \frac{\Delta T}{T}(\boldsymbol{n}) = \sum_{l,m} a_{lm} Y_l^m(\boldsymbol{n}). \tag{4.10}$$

The 2-point correlation between two directions in the sky is then

$$\left\langle \Delta(\boldsymbol{n})\Delta(\boldsymbol{n}')\right\rangle = \sum_{l,l',m,m'} \langle a_{lm} a^*_{l'm'}\rangle Y_l^m(\boldsymbol{n}) \left(Y_{l'}^{m'}(\boldsymbol{n}')\right)^* \tag{4.11}$$

One now assumes that the angle $\mu \equiv \boldsymbol{n}\cdot\boldsymbol{n}'$ between the directions is statistically independent of the orientation, i.e. one can write

$$\langle a_{lm} a^*_{l'm'}\rangle = \delta_{ll'}\delta_{mm'} C_l, \tag{4.12}$$

with coefficients C_l. From Equation (4.11) we then get

$$\begin{aligned} \left\langle \Delta(\boldsymbol{n})\Delta(\boldsymbol{n}')\right\rangle &= \sum_l C_l \sum_{m=-l}^{l} Y_l^m(\boldsymbol{n}) \left(Y_l^m(\boldsymbol{n}')\right)^* && (4.13)\\ &= \frac{1}{4\pi}(2l+1) C_l P_l(\mu), && (4.14) \end{aligned}$$

where $P_l(\mu)$ are Legendre polynomials. In Fourier space, C_l's can be expressed as

$$C_l = (4\pi)\int k^2 \mathrm{d}k P(k) |\Delta_l(k,\tau_0)|, \tag{4.15}$$

where $\mathcal{P}(k)$ is the initial power spectrum and $\Delta_l(k,\tau_0)$ are coefficients of the Legendre series

$$\Delta(k,\mu,\tau_0) = \sum_l (-i)^l (2l+1)\Delta_l(k,\tau_0) P_l(\mu). \tag{4.16}$$

4.3 The Liouville Equation for Photons

At redshift $z \approx 1100$, the universe was cool enough for electrons and protons to recombine and form neutral hydrogen. The less free electrons there were, the less opaque the universe became for photons. From the recombination period on, the description of photons and baryons as one single fluid is not appropriate anymore. One therefore uses the phase-space distribution function f. For a start, let us consider the simple case of a spatially homogenous distribution $f = \bar{f}(p,\tau)$ (forgetting

[3] We suppress the arguments $\boldsymbol{x}_0$ ('here') and τ_0 ('now') in this section for ease of notation.

[4] The calculation here follows 'textbook' standard and can in similar form be found for instance in [18].

for a moment that it might resemble the one in (4.1)). In the argument we have defined $p \equiv \delta_{ij}\, p^i p^j$. The general relativistic Liouville equation is [47]

$$p^\mu (\partial_\mu \bar{f})_{|p} - \Gamma^i_{\mu\nu} p^\mu p^\nu \frac{\partial \bar{f}}{\partial p^i} = 0, \tag{4.17}$$

where $|p$ stands for evaluation at constant p. From $p = \delta_{ij}\, p^i p^j$ one has

$$\frac{\partial p}{\partial p^i} = \frac{p^k}{p}\delta_{ik}. \tag{4.18}$$

Using this, $p^0 = p \neq 0$ for photons and the unperturbed Christoffel symbols of Appendix A yields

$$\left(\partial_\tau \bar{f}\right)_{|p} - 2p\frac{\dot{a}}{a}\left(\frac{\partial \bar{f}}{\partial p}\right)_{|\tau} = 0. \tag{4.19}$$

Now, a photon observed by some observer with 4-velocity u^μ has energy $E = u_\mu p^\mu$ [46] and therefore with $u_0 = -a$ from Equation (3.31),

$$E = -ap. \tag{4.20}$$

The time derivative of E at *constant* p is therefore[5]

$$(\partial_\tau E)_{|p} = -\dot{a}p = \frac{\dot{a}}{a}E. \tag{4.21}$$

Moving from the variables$\{\tau, p\}$ of Equation (4.19) to $\{\tau, E\}$ and using $p\frac{\partial \bar{f}}{\partial p} = E\frac{\partial \bar{f}}{\partial E}$ yields

$$\begin{aligned} 0 &= (\partial_\tau \bar{f})_{|E} + \left(\frac{\partial \bar{f}}{\partial E}\right)_{|\tau}\left(\frac{\partial E}{\partial \tau}\right)_{|p} - 2E\frac{\dot{a}}{a}\left(\frac{\partial \bar{f}}{\partial E}\right)_{|\tau} \\ &= (\partial_\tau \bar{f})_{|E} - E\frac{\dot{a}}{a}\left(\frac{\partial \bar{f}}{\partial E}\right)_{|\tau}. \end{aligned} \tag{4.22}$$

Now, for any function $\bar{f}(x \equiv aE)$,

$$(\partial_\tau \bar{f})_{|E} = \frac{\partial \bar{f}}{\partial x}\left(\frac{\partial x}{\partial \tau}\right)_{|E} = \dot{a}E\frac{\partial \bar{f}}{\partial x}, \tag{4.23}$$

and

$$(\partial_E \bar{f})_{|\tau} = \frac{\partial \bar{f}}{\partial x}\left(\frac{\partial x}{\partial E}\right)_{|\tau} = a\frac{\partial \bar{f}}{\partial x}. \tag{4.24}$$

Inserting this in Equation (4.22), we see that any distribution that solely depends on aE is unchanged by the cosmological expansion. Looking back at the distribution function for a thermal photon gas (4.1) one finds that for $T \propto a^{-1}$, f is preserved just as before.

[5] If one happens to know that $Ea = const.$ (e.g. from the last section), one is tricked into the conclusion that $\dot{E} = -\frac{\dot{a}}{a}E$. However, at constant p, one gets the opposite sign.

4.4 The Perturbed Photon Distribution

The last section showed that $\bar{f}$ is a function of $aE = -a^2 p$ only. Following [18], we define $v \equiv a^2 p^i p^j \delta_{ij}$ and $f(\tau, \boldsymbol{x}, v, \boldsymbol{n}) = \bar{f}(v) + F(\tau, \boldsymbol{x}, v, \boldsymbol{n})$, where $\boldsymbol{n}$ is the unit vector of the photon momentum. Including collisions, Liouville's equation (4.17) becomes Boltzmann's Equation [47]

$$p^\mu (\partial_\mu f)_{|p^\mu} - \Gamma^i_{\mu\nu} p^\mu p^\nu \frac{\partial f}{\partial p^i} = C[f], \tag{4.25}$$

where $C[f]$ contains collision terms. We will not calculate the collision term in this work, but state the result as derived in [18] at the end of this section. The unperturbed distribution $\bar{f}$ is by definition thermal with Temperature $\bar{T} = \bar{T}(\tau) = \bar{T}_0 a^{-1}$:

$$\bar{f}(v) = \left[\exp\left(-\frac{v}{\bar{T}_0} \right) - 1 \right]^{-1}. \tag{4.26}$$

One then defines the temperature perturbation by

$$f(\tau, \boldsymbol{x}, v, \boldsymbol{n}) = \bar{f}\left(\frac{v}{1+\Delta} \right), \tag{4.27}$$

where the term in brackets *is the argument* of $\bar{f}$, and

$$\Delta(\tau, \boldsymbol{x}, \boldsymbol{n}) \equiv \frac{\Delta T}{\bar{T}}, \tag{4.28}$$

is the relative temperature anisotropy. Plugging this into (4.26) one indeed sees that $\bar{T}_0 \to \bar{T}_0(1+\Delta)$ making the definition plausible. Taylor expanding (4.27)

$$f(\tau, \boldsymbol{x}, v, \boldsymbol{n}) \approx \bar{f}(v) - v\Delta \frac{\mathrm{d}\bar{f}}{\mathrm{d}v}, \tag{4.29}$$

one sees that

$$F(\tau, \boldsymbol{x}, v, \boldsymbol{n}) = -v \frac{\mathrm{d}\bar{f}}{\mathrm{d}v} \Delta(\tau, \boldsymbol{x}, \boldsymbol{n}), \tag{4.30}$$

connecting F with Δ. In order to obtain an equation for the temperature perturbation Δ, one uses [18] Boltzmann's equation (4.25) with the perturbed Christoffel symbols and replaces F by Δ by means of relation (4.30). The intermediate result is [18]:

$$\partial_\tau \Delta + n^i \partial_i \Delta = -n^i A_{,i} - n^i n^j \left(B_{i,j} + \dot{H}_{ij} \right) + \tilde{C}[f], \tag{4.31}$$

where $\tilde{C}[f] \equiv -C[f]/(v\bar{f}')$. The next step consists in an expansion of

$$\Delta(\tau, \boldsymbol{x}, \boldsymbol{n}) = \sum_{l=0}^{\infty} \alpha_{i_1, \ldots i_l}(\tau, \boldsymbol{x}) n^{i_1} \ldots n^{i_l}, \tag{4.32}$$

where $\alpha_{i_1,\ldots i_l}(\tau, \boldsymbol{x})$ are symmetric traceless tensor fields. It turns out that tensor components beyond the 2-tensor are negligible [18]. Furthermore, scalar field quintessence will not source tensor or vector perturbations and hence, we will only treat the scalar temperature anisotropy in the following. Keeping only the scalar and using the decomposition of Chapter (3), one simply has

$$\Delta(\tau, \boldsymbol{x}, \boldsymbol{n}) = \Delta^{(S)}(\tau) Q(\boldsymbol{x}). \tag{4.33}$$

Inserting this in Equation (4.31) yields

$$\partial_\tau \Delta^{(S)} + ik\mu\Delta^{(S)} = -ik\mu A + \mu^2 k\sigma - \frac{1}{3}\dot{H}_T - \dot{H}_L + \tilde{C}[f], \tag{4.34}$$

where μ is the direction cosine defined via $n^j Q_{,j} = ik\mu Q$ and $\sigma = k^{-1}\dot{H}_T - B$. In flat space, where $Q = \exp(i\boldsymbol{k}\boldsymbol{x})$, μ given by $\mu = k^{-1}\boldsymbol{k}\cdot\boldsymbol{n}$. Unfortunately, the above Equation (4.34) is not gauge invariant. However with

$$\mathcal{M} \equiv \Delta^{(S)} + H_L + \frac{1}{3}H_T + i\mu\sigma, \tag{4.35}$$

Equation (4.34) becomes

$$\partial_\tau \mathcal{M} + ik\mu\mathcal{M} = ik\mu(\Phi - \Psi) + \tilde{C}[f]. \tag{4.36}$$

One can show [18] that $\mathcal{M} = \Delta^{(S)}$ up to a gauge dependent monopole and dipole contribution and indeed $\mathcal{M}$ is gauge invariant [48]. It is this quantity $\mathcal{M}$ that plays the central role in the calculation of the CMB anisotropy spectrum. Let us stop for a moment to recapitulate the steps: from the Boltzmann Equation and the distribution $f(\tau, \boldsymbol{x}, v, \boldsymbol{n}) = \bar{f}(v) + F(\tau, \boldsymbol{x}, v, \boldsymbol{n})$ one moves to $\Delta(\tau, \boldsymbol{x}, \boldsymbol{n})$, decomposes this into scalar, vector etc. and singles out the equation for $\Delta^{(S)}(\tau)$ for one Fourier mode $\boldsymbol{k}$. It turns out that this equation depends on $\boldsymbol{k}$ and $\boldsymbol{n}$ only through $\boldsymbol{k}\cdot\boldsymbol{n}$ and that by moving from $\Delta^{(S)}$ to $\mathcal{M}$, the Equation (4.34) becomes gauge invariant.

One can now make contact to the fluid description of Section (3.2) by means of

$$T^{\mu\nu} = \int p^\mu p^\nu f(p, x) p^2 \frac{\mathrm{d}p}{p^0} \mathrm{d}\Omega_p. \tag{4.37}$$

Comparison with the fluid perturbations, yields [18]

$$D_g^\gamma = \frac{1}{\pi}\int \mathcal{M}\mathrm{d}\Omega \tag{4.38}$$

$$V_\gamma = \frac{3i}{4\pi}\int \mu\mathcal{M}\mathrm{d}\Omega \tag{4.39}$$

$$\Pi_\gamma = -\frac{3}{\pi}\int \frac{1}{2}\left(3\mu^2 - 1\right)\mathcal{M}\mathrm{d}\Omega. \tag{4.40}$$

The appearance of Legendre polynomials in the integrals of (4.38 -4.40) suggests, that an expansion of $\mathcal{M}$ in terms of spherical harmonics is helpful. Following [49,18], we use

$$\mathcal{M} = \sum_l M_{l\ 0} G_l^0 \tag{4.41}$$

with

$$ {}_sG_l^m(\boldsymbol{n}) = (-i)^l \sqrt{\frac{4\pi}{2l+1}}\, {}_sY_l^m, \tag{4.42} $$

where ${}_sY_l^m$ are spin weighted harmonics [50,51]. The use of spin-weighted harmonics is of advantage, because the *polarization* turns out to be a spin-2 quantity which is best quoted in terms of the variables E and B. For scalars B vanishes, and E is related to the Stokes parameter Q via [52,53,18]

$$ \frac{1}{4}Q = \sum_l E_l\, {}_2G_l^0(\boldsymbol{n}). \tag{4.43} $$

With the multipole decomposition of $\mathcal{M}$, we can rewrite Equations (4.38-4.40) as

$$ D_g^\gamma = 4\mathcal{M}_0 \tag{4.44} $$

$$ V_\gamma = \mathcal{M}_1 \tag{4.45} $$

$$ \Pi_\gamma = \frac{12}{5}\mathcal{M}_2 \tag{4.46} $$

Including polarization and the collision terms due to Thomson scattering [49,18], one finally arrives at

$$ \dot{\mathcal{M}} + i\mu k\mathcal{M} + \dot{\kappa}\mathcal{M} = i\mu k(\Phi - \Psi) + \dot{\kappa}\left(\frac{1}{4}D_g^\gamma - i\mu V_b - \frac{1}{2}(3\mu^2 - 1)\mathcal{C}\right), \tag{4.47} $$

where $\dot{\kappa} \equiv a\, n_e \sigma_T$ is the differential optical depth with n_e the number density of free electrons and σ_T the Thomson scattering cross section. The quantity $\mathcal{C}$ in the above, is given by $\mathcal{C} \equiv (M_2 - \sqrt{6}E_2)/10$. In principle, one could now insert the multipole decomposition of $\mathcal{M}$ and E in Equation (4.47) (and a corresponding equation for E), get an hierarchy of equations for each multipole l and from this infer the coefficients C_l of the temperature anisotropy correlation. However, for C_l up to $l \approx 1500$, this translates into more than 3000 coupled differential equations. Luckily, the *line of sight* strategy to solve Equation (4.47) has been developed [16]. It only needs a few ($l \lessapprox 8$) M_l's and is hence much faster. As we still need the multipole hierarchy (even though to much smaller extent), we note that this hierarchy for $\mathcal{M}$ is given by [52]

$$ \dot{\mathcal{M}}_0 = -\frac{k}{3}V_\gamma \tag{4.48} $$

$$ \dot{\mathcal{M}}_1 = \dot{\kappa}(V_b - V_\gamma) + k(\Psi - \Phi) + k\left(\mathcal{M}_0 - \frac{2}{5}\mathcal{M}_2\right) \tag{4.49} $$

$$ \dot{\mathcal{M}}_2 = -\dot{\kappa}\,(\mathcal{M}_2 - \mathcal{C}) + k\left(\frac{2}{3}V_\gamma - \frac{3}{7}\mathcal{M}_3\right) \tag{4.50} $$

$$ \dot{\mathcal{M}}_l = -\dot{\kappa}\,\mathcal{M}_l + k\left(\frac{l}{2l-1}\mathcal{M}_{l-1} - \frac{l+1}{2l+3}\mathcal{M}_{l+1}\right) \quad ; l > 2, \tag{4.51} $$

whereas the one for E is [52]

$$\dot{E}_2 = -\frac{k\sqrt{5}}{7}E_3 - \dot{\kappa}\left(E_2 + \sqrt{6}\,\mathcal{C}\right) \tag{4.52}$$

$$\dot{E}_l = k\left(\frac{{}_2\kappa_l}{2l-1}E_{l-1} - \frac{{}_2\kappa_{l+1}}{2l+3}E_{l+1}\right) - \dot{\kappa}\,E_l \quad ; l > 2. \tag{4.53}$$

Here, $\mathcal{C} = (M_2 - \sqrt{6}E_2)/10$ as above and ${}_2\kappa_l = \sqrt{l^2-4}$ are combinatorial factors [52] that should not be confused with the differential optical depth $\dot{\kappa}$.

Massless neutrinos

Massless neutrinos follow the same multipole hierarchy as $\mathcal{M}$, however without polarization and Thomson scattering. Hence, the perturbed neutrino distribution is

$$\dot{\mathcal{N}}_0 = -\frac{k}{3}V_\nu \tag{4.54}$$

$$\dot{\mathcal{N}}_1 = k(\Psi - \Phi) + k\left(\mathcal{N}_0 - \frac{2}{5}\mathcal{N}_2\right) \tag{4.55}$$

$$\dot{\mathcal{N}}_l = k\left(\frac{l}{2l-1}\mathcal{N}_{l-1} - \frac{l+1}{2l+3}\mathcal{N}_{l+1}\right) \quad ; l > 1, \tag{4.56}$$

where $V_\nu = \mathcal{N}_1$. In contrast to photons, there is no tight coupling to baryons. Thus, moments beyond the dipole may built up from the beginning. However, as $\dot{\mathcal{N}}_l \propto k\mathcal{N}_{l-1}$ for $l > 1$, it follows that $\mathcal{N}_l \propto (k\tau)^{(l-1)}\mathcal{N}_1$ at early times. As $k\tau \ll 1$ for super-horizon modes, higher order moments of $\mathcal{N}$ are suppressed.[6]

4.5 The Line of Sight Strategy

Inspecting (4.47), one notices that the LHS can be written as

$$e^{-i\mu k\tau}e^{-\kappa(\tau)}\dot{L}, \tag{4.57}$$

where

$$L \equiv e^{i\mu k\tau}e^{\kappa(\tau)}\mathcal{M}. \tag{4.58}$$

Hence, (4.47) translates into

$$\dot{L} = e^{i\mu k\tau}e^{\kappa(\tau)}\left[i\mu k(\Phi - \Psi) + \dot{\kappa}\left(\frac{1}{4}D_g^\gamma - i\mu V_b - \frac{1}{2}(3\mu^2 - 1)C\right)\right], \tag{4.59}$$

[6] This is a bit of a circular reasoning. *If* each moment $\mathcal{N}_{l+1}$ is small compared to $\mathcal{N}_{l-1}$, *then* $\dot{\mathcal{N}}_l \propto k\mathcal{N}_{l-1}$. That this leads to the suppression of higher order moments is no wonder, for we have assumed this from the start. Yet, $\mathcal{N}_2$ corresponds to Π_ν and this in turn determines $\Psi - \Phi$ from Einstein's equation. As this difference is not substantial, one concludes that N_2 (and all higher moments) are small initially.

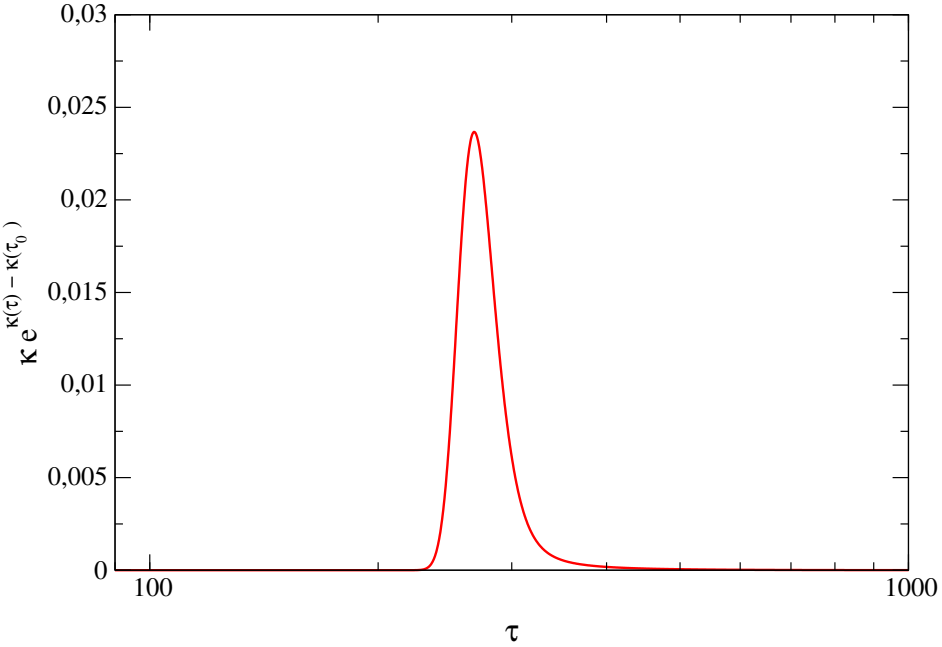

Figure 4.2: The visibility $g \equiv \dot{\kappa}\exp(\kappa(\tau) - \kappa(\tau_0))$ as a function of conformal time τ in Mpc. Its peak at about $\tau \approx 300\,\mathrm{Mpc}$ defines the epoch of last scattering.

and integrated over conformal time,

$$L(\tau_0) = \int_0^{\tau_0} \mathrm{d}\tau e^{i\mu k\tau} e^{\kappa(\tau)} \left[i\mu k(\Phi - \Psi) + \dot{\kappa}\left(\frac{1}{4}D_g^\gamma - i\mu V_b - \frac{1}{2}(3\mu^2 - 1)C\right)\right]. \tag{4.60}$$

According to Equation (4.58), the photon perturbation today is given by $M(\mu, \tau_0) = e^{-i\mu k\tau_0} e^{-\kappa(\tau_0)} L(\tau_0)$, so

$$M(\mu, \tau_0) = \int_0^{\tau_0} \mathrm{d}\tau\, e^{i\mu k(\tau - \tau_0)} e^{\kappa(\tau) - \kappa(\tau_0)} \times \left[i\mu k(\Phi - \Psi) + \dot{\kappa}\left(\frac{1}{4}D_g^\gamma - i\mu V_b - \frac{1}{2}(3\mu^2 - 1)C\right)\right]. \tag{4.61}$$

The product $g \equiv \dot{\kappa}\exp(\kappa(\tau) - \kappa(\tau_0))$ plays an important role[7] and is called the visibility function. Its peak defines the epoch of recombination (see also Figure 4.5). Each term in the above Equation (4.61) containing factors of μ, can be

[7] Please note that in [16], $\kappa(\tau) = \int_\tau^{\tau_0} \dot{\kappa}(\tau')\mathrm{d}\tau'$ and hence $\kappa(\tau_0) = 2\kappa(\tau)$. Therefore the factor $\exp(\kappa(\tau) - \kappa(\tau_0))$ equals $\exp(-\kappa(\tau))$. However, this obscures the derivation a bit and we therefore choose to display $\kappa(\tau_0)$.

integrated by parts, in order to get rid of μ. For instance

$$\int_0^{\tau_0} \left[e^{i\mu k(\tau-\tau_0)} i\mu k\right] g V_b \mathrm{d}\tau = \left[\,\right] - \int_0^{\tau_0} e^{i\mu k(\tau-\tau_0)} k^{-1} \left(g\dot{V}_b + V_b\,\dot{g}\right) \mathrm{d}\tau, \qquad (4.62)$$

where $[\,]$ stands for the boundary term that here and for all of the terms above can be dropped, as it vanishes for $\tau \to 0$ and only contributes to C_0 for $\tau = \tau_0$. Applying this procedure to all terms involving μ yields

$$\mathcal{M}(\mu, \tau_0) = \int_0^{\tau_0} e^{i\mu k(\tau-\tau_0)} S(k,\tau)\mathrm{d}\tau, \qquad (4.63)$$

where the *source* is

$$S = -e^{\kappa(\tau)-\kappa(\tau_0)} \left[\dot{\Phi} - \dot{\Psi}\right] + g\left[\frac{1}{4}D_g^\gamma + \frac{\dot{V}_b}{k} - (\Phi - \Psi) + \frac{\mathcal{C}}{2} + \frac{3}{2k^2}\ddot{\mathcal{C}}\right] + \dot{g}\left[\frac{V_b}{k} + \frac{3}{k^2}\dot{\mathcal{C}}\right] + \ddot{g}\frac{3}{2k^2}\mathcal{C}. \qquad (4.64)$$

Let us pause to discuss this result (4.63, 4.64) in detail. First, we note that the visibility function g is sharply peaked at the epoch of decoupling (see Figure 4.5). Hence, $\mathcal{M}(\tau_0)$ gets contributions from D_g^γ and V_b^γ at about this epoch: whatever the density contrast of the photon fluid and the baryon fluid velocity has been at decoupling, will be imprinted in the temperature anisotropy today. The term from the density contrast D_g^γ is the most important one on scales smaller than the sound horizon. It is the main contributor towards the oscillatory behaviour of the C_l spectrum. Its appearance is plausible, because for a photon gas, $\rho \propto T^4$ and therefore $\delta T/T \propto \frac{1}{4}\delta\rho/\rho$. The V_b^γ-term appears, because a baryon moving in the direction towards the observer will cause a Doppler shift of the emitted photon. For adiabatic initial conditions, this Doppler shift fills the region before the first peak (at $l \approx 220$), which is mainly due to D_g^γ [44]. The first term in the source (involving $\dot{\Phi} - \dot{\Psi}$) accounts for the integrated Sachs-Wolfe (ISW) effect [54]: if the gravitational potential decays, the photons have to climb out of a more shallow potential than they have been in before. Quintessence, for instance can lead to a more pronounced ISW than standard CDM models. The terms involving $\mathcal{C}$ and its derivatives describe polarization effects and are far less important than the D_g^γ term. Finally, the $(\Phi - \Psi)$ term is the (ordinary) Sachs-Wolfe effect. On scales that at decoupling were well outside the horizon, this gives the main contribution.

4.5.1 The Multipole Power Spectrum from the Line of Sight

In order to find the multipole power spectrum, one expands[8] the plane wave $\exp(ik\mu[\tau - \tau_0])$ in Equation (4.63) in terms of Legendre polynomials

$$\begin{aligned} e^{ik\mu[\tau-\tau_0]} &= e^{-ik\mu[\tau_0-\tau]} = \left[e^{ik\mu[\tau_0-\tau]}\right]^* && (4.65)\\ &= \left[\sum_l (i)^l (2l+1) j_l\left(k[\tau_0-\tau]\right) P_l(\mu)\right]^* && (4.66)\\ &= \sum_l (-i)^l (2l+1) j_l\left(k[\tau_0-\tau]\right) P_l(\mu). && (4.67) \end{aligned}$$

Comparing with (4.16) one finds [16]

$$\mathcal{M}_l(k,\tau_0) = \int_0^{\tau_0} \mathrm{d}\tau S(k,\tau)\, j_l\left(k[\tau_0-\tau]\right). \tag{4.68}$$

Inserting this in Equation (4.15), the C_l spectrum follows.

4.5.2 Putting it all together

As far as the CMB is concerned what one really wants is the temperature[9] anisotropy correlation functions, commonly quoted using the coefficients C_l. The slow way would be to get the C_l's directly from the (vast) multipole hierarchy of the photon distribution via Equation (4.15). In contrast, the line of sight integration gets the Δ_l's (in our case the gauge-invariant $\mathcal{M}_l$'s) by folding the source term S with the spherical Bessel functions j_l. While the Bessel functions oscillate rapidly in this convolution, the source term is most of the time rather slowly changing. It thus suffices to calculate the sources at few (cleverly chosen) points and interpolate between. In order to determine the sources, one needs to know (among other things) D_g^γ and $\mathcal{C}$. Therefore, one still needs to solve a multipole hierarchy for $\mathcal{M}$ and E. However, for sufficient precision, only a few multipoles are needed: they built up rather slowly starting from initially shear-free conditions ($M_l = 0,\ l > 1$) due to the tight coupling to baryons. In order to suppress truncation effects, the multipole beyond the highest one in the hierarchy is approximated by the recursion relation of Bessel functions (see Appendix C).

[8] See Abramowitz, M. and Stegun, I. A. (Eds.)., Chapter on Bessel functions of fractional order, addition theorems.

[9] And some more, like polarization etc.

5

Initial Conditions

In order to classify initial conditions the introduction of

$$S_{a:b} \equiv \frac{\delta_a}{1+w_a} - \frac{\delta_b}{1+w_b} \tag{5.1}$$

$$= \frac{D_g^a}{1+w_a} - \frac{D_g^b}{1+w_b} \tag{5.2}$$

is useful. It is gauge invariant and characterizes the entropy exchange between two components 'a' and 'b'. As an illustration, suppose the two components were cold dark matter and radiation and $S_{cdm:r}$ would vanish. Then the perturbation in the number density of cdm particles n would be

$$\frac{\Delta n}{n} = \delta_{\rm cdm} = \frac{3}{4}\frac{\Delta\rho_r}{\rho_r} = \frac{\Delta s_r}{s_r}, \tag{5.3}$$

since the entropy of radiation $s_r \propto T^3$ and $\rho_r \propto T^4$. Hence, the radiation entropy per cdm particle would vanish:

$$\Delta\left(\frac{s_r}{n}\right) = \frac{n\,\Delta s_r - s_r \Delta n}{n^2} = 0. \tag{5.4}$$

If

$$S_{a:b} = 0, \tag{5.5}$$

for all pairs of components in the early universe, one speaks of *isentropic* or *adiabatic* initial conditions.

5.1 Initial Conditions without Quintessence

The initial conditions are most easily derived without quintessence first. Later in this chapter, we will add quintessence to the picture. With *initial conditions*, we mean the value of all perturbation variables at early time (i.e. radiation domination) for modes that are well outside the horizon. Therefore $x \equiv k\tau$ is a small number.

The multipole hierarchy of photons (4.48-4.53) and neutrinos (4.54-4.56) shows that each higher order moment is suppressed by a power of x with respect to the one below (see also Section 4.4). As $x \ll 1$, it suffices to truncate the expansion beyond the quadrupole, i.e. we have $N_3 = \mathcal{M}_3 = 0$. For photons, the tight coupling to baryons suppresses even the quadrupole and together they behave like one single fluid. From the equations governing the time evolution of the photon and baryon velocities one can derive a single equation for the baryon-photon fluid velocity. One starts from the equations for the separate fluids (neglecting baryon sound speed and photon dipole here),

$$\begin{aligned} \dot{V}_\mathrm{b} &= -\frac{\dot{a}}{a}V_\mathrm{b} + k\Psi + \dot{\kappa}\, R(V_\gamma - V_\mathrm{b}) \\ \dot{V}_\gamma &= \frac{k}{4}D_{g,\gamma} + k(\Psi - \Phi) + \dot{\kappa}(V_\mathrm{b} - V_\gamma), \end{aligned} \tag{5.6}$$

where $R \equiv 4\rho_\gamma/(3\rho_b)$. In the above, the Thomson drag term [18] has been added to the Equation for the Baryon velocity. As $\dot{\kappa}$ is overwhelmingly large in the early universe, both velocities are forced to coincide. This is the so called tight coupling limit. Adding the two Equations (5.6) , one gets

$$R\dot{V}_\gamma + \dot{V}_\mathrm{b} = k\left(R(\Psi - \Phi) + \Psi + R\frac{1}{4}D_{g,\gamma}\right) - \frac{\dot{a}}{a}V_\mathrm{b}, \tag{5.7}$$

and finally using $R\dot{V}_\gamma + \dot{V}_\mathrm{b} = (R+1)\dot{V}_\mathrm{b} - R\dot{V}_\mathrm{b} + R\dot{V}_\gamma$,

$$(R+1)\dot{V}_\mathrm{b} = k\left((R+1)\Psi - R\Phi + R(\dot{V}_\mathrm{b} - \dot{V}_\gamma) + \frac{1}{4}RD_{g,\gamma}\right) - \frac{\dot{a}}{a}V_\mathrm{b}. \tag{5.8}$$

It is this equation that in the tight coupling limit replaces the two equations (5.6). To proceed further we note that in the early universe, $R \gg 1$ and hence $R+1 \approx R$. In addition, $\dot{V}_\mathrm{b} - \dot{V}_\gamma = 0$ due to the tight coupling. Therefore Equation (5.8) simplifies to

$$\dot{V}_\mathrm{b} = k\left(\Psi - \Phi + \frac{1}{4}D_{g,\gamma}\right) - R^{-1}\frac{\dot{a}}{a}V_\mathrm{b}. \tag{5.9}$$

Now,

$$R^{-1} = \frac{3\rho_b}{4\rho_\gamma} = \frac{3\,\Omega_0^\mathrm{b}\,h^2}{4\,\Omega_0^\gamma\,h^2}\,a \approx 500\,a. \tag{5.10}$$

At the early times we are interested in, a is small and we can also drop the term proportional to V_b.[1]

The perturbed Einstein equations (3.53 - 3.55) simplify in the deep radiation dominated era, because then $a \propto \tau$, $\dot{a}/a = \tau^{-1}$ and the Friedmann equation (2.7) yields

$$3\mathrm{M}_\mathrm{P}^2 a^{-2}\left(\frac{\dot{a}}{a}\right)^2 = 3\mathrm{M}_\mathrm{P}^2 a^{-2}\tau^{-2} = \bar{\rho}, \tag{5.11}$$

[1] After these simplifications, the evolution equation for the common baryon-photon velocity V_b has become the one for a single photon fluid (see Equation (5.16) below).

hence

$$\mathrm{M_P^{-2}}\, a^2\, \bar{\rho} = 3\tau^{-2}. \tag{5.12}$$

Using this and (5.8), the set of equations determining the perturbation evolution is therefore

$$\begin{aligned}
0 &= \dot{D}_c + kV_\mathrm{c} && (5.13)\\
0 &= \dot{V}_\mathrm{c} + \frac{\dot{a}}{a}V_\mathrm{c} - k\Psi && (5.14)\\
0 &= \dot{D}_{g,\gamma} + \frac{4}{3}kV_\gamma && (5.15)\\
0 &= \dot{V}_\gamma - k\left(\Psi - \Phi + \frac{1}{4}D_{g,\gamma}\right) && (5.16)\\
0 &= \dot{D}_{g,\nu} + \frac{4}{3}kV_\nu && (5.17)\\
0 &= \dot{V}_\nu - k\left(\Psi - \Phi + \frac{1}{4}D_{g,\gamma} - \frac{1}{6}\Pi_\nu\right) && (5.18)\\
0 &= \dot{\Pi}_\nu - \frac{8}{5}kV_\nu && (5.19)\\
0 &= \Phi + \Psi + \Omega_\star^\nu \Pi_\nu x^{-2} && (5.20)\\
0 &= -\Phi(12[\Omega_\star^\nu + \Omega_\star^\gamma] + 9\Omega_\star^\mathrm{c} + x^2) + 3\Omega_\star^\gamma\left[D_{g,\gamma} + 4V_\gamma x^{-1}\right]\\
&\quad +3\Omega_\star^\nu\left[D_{g,\nu} + 4V_\nu x^{-1}\right] + 3\Omega_\star^\mathrm{c}\left[D_c + 3V_\mathrm{c} x^{-1}\right]. && (5.21)
\end{aligned}$$

Here, Equation (5.20) corresponds to (3.54) and the last Equation is just Poisson's equation (3.53). The $\Omega_\star$'s denote quantities at initial time. We keep the minute cold dark matter contribution in (5.21), until we have shown that V_γ vanishes to lowest order in x. Thereafter, we drop cold dark matter from Poisson's equation. Please note that we do not need to consider baryons separately, as their velocity coincides with the one for photons and $D_{g,b}$ will be determined from the type of initial conditions later. In addition, adding baryons to Poisson's equation wouldn't change the reasoning with respect to V_γ, which is why we omit it from (5.21). The easily obtained solutions for a single photon fluid, (3.86) suggest that a power-law ansatz of the form

$$Y(x) = Y^0 + Y^1 x^2 + Y^2 x^2, \tag{5.22}$$

with coefficients Y^i is sensible. As Φ and Ψ are related to Π_ν via Equation (5.19), consistency requires that we keep only the constant[2] term for Φ and Ψ [56]. All other perturbation variables are expanded up to x^2. In a first step, Equation (5.20) requires

$$\Pi_\nu^0 = \Pi_\nu^1 = 0, \tag{5.23}$$

[2] In principle, we can add the terms up to x^2, a detailed calculation shows however, that $\Phi^1 = \Psi^1 = 0$ and the second order terms don't influence other quantities.

and hence using Equation (5.19), we find

$$V_\nu^0 = 0. \tag{5.24}$$

Similarly, Equation (5.14) gives

$$V_\mathrm{c}^0 = 0, \tag{5.25}$$

and combining the two, Poisson's equation (5.21) forces

$$V_\gamma^0 = 0. \tag{5.26}$$

Hence, all zero order velocities vanish. Comparing terms proportional to τ in our equation system, we get

$$\begin{aligned}
D_{g,\gamma}^2 &= -2/3 V_\gamma^1 && (5.27)\\
D_{g,\nu}^2 &= -2/3 V_\nu^1 && (5.28)\\
D_c^2 &= -1/2 V_\mathrm{c}^1 && (5.29)\\
V_\gamma^2 &= 1/8 D_{g,\gamma}^1 && (5.30)\\
V_\nu^2 &= 1/8 D_{g,\nu}^1 && (5.31)\\
V_\mathrm{c}^2 &= 0 && (5.32)
\end{aligned}$$

Turning subsequently to the constant terms in the equation system, one gets

$$\begin{aligned}
D_c^1 &= 0 && (5.33)\\
V_\mathrm{c}^1 &= \Psi^0/2 && (5.34)\\
D_{g,\gamma}^1 &= 0 \quad \rightarrow V_\gamma^2 = 0 && (5.35)\\
D_{g,\nu}^1 &= 0 \quad \rightarrow V_\nu^2 = 0 && (5.36)\\
\Pi_\nu^2 &= -\left(\Omega_\star^\nu\right)^{-1}\left(\Psi^0 + \Phi^0\right) && (5.37)
\end{aligned}$$

In addition, Equation (5.16) relates

$$\Psi^0 = \Phi^0 + V_\gamma^1 - \frac{1}{4} D_{g,\gamma}^0, \tag{5.38}$$

and

$$\Phi^0 = \frac{1}{8} D_{g,\gamma}^0 - \frac{2}{5}\Omega_\star^\nu V_\nu^1 - \frac{1}{2} V_\gamma^1. \tag{5.39}$$

After all these considerations, we are left with

$$\begin{aligned}
V_\gamma^1 - V_\nu^1 &= \frac{1}{4}\left(D_{g,\gamma}^0 - D_{g,\nu}^0\right) && (5.40)\\
\Omega_\star^\gamma\left[6V_\gamma^1 + \frac{1}{2} D_{g,\gamma}^0\right] &= -\Omega_\star^\nu\Bigg[V_\nu^1\left\{\frac{6}{5}(\Omega_\star^\nu + \Omega_\star^\gamma) + 4\right\} && (5.41)\\
&\qquad + D_{g,\nu}^0 - \frac{1}{2} D_{g,\gamma}^0 + 2V_\gamma^1\Bigg] && (5.42)\\
& && (5.43)
\end{aligned}$$

The relation between $D_{g,\gamma}$ and $D_{g,\nu}$ imposed by the type of initial conditions, determines then all variables in terms of an overall constant. Let us look closer at adiabatic conditions.

5.1.1 Adiabatic Initial Conditions

According to Equation (5.5), adiabaticity forces $D_{g,\gamma} = D_{g,\nu}$. In this case, Equation (5.40) yields $V_\gamma^1 = V_\nu^1$. Also, $D_c = 3/4 D_{g,\gamma}$ is implied by adiabatic conditions. Solving Equation (5.42) for V_γ^1 then completely determines all perturbations,

$$D_{g,\nu} = D_{g,\gamma} = 1 + \frac{5}{6} Q x^2 \tag{5.44}$$

$$D_c = D_\mathrm{b} = \frac{3}{4} + \frac{15}{24} Q x^2 \tag{5.45}$$

$$V_\nu = V_\mathrm{c} = V_\mathrm{b} = V_\gamma = -\frac{5}{4} \mathcal{Q}\, x \tag{5.46}$$

$$\Pi_\nu = -\mathcal{Q}\, x^2 \tag{5.47}$$

$$\Phi = \frac{1}{2}[2\Omega_\star^\nu + 5]\,\mathcal{Q} \tag{5.48}$$

$$\Psi = -\frac{5}{2}\mathcal{Q}, \tag{5.49}$$

where $\mathcal{Q} = [4\Omega_\star^\nu + 15]^{-1}$. Having found the early time behaviour of the perturbations, we are now going to turn to the quintessence field.

5.2 Early Time Quintessence Perturbations

As such, there is no 'canonical' quintessence. To our knowledge, however, the early time behaviour of the field perturbation has been studied either for pure exponentials [28] or for negligible quintessence content in the early universe [55].[3] The reason for these assumptions is simply the fact that a closed solution for *all* types of quintessence is impossible to find.

However, for tracker solutions, this is possible. We owe this to the fact that in these cases, V', $\dot{\bar{\varphi}}$ etc., occurring in the equation of motion for the perturbation (3.73) have a well defined scaling with τ (see Section 2.3.1). The equation of motion (3.73) contains a term $\dot{\bar{\varphi}}\left(\dot{\Psi} - 3\dot{\Phi}\right)$. We will in the following assume that quintessence doesn't change the almost constant behaviour of the gravitational potentials and hence drop this term.[4] In addition, for super-horizon modes, $a^2 V'' \gg k^2$, and hence the equation of motion reduces to

$$\ddot{X} = -2a^2 V' \Psi - a^2 V'' X - 2\frac{\dot{a}}{a}\dot{X}. \tag{5.50}$$

We will solve this equation using the power law solutions for the derivatives of V obtained in Section 2.3.1. Our assumptions are hence that

(i) The energy density of the universe scales as a^{-4} at the time of interest, implying

[3] Unfortunately, the solution given in [55] seems incorrect, though the scaling with τ is correct.

[4] This is very well justified in practice.

$\dot{a}/a = \tau^{-1}$.

(*ii*) The equation of state w^φ is (nearly) constant.

In order to manifestly display the power laws, we write

$$\begin{aligned} V' &= \hat{V}^{(1)} \tau^{-(7+3w^\varphi)/2} && (5.51)\\ V'' &= \hat{V}^{(2)} \tau^{-4} && (5.52)\\ a &= \hat{a}\tau && (5.53)\\ X &= \hat{X}\tau^q, && (5.54) \end{aligned}$$

where $\hat{a}$ etc. are proportionality constants and we seek a power-law solution for $X(\tau)$. Inserting these relations in (5.50), one gets

$$q(q+1) = -\hat{a}^2 \left[2\Psi \hat{V}^{(1)} \hat{X}^{-1} \tau^{\left(\frac{1}{2} - \frac{3}{2}w^\varphi - q\right)} + \hat{V}^{(2)} \right]. \tag{5.55}$$

Except for the factor $\tau^{(1-3w^\varphi)/2-q}$, all quantities are constant in this equation.[5] Hence, the solution is given by $q = (1-3w^\varphi)/2$ and therefore

$$X(\tau) = \hat{X}\, \tau^{\frac{1}{2}(1-3w^\varphi)}, \tag{5.56}$$

with $\hat{X}$ given by

$$\hat{X} = -\frac{8\hat{a}^2 \hat{V}^{(1)} \Psi}{3(1-w^\varphi)(1-3w^\varphi) + 4\hat{a}^2 \hat{V}^{(2)}}, \tag{5.57}$$

and upon re-substituting $\hat{a} \to a(\tau)\tau^{-1}$ etc,

$$X(\tau) = -\frac{8a^2\tau^2 V' \Psi}{3(1-w^\varphi)(1-3w^\varphi) + 4a^2\tau^2 V''}. \tag{5.58}$$

Let us briefly denote this particular solution by $\tilde{X}$. Adding another power-law to this, i.e. making the ansatz $X(\tau) = \tilde{X}(\tau) + c\tau^p$, one observes that this also solves the equation of motion, if $p = \frac{1}{2}\left[-1 + \sqrt{1 - 4\hat{a}^2\hat{V}^{(2)}}\right]$. In fact, the *general* solution is obtained by adding the particular solution and two complementary solutions:

$$X(\tau) = \tilde{X}(\tau) + c\,\tau^{-\frac{1}{2}\left(1-\sqrt{1-4\hat{a}^2\hat{V}^{(2)}}\right)} + c_2\,\tau^{-\frac{1}{2}\left(1+\sqrt{1-4\hat{a}^2\hat{V}^{(2)}}\right)}, \tag{5.59}$$

where the mode proportional to c_2 is at least as rapidly decaying as the one proportional to c. From Equations (5.52) and (5.53), we know that $4\hat{a}^2\hat{V}^{(2)} = 4a^2V''\tau^2$.

[5] As already mentioned, we assume that the time behaviour of Ψ, i.e. its (near) constancy remains unaltered by quintessence. It is clear, that this is true for subdominant quintessence. As we will see, it is also true for exponential potential quintessence and its relatives like the LKT model.

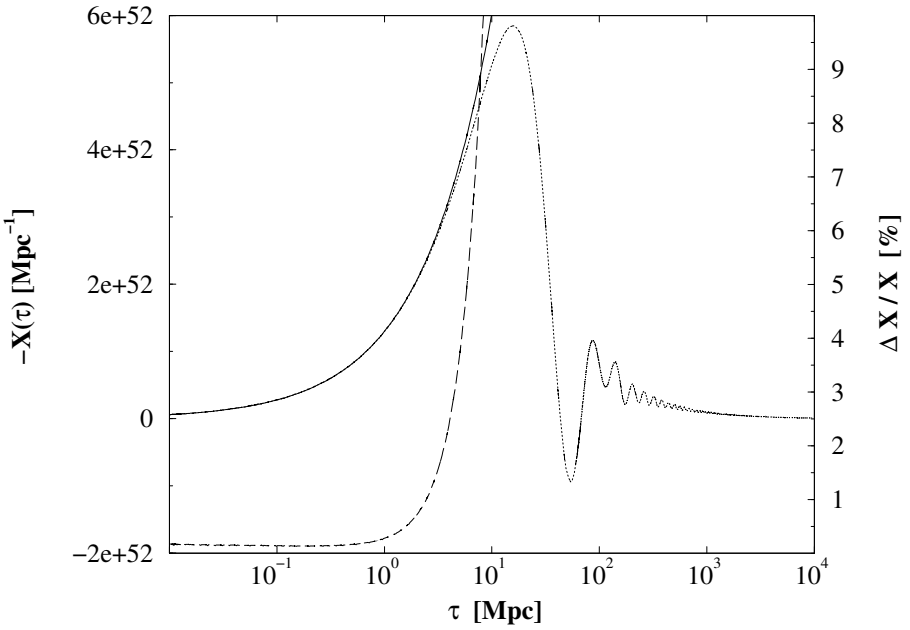

Figure 5.1: Gauge invariant quintessence field fluctuation $X(\tau)$ as simulated (dotted), compared to the analytic solution of Equation (5.58) (solid). The relative deviation is plotted as long dashed line. The quintessence model used was an IPL with $\alpha = 4$, leading to $w^{\varphi}_{\text{early}} \approx -0.111$ and hence according to (5.56), $X \propto \tau^{0.667}$. Shown is the mode for $k = 0.1\,\text{Mpc}^{-1}$ and the cosmological parameters have been $\Omega_0^{\text{b}} h^2 = 0.02$, $h = 0.65$, $\Omega_0^{\varphi} = 0.1$, $\Omega_0^{\text{c}} = 1 - \Omega_0^{\text{b}} - \Omega_0^{\varphi}$.

As V'' is the mass square of the quintessence field and as in the attractor, the only available scale is the Hubble parameter, it follows that V'' is $\mathcal{O}(H^2)$. Therefore,

$$\begin{aligned} 4a^2 V'' \tau^2 &\approx 4a^2 \left(\frac{\dot{a}}{a}\right)^2 a^{-2} \tau^2 \\ &= 4 \left(\frac{\dot{a}}{a}\right)^2 \tau^2 \\ &= 4. \end{aligned} \tag{5.60}$$

This order of magnitude result is in practice rather under estimating $4a^2 V'' \tau^2$. In most situations, the square root in p is therefore imaginary and one is left with a decaying oscillating mode. Even if $4a^2 V'' \tau^2$ *would* vanish, the mode would at most be constant. For as long as $w^{\varphi} < 1/3$, this mode will even then be subdominant. In all practical settings, it is decaying $\propto 1/\sqrt{\tau}$ in an oscillating fashion. Coming back to the dominating particular solution (5.58), Figure 5.1 shows that the accuracy of this analytic result is indeed high at early times, when compared to numerical simulations.

5.2.1 Quintessence Energy Density Perturbation

Intuitively, one expects that the energy density perturbation D_g^φ should remain constant on super-horizon scales[6]. This is true, at least for tracking solutions, because from the scaling relations of Section 2.3.1 and Equation (5.56), it follows that

$$\frac{\dot{X}}{\dot{\bar{\varphi}}} = const, \qquad\qquad X\,\frac{V'}{\rho} = const. \tag{5.61}$$

Hence, making use of $X \propto \tau^{(1-3w)/2}$ and Equations (2.29, 2.27)

$$D_g^\varphi = const \;=\; (1+w^\varphi)\left[3\Phi - \Psi \;+ \frac{1-3w^\varphi}{2}\frac{X(\tau)}{\tau\dot{\bar{\varphi}}}\right] + X(\tau)\frac{V'(\varphi)}{\bar{\rho}_\varphi} \tag{5.62}$$

$$= \;(1+w^\varphi)\left[3\Phi - \Psi \;- X(\tau)\left\{\frac{1+3w^\varphi}{\mathrm{M_P}\sqrt{3(1+w^\varphi)\Omega^\varphi}}\right\}\right] \tag{5.63}$$

with $X(\tau)$ given by Equation (5.58). For $w^\varphi = -1/3$, the X-dependent contribution cancels. However, this doesn't mean that there is no quintessence energy fluctuation, because there is still the time fluctuation Ψ present. This accounts for the apparent energy fluctuation of observers measuring the same background density, yet disagreeing about the corresponding time. For exponential potentials, it turns out that D_g^φ is particularly simple.

Early time exponential potentials

For the exponential potential the derivatives of the potential are $V' = -\lambda \mathrm{M_P}^{-1} V$ and $V'' = \lambda^2 \mathrm{M_P}^{-2} V$. Hence, Equation (5.58) simplifies to

$$X(\tau) = 2\lambda^{-1}\Psi \mathrm{M_P}. \tag{5.64}$$

Thus, the field fluctuation remains constant during the early universe on super-horizon scales for exponential potentials and their relatives (like LKT). In addition, Equation (5.62) simplifies to

$$D_g^\varphi = 4\Phi - 2\Psi, \tag{5.65}$$

where we have used $V'_{\mathrm{E}p}/\bar{\rho}_\varphi = -\lambda/(3\mathrm{M_P})$. The constant behaviour of X and D_g^φ is depicted in Figure 5.2.

5.2.2 Adiabatic Initial Conditions including Quintessence

From the definition of $S_{a:b}$ (5.1), we see that adiabaticity requires

$$D_g^\varphi = (1+w^\varphi) D_g^c. \tag{5.66}$$

[6] If not by some initial condition forced out of this solution

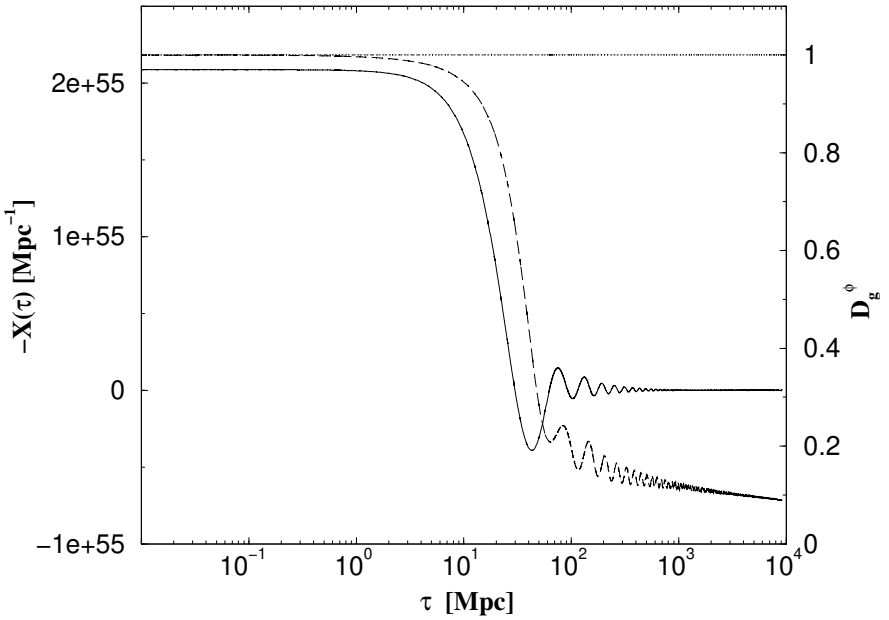

Figure 5.2: Gauge invariant quintessence field fluctuation $X(\tau)$ (solid line) and energy density perturbation D_g^φ (long dashed line) as a function of conformal time for an exponential potential. Also drawn is the line $const = 1$. According to Equation (5.65), $D_g^\varphi = 4\Phi - 2\Psi$ and for the adiabatic conditions used, $4\Phi - 2\Psi = 1$. The agreement of numerical and analytic results is very good. The mode shown has $k = 0.1\,\mathrm{Mpc}^{-1}$ and the cosmological parameters are $\Omega_0^\mathrm{b}h^2 = 0.02$, $h = 0.65$, $\Omega_0^\varphi = 0.1$, $\Omega_0^\mathrm{c} = 1 - \Omega_0^\mathrm{b} - \Omega_0^\varphi$. The horizon at equality and today are $\tau_0 \approx 9130\mathrm{Mpc}$ and $\tau_\mathrm{eq} = 40\mathrm{Mpc}$.

In addition, this shouldn't change instantly after specifying the initial condition, leading to the demand

$$\dot{D}_g^\varphi = \dot{w}^\varphi D_g^c, \tag{5.67}$$

where we assumed that D_g^c is at least nearly constant. Using the first constraint yields

$$\begin{aligned} X &= -\frac{\bar{\rho}_\varphi}{V'}(1+w^\varphi)\left[3\Phi - \Psi + D_c + \dot{X}\dot{\bar{\varphi}}^{-1}\right] \\ &= -\frac{\bar{\rho}_\varphi}{V'}(1+w^\varphi)\left[\frac{1}{2}\Psi + \frac{\dot{X}}{\dot{\bar{\varphi}}}\right], \end{aligned} \tag{5.68}$$

where

$$\frac{\frac{1}{2}\Psi\left[\dot{\bar{\varphi}}\left(\bar{\rho}_\varphi \mathcal{W}\dot{\mathcal{A}} - \dot{w}^\varphi\dot{\bar{\varphi}}V'\right) + a^2\mathcal{W}\left\{4(V')^2 - \bar{\rho}_\varphi\mathcal{W}V''\right\}\right]}{\left[\dot{w}^\varphi - \mathcal{W}\left(2\tau^{-1} + \dot{\bar{\varphi}}^{-1}\ddot{\bar{\varphi}}\right) + \dot{\bar{\varphi}}\dot{\mathcal{A}}\right]V' + \left(\dot{\bar{\varphi}}^{-1}\mathcal{W}a^2V'' - \mathcal{A}\right)\mathcal{W}\bar{\rho}_\varphi} \tag{5.69}$$

is fixed by the second requirement and the equation of motion for X (3.73) and $\mathcal{W} \equiv (1+w^\varphi)$, $\mathcal{A} \equiv V'/\bar{\rho}_\varphi$. In our numerical simulation, these rather complicated

expressions give the initial conditions for X and $\dot{X}$. In the next few lines, we will prove that for tracking quintessence, X given by the above and the tracking value (5.58) coincide.

For tracking quintessence, $\dot{w}^\varphi$ vanishes. Thus $\dot{D}_g^\varphi = 0$ from which it follows that

$$(1+w^\varphi)\frac{\dot{X}}{\dot{\bar{\varphi}}} + X\left(\frac{V'}{\bar{\rho}_\varphi}\right) = const, \tag{5.70}$$

where we have assumed that Ψ and Φ are (at least nearly) constant. As both $\dot{\bar{\varphi}}$ and $V'/\bar{\rho}_\varphi$ follow a power law in the attractor, Equation (5.70) forces X to follow a power law in τ also. If each of the two terms in Equation (5.70) is constant by itself, then the scaling relation (2.33) determines $X \propto \tau^{(1-3w^\varphi)/2}$. This is just the behaviour of X from Equation (5.56). Thus, the solution for X from the adiabaticity requirement and the 'tracking solution' for X from Equation (5.56) are proportional to each other. However, the 'adiabatic' X (5.69) has been derived using the equation of motion for X (3.73). The very same equation that is used to derive (5.56). As both solve the equation of motion and as they are proportional to each other, we are lead to conclude that they coincide.[7] To complete the proof, we have to show that each of the two terms in Equation (5.70) is conserved separately. Suppose that this wouldn't be the case, but still, the sum (5.70) is conserved. Then, the power-law of X differs from $X \propto \tau^{(1-3w^\varphi)/2}$ and the only possibility left for (5.70) to hold is a cancellation of the two terms. Using the relations (2.29) and (2.27), Equation (5.70) then becomes

$$\tau\dot{X} + \frac{3}{2}(1+w^\varphi)\sigma X = 0, \tag{5.71}$$

where $\sigma = \mathrm{sign}(V')$ and $\sigma = -1$ in the case we are interested in. The solution to Equation (5.71) is $X = \hat{X}\tau^{3(1+w^\varphi)/2}$. However, for $w^\varphi \neq -1/3$, this solution is not the one of (5.56), (5.59). As this is the only solution to the equation of motion in the tracking regime, we are led to conclude that a cancellation in the sum (5.70) is not possible, except for $w^\varphi = -1/3$. In this case, the solutions coincide anyway and both terms are once again conserved separately (and as we know from Equation (5.63), they cancel each other). This completes the proof.

A problem arises, because to evaluate (5.69), one needs Ψ. This in turn is given by Π_ν and Φ. To get Φ, one needs to solve Poisson's equation including quintessence

$$\begin{aligned}\Phi(12[\Omega_\star^\nu + \Omega_\star^\gamma] + 9(1+w^\varphi)\Omega^\varphi) = 3[\Omega_\star^\gamma + \Omega_\star^\nu]\left[D_{g,\gamma} + 4V_\gamma x^{-1}\right] \\ + 3\Omega^\varphi\left[D_g^\varphi + 3(1+w)V_\varphi x^{-1}\right],\end{aligned} \tag{5.72}$$

where we have used the (still valid) relations $V_\nu = V_\gamma$, $D_{g,\nu} = D_{g,\gamma}$ and neglected the (small) matter contribution.[8] Practically all relations of the previous section

[7] To prove this by direct calculation seems rather difficult.

[8] We have also dropped the term proportional to x^2, as it is negligible for early times and never used in the derivation of Φ^0, etc.

between the perturbation variables are still valid, as only Poisson's equation is changed. It is clear from this Poisson equation (5.72), that *if* $3(1+w^\varphi)V_\varphi = 4V_\gamma$, then solutions for Φ from Poisson's equation without quintessence (5.21) also solve (5.72). For arbitrary quintessence, this is not clear, as X is given by the complicated expressions (5.68) and (5.69).

Yet, if Ω^φ is subdominant at early times, Poisson's equation will practically stay the same as without quintessence and Φ will be given by Equation (5.48). In addition, even if Ω^φ is relevant, then usually potentials that look exponential at the time of interest are involved. Luckily, exponential potentials lead to $w = 1/3$ and therefore $a \propto \tau$ is still valid. In addition, their tracking assures that the relations of section 2.3.1 are fully applicable. Using the fact that $X = const$, and Equations (2.27, 2.33) yields

$$\begin{aligned} V_\varphi &= \frac{kX}{\dot{\bar{\varphi}}} = -k\Psi \frac{1+w^\varphi}{1-w^\varphi} \frac{V}{V'\dot{\bar{\varphi}}} \\ &= \frac{k\Psi}{3(1-w^\varphi)\frac{\dot{a}}{a}} = \frac{1}{2}k\tau\Psi \\ &= V_\gamma \end{aligned} \tag{5.73}$$

Thus, quintessence models with potentials that behave like an exponential at the time of interest, do not alter the value of Φ (and Ψ). Unfortunately, we can say nothing generic[9] about the influence on Φ in the case of a substantial quintessence contribution at early times with *arbitrary* potential.

To put it in a nutshell: for most models of practical interest, Ω_0^φ is either negligible at initial times, or the potential behaves like an exponential. In both cases, Φ stays the same as without quintessence. One can therefore use Equations (5.44-5.49) together with (5.68) and (5.69) to specify the initial adiabatic conditions.[10]

[9] At least nothing notable. In principle, one can solve the problem, however the result is rather lengthy and of little practical use. We therefore omit it here.

[10] Making a mistake, whenever quintessence is non-negligible at early times and the potential is not exponential.

6

Footprints of Quintessence

The non-genericness of quintessence makes it difficult to detect it and even more difficult to rule it out. In this chapter, we are going to dicuss possibilities to find the traces dark energy could have left behind. We will mainly focus on CMB and SNe Ia experiments, touching only briefly structure formation. In addition to these three observation possibilites, lensing [57] as well as bounds from big bang nucleosynthesis (BBN) [11,59] play an important role. For an overview of observation strategies, see for instance [58,60]. If dark energy is not a cosmological constant, then its time varying behaviour may be imprinted at different epochs. For instance, a detection of, say 5% dark energy at last scattering would mean that the dark energy must be dynamical. But even if observational tests do not lead to a detection, they still put stringent bounds on each model. Already, it is by no means trivial to find a model with sensible parameters that passes observational tests. The current constraints available together with the epoch each test probes are summarized in Figure 6.1.

Our aim is not to constrain a particular model as good as possible. In fact, there is no particular reason why any of the models on the market should be *the* quintessence realization. Therefore, we will describe main features of quintessence relevant for CMB and SNe Ia in a model independent way. With very few parameters, e.g. the influence of quintessence on the CMB can be determined. Apart from the better understanding due to this analytic description (compared to simulations), one can also estimate whether a given model will pass CMB constraints without explicitly using a CMB Boltzmann code. Of course, our findings are applicable in universes *without* quintessence also. For instance, the phase shift of the third peak in the CMB multipole spectrum is quite insensitive to the details of the cosmological model.

6.1 Introducing Quintessence in the CMB

In the following sections, we will discuss in which ways quintessence influences the CMB. For as long as quintessence is not coupled to any other form of matter or radiation, it can only change the expansion history and - less importantly - the integrated Sachs-Wolfe effect. We will see that changing the expansion history leads

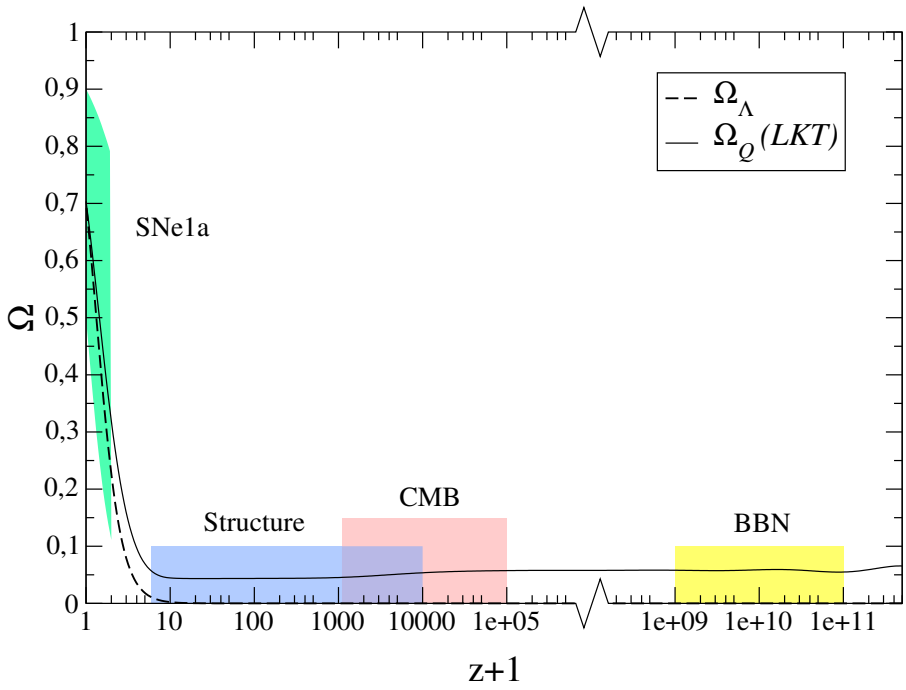

Figure 6.1: Constraints on dark energy versus redshift. The upper bound each test places on Ω^{φ} is indicated by shaded boxes. A viable model needs to stay within these regions. Very short termed violations of the bounds (though seemingly unnatural) are of course still possible.

to a different spacing between the peaks in the CMB. In principle, one could use this effect to detect the amount of quintessence before recombination. However, the Hubble parameter can mimic the influence of quintessence, spreading the separation between peaks. Hence, one needs independent information about the Hubble constant, in order to determine the amount of quintessence at last scattering.

In a flat universe, the *acoustic* scale l_A, we will be calculating determines the average spacing Δl between the peaks. We will derive an analytic expression depending only on the averaged equation of state $\overline{w}_0$ from Equation (2.44), the averaged amount of quintessence before recombination, $\bar{\Omega}^{\varphi}_{\rm ls}$, and the amount of quintessence today, Ω^{φ}_0. When comparing this analytic formula for the acoustic scale to numerical simulations, the typical precision turns out to be better than 1%.

Even though the acoustic scale yields the average spacing between CMB peaks, it is inappropriate to estimate the *location* of the peaks. Hence, in a second step, we

are going to quantify the relation between the acoustic scale and the peak locations. The results on these *peak shifts* are applicable to universes without quintessence as well and have been used to analytically describe main features of the CMB [61]. As a side effect, we will be in the position to *determine* the acoustic scale from measurements - an extremely valuable result. But let us first turn to the acoustic scale.

6.2 The Acoustic Scale of the CMB

The equation of state of quintessence influences the expansion rate of the Universe and thus the locations of the CMB peaks [3,28,62–64]. The influence of dark energy on the present horizon and therefore on the CMB has been discussed in [39]. A likelihood analysis on combined CMB, large scale structure and supernovae data [65,66] can also give limits on the equation of state. Several of these analysis concentrate on models where the dark energy component is negligible at last scattering. In contrast, we are interested particularly in getting information about dark energy in early cosmology. Therefore, the amount of dark energy at last scattering is an important parameter in our investigation.

The inter-peak spacing is to a good approximation [44,45] given by the acoustic scale[1]

$$l_{\mathrm{A}} = \pi \frac{\tau_0 - \tau_{\mathrm{ls}}}{\bar{c}_s \tau_{\mathrm{ls}}}. \tag{6.1}$$

The acoustic scale depends directly on the present geometry through τ_0 as well as indirectly through the dependence of τ_{ls} on the amount of dark energy today (see Equation (6.5)). In section (2.4), we have already calculated τ_0 using a suitably defined average equation of state $\overline{w}_0$ for the quintessence component. In addition, the average sound speed until decoupling is $\bar{c}_s \approx 1/\sqrt{3}$. According to Equation (4.9), we then only need to estimate τ_{ls} to get l_A. To this end, we assume that the fraction of quintessential energy $\Omega^{\varphi}(\tau)$ does not change rapidly for a considerable period before decoupling and define an effective average

$$\bar{\Omega}^{\varphi}_{\mathrm{ls}} \equiv \tau_{\mathrm{ls}}^{-1} \int_0^{\tau_{\mathrm{ls}}} \Omega^{\varphi}(\tau) \mathrm{d}\tau. \tag{6.2}$$

This average is dominated for τ near τ_{ls} whereas very early cosmology is irrelevant. Approximating Ω^{φ} by the constant $\bar{\Omega}^{\varphi}_{\mathrm{ls}}$ for the period around last scattering, the Friedmann equation (2.7) is just

$$3\mathrm{M}_{\mathrm{P}}^2 H^2 (1 - \bar{\Omega}^{\varphi}_{\mathrm{ls}}) = \rho^{\mathrm{m}} + \rho^{\mathrm{r}} = \rho_0^{\mathrm{m}} a^{-3} + \rho_0^{\mathrm{r}} a^{-4}. \tag{6.3}$$

Here ρ_0^{m} and ρ_0^{r} are the matter and relativistic (photons and 3 species of neutrinos) energy densities today. Neglecting radiation contributions today, we have

[1] See also section 4.1.

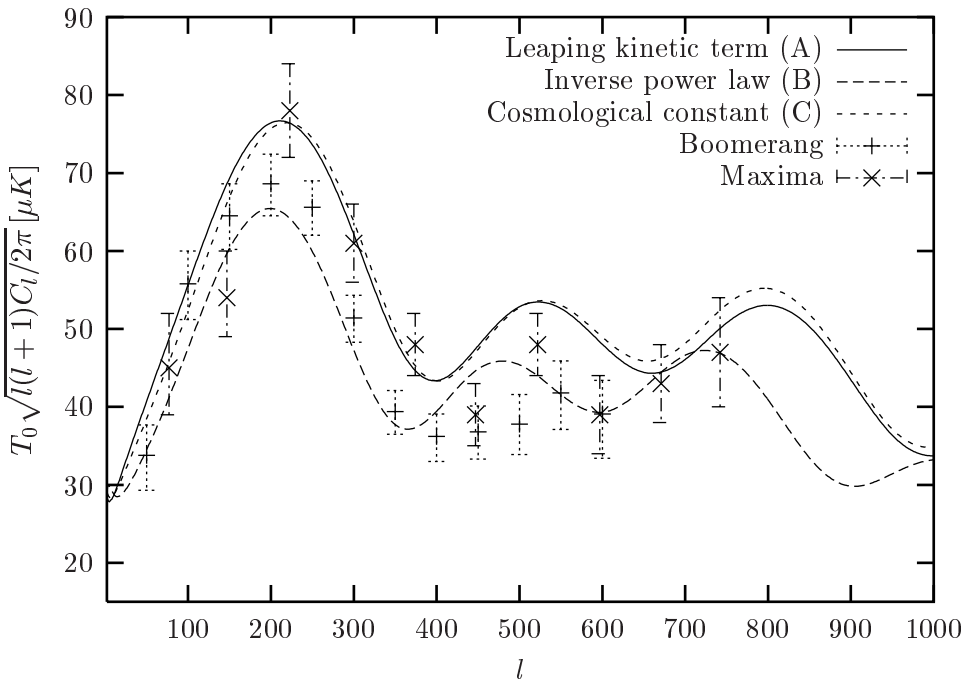

Figure 6.2: The CMB Spectrum for Λ-CDM (model C), leaping kinetic term (model A) and inverse power law (model B) quintessence universes with $\Omega_0^\varphi = 0.6$. The data points from the Boomerang [67] and Maxima [68] experiments are shown for reference.

$3\mathrm{M}_\mathrm{P}^2 H_0^2(1-\Omega_0^\varphi) = \rho_0^\mathrm{m}$, which we insert in Equation (6.3) to obtain

$$\left(\frac{\mathrm{d}a}{\mathrm{d}\tau}\right)^2 = H_0^2(1-\bar{\Omega}_\mathrm{ls}^\varphi)^{-1}\left[(1-\Omega_0^\varphi)a(\tau)+\Omega_0^\mathrm{r}\right]. \tag{6.4}$$

Separating the variables and integrating gives

$$\tau_\mathrm{ls} = 2H_0^{-1}\sqrt{\frac{1-\bar{\Omega}_\mathrm{ls}^\varphi}{1-\Omega_0^\varphi}}\left\{\sqrt{a_\mathrm{ls}+\frac{\Omega_0^\mathrm{r}}{1-\Omega_0^\varphi}}-\sqrt{\frac{\Omega_0^\mathrm{r}}{1-\Omega_0^\varphi}}\right\}, \tag{6.5}$$

which is well known for vanishing $\bar{\Omega}_\mathrm{ls}^\varphi$. For fixed H_0, Ω_0^φ, Ω_0^r and a_ls, we see that $\tau_\mathrm{ls} = \tau_\mathrm{ls}^\mathrm{vac}\,(1-\bar{\Omega}_\mathrm{ls}^\varphi)^{(1/2)}$, where $\tau_\mathrm{ls}^\mathrm{vac}$ is the last scattering horizon for a Λ-CDM universe (which we treat here to be just a special realization of dark energy with $w=-1$). Inserting Equations (6.5) and (2.48) in Equation (4.9), we get the desired expression for the acoustic scale

$$l_\mathrm{A} = \pi\bar{c}_s^{-1}\left[\frac{F(\Omega_0^\varphi,\overline{w}_0)}{\sqrt{1-\bar{\Omega}_\mathrm{ls}^\varphi}}\left\{\sqrt{a_\mathrm{ls}+\frac{\Omega_0^\mathrm{r}}{1-\Omega_0^\varphi}}-\sqrt{\frac{\Omega_0^\mathrm{r}}{1-\Omega_0^\varphi}}\right\}^{-1}-1\right], \tag{6.6}$$

with F given by Equation (2.49) and today's radiation component $\Omega_0^{\mathrm{r}}h^2 = 4.2 \times 10^{-5}$. Please note, that since it is the combination $\Omega_0^{\mathrm{r}}h^2$ that is measurable, the expression (6.6) above depends strongly on the Hubble parameter. Both, an *increase* in $\bar{\Omega}_{\mathrm{ls}}^{\varphi}$ and a *decrease* in h lead to an increase in l_A. The sound velocity c_s and the scale factor of decoupling a_{ls} have to be determined numerically to achieve high accuracy in l_A. In our case ($\Omega_0^{\mathrm{b}} = 0.05$ and $h = 0.65$), they are $a_{\mathrm{ls}}^{-1} = 1130$ and $\bar{c}_s = 0.52$. However, using $a_{\mathrm{ls}} \approx 1100$ and $c_s = 1/\sqrt{3} \approx 0.57$, is still enough for a quick estimate at the 10% level.[2] We have evaluated Equation (6.6) for quintessence models with various parameters (see section 2.3 for definitions of the models):

A. A Leaping kinetic term model with $\sigma = 1$, $k_{\mathrm{min}} = 0.05$, 0.1, 0.2 and 0.26 and φ_1 is adjusted to ≈ 277 in order to obtain $\Omega_0^{\varphi} = 0.6$. The value of $\bar{\Omega}_{\mathrm{ls}}^{\varphi}$ is determined by these parameters.

B. An inverse power law potential, with $\alpha = 6, 22$ and 40, and A adjusted such that $\Omega_0^{\varphi} = 0.6$. Once again, $\bar{\Omega}_{\mathrm{ls}}^{\varphi}$ follows.

C. A cosmological constant tuned such that $\Omega_0^{\varphi} \equiv \Omega_0^{\Lambda} = 0.6$.

D. The pure exponential potential with $\lambda = \sqrt{3/\Omega_0^{\varphi}}$.

The results are summarized in Table 6.1, where we give l_A together with the locations l_1, l_2 of the first two peaks computed by CMBEASY. The last entry contains the peak spacing Δl averaged over 6 peaks for the numerical solution. Of course, when running CMBEASY, one can also determine l_A directly from the background evolution via Equation (4.9). The formula (6.6), the numerical value of l_A and the averaged peak spacing Δl are found to be in very good agreement.

In Table 6.2, we determine the accuracy of the estimates of τ_{ls} (6.5) and τ_0 (2.48) by comparison with the numerical solution. The good agreement demonstrates that the averaging prescriptions Equation (2.44) and (6.2) are indeed meaningful. We conclude that the influence of a wide class of different quintessence models (beyond the ones discussed here explicitly) on τ_{ls}, τ_0 and l_A can be characterized by the three quantities Ω_0^{φ}, $\bar{\Omega}_{\mathrm{ls}}^{\varphi}$ and $\overline{w}_0$.

For the models (A) and (D), quintessence is not negligible at last scattering. The pure exponential potential requires $\Omega_0^{\varphi} \leq 0.2$ for consistency with nucleosynthesis and structure formation. It does not lead to a presently accelerating universe. We quote results for $\Omega_0^{\varphi} = 0.6$ for comparison with other models and in order to demonstrate that a measurement of l_{A} can serve as a constraint for this type of models, independently of other arguments. The inverse power law models (B) are compatible with a universe accelerating today only if $\bar{\Omega}_{\mathrm{ls}}^{\varphi}$ is negligible. Again, our parameter list includes cases which are not favoured by phenomenology. As an illustration we quote in Table 6.1 the value of σ_8, which should typically range between 0.6 and 1.1 for the models considered. For example, the exponential

[2] Generically, the sound velocity is smaller than the theoretical upper limit $1/\sqrt{3}$ and hence using this upper limit, Equation (6.6) will give a lower bound on l_A.

$\bar{\Omega}_{\rm ls}^{\varphi}$	$\overline{w}_0$	$\mathbf{l_1}$	$\mathbf{l_2}$	$\mathbf{l_A^{estim.}}$	$\mathbf{\Delta l^{num.}}$	σ_8
Leaping kinetic term (A), $\Omega_0^{\varphi}= 0.6$						
8.4×10^{-3}	-0.76	215	518	292	291	0.86
0.03	-0.69	214	520	294	293	0.78
0.13	-0.45	211	523	299	300	0.47
0.22	-0.32	207	524	302	307	0.29
Inverse power law potential (B), $\Omega_0^{\varphi}= 0.6$						
8.4×10^{-8}	-0.37	199	480	271	269	0.61
9.9×10^{-2}	-0.13	178	443	252	252	0.18
0.22	-8.1×10^{-2}	172	444	257	257	0.09
Pure exponential potential, $\Omega_0^{\varphi}= 0.6$						
0.70	7×10^{-3}	190	573	368	377	0.01
Pure exponential potential, $\Omega_0^{\varphi} = 0.2$						
0.22	4.7×10^{-3}	194	490	282	281	0.38
Cosmological constant (C), $\Omega_0^{\varphi}= 0.6$						
0	-1	219	527	296	295	0.97
Cold Dark Matter - no dark energy, $\Omega_0^{\varphi}= 0$						
0	–	205	496	269	268	1.49

Table 6.1: Location of the first two CMB peaks l_1, l_2 for several models of dark energy. We also show the analytic (from Equation (6.6)) and numerical (from CMBEASY) average spacing of the peaks and σ_8, the normalization of the power spectrum on scales of $8h^{-1}$Mpc.

potential model with large $\bar{\Omega}_{\rm ls}^{\varphi}$ is clearly ruled out by its tiny value of σ_8[3]. The main interest for listing also phenomenologically disfavored models arises from the question to what extent the location of the peaks can give independent constraints. From the point of view of naturalness, only the models (A) and (D) do not involve tiny parameters or small mass scales.

The horizons and $l_{\rm A}$ for the models considered are shown in Tables 6.2 and 6.1. We note that the estimate and the exact numerical calculation are in very good agreement. A different choice of $a_{\rm ls}$, say $a_{\rm ls}^{-1} = 1150$, would have affected the outcome on the low-percent level. Also, the average spacing obtained from CMBEASY varies slightly (at most 2%) when averaging over 4, 5 or 6 peaks. For a fixed value of the equation of state, $\overline{w}_0 = -0.7$, we plot the peak spacing as a function of Ω_0^{φ} and $\bar{\Omega}_{\rm ls}^{\varphi}$ in Figure 6.3.

[3]Of course σ_8 itself also depends on other cosmological parameters and so it alone cannot be used to determine $\bar{\Omega}_{\rm ls}^{\varphi}$.

$\bar{\Omega}^{\varphi}_{\rm ls}$	w_0	$\overline{w}_0$	$\tau_0^{\rm estim.}$	$\Delta\tau_0$	$\tau_{\rm ls}^{\rm estim.}$	$\Delta\tau_{\rm ls}$
Leaping kinetic term (A), $\Omega^{\varphi}_0 = 0.6$						
8.4×10^{-3}	-0.79	-0.76	13073	0.1%	266	0.3%
0.03	-0.79	-0.69	12971	0.2%	263	0.3%
0.13	-0.78	-0.45	12470	1.0%	248	0.2%
0.22	-0.75	-0.32	12012	1.3%	236	0.0%
Inverse power law potential (B), $\Omega^{\varphi}_0 = 0.6$						
8.4×10^{-8}	-0.32	-0.37	12205	0.5%	267	0.0%
9.9×10^{-2}	-0.16	-0.13	10774	0.2%	253	0.2%
0.22	-0.1	-8.1×10^{-2}	10241	0.3%	236	0.2%
Pure exponential potential, $\Omega^{\varphi}_0 = 0.6$						
0.70	0.00	7×10^{-3}	9014	0.4%	146	2.3%
Pure exponential potential, $\Omega^{\varphi}_0 = 0.2$						
0.22	5×10^{-5}	4.7×10^{-3}	9107	0.1%	191	0.3%
Cosmological constant (C), $\Omega^{\varphi}_0 = 0.6$						
0	-1	-1	13330	0.0%	267	0.0%
Cold Dark Matter - no dark energy, $\Omega^{\varphi}_0 = 0$						
0	–	–	9133	0.0%	201	0.5%

Table 6.2: Horizons in Mpc at last scattering and today for various kinds of quintessence. The deviation of our analytic estimates and numerically obtained values for τ_0 and $\tau_{\rm ls}$ are also given.

For fixed $\overline{w}_0$ and Ω^{φ}_0, we see from Equation (6.6) that $l_{\rm A} \propto (1 - \bar{\Omega}^{\varphi}_{\rm ls})^{(-1/2)}$. Hence, when combining bounds on Ω^{φ}_0 and $\overline{w}_0$ from the structure of the Universe, supernovae redshifts and other sources with CMB data, the amount of dark energy in a redshift range of $z \sim 10^5$ to last scattering $z \sim 1100$ may be determined. However, as the Hubble parameter can mimic the effects of $\bar{\Omega}^{\varphi}_{\rm ls}$, one needs to know H_0 from an independent measurement.

6.3 CMB Peak Positions and Quintessence

The locations of the peaks and troughs of the CMB anisotropy spectrum can serve as a sensitive probe of cosmological parameters [69–72,39,63].

There are however many processes which contribute to the final anisotropies, and these must be calculated from the systems of coupled partial differential equations of section 4.4. As such it is not possible *a priori* to derive an accurate analytic

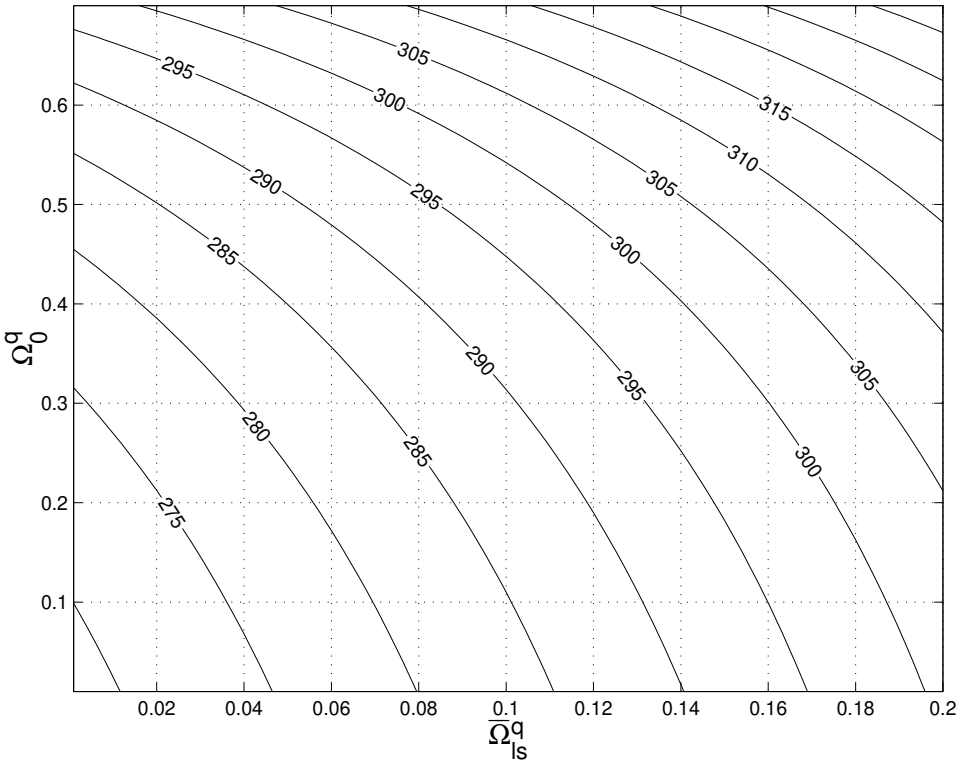

Figure 6.3: Contours of equal peak spacing l_A as a function of Ω_0^φ and $\bar{\Omega}_{ls}^\varphi$.The average equation of state is kept fixed, $\overline{w}_0 = -0.7$. Increasing $\bar{\Omega}_{ls}^\varphi$ leads to a pronounced stretching of the spacing.

formula for the peak locations. There exists a numerically-obtained estimate of the location of the first peak [73] for a universe with no cosmological constant, namely $l_1 \sim 200\ \Omega_m^{-1/2}$. This was extended to universes with $\Lambda \neq 0$, by perturbing around the $\Lambda = 0$ value [74], but holding all other parameters fixed. In this section, we calculate the locations of the first three peaks as a function of several cosmological parameters, including universes with a large dark energy component. We show how these results can be used to extract cosmological information about, for instance the history of quintessence, from just a handful of CMB data points and also to speed up multi-parameter likelihood analysis.

Before last scattering, the photons and baryons are tightly bound by Compton scattering and behave as a fluid. The oscillations of this fluid, occurring as a result of the balance between the gravitational interactions and the photon pressure, lead to the familiar spectrum of peaks and troughs in the averaged temperature anisotropy spectrum which we measure today. The odd peaks correspond to maximum compression of the fluid, the even ones to rarefaction [45]. In an idealized

Ω_m	Ω_Λ	l_1 (estim.)	l_1 (numeric.)	% error
0.4	0.6	296	219	35
1.0	0.0	269	205	31

Table 6.3: Values of the location of the first peak l_1 estimated by $l_1 \approx l_A$ and calculated numerically via CMBEASY. The intuitive model clearly does not describe the location of the first peak well, though the spacings between other peaks is better. The above values were calculated assuming $h = 0.65$, $\Omega_b = 0.05$, $n = 1$ and $a_{\rm ls} = 1100^{-1}$.

model of the fluid, there is an analytic relation for the location of the m-th peak: $l_m \approx m\, l_A$ [75,44] where l_A is the *acoustic scale* which may be calculated analytically [72] and depends on both pre- and post-recombination physics as well as the geometry of the universe.

The simple relation $l_m \approx m\, l_A$ however does not hold very well for the first peak (see Table 6.3) although it is better for higher peaks [69]. Driving effects from the decay of the gravitational potential as well as contributions from the Doppler shift of the oscillating fluid introduce a shift in the spectrum. In order to compensate for this, we parameterize the location of the peaks and troughs as in [75] by[4]

$$l_m \equiv l_A\,(m - \varphi_m) \equiv l_A\,(m - \bar{\varphi} - \delta\varphi_m)\,. \tag{6.7}$$

For convenience, we define $\bar{\varphi} \equiv \varphi_1$ to be the overall peak shift, and $\delta\varphi_m \equiv \varphi_m - \bar{\varphi}$ the shift of the m-th peak relative to the first.[5] The reason for this parameterization is that the phase shifts of the peaks are determined predominantly by pre-recombination physics, and are independent of the geometry of the Universe. In particular, the ratio of the locations of the first and m-th peaks

$$\frac{l_m}{l_1} = \frac{l_A}{l_A}\frac{(m - \bar{\varphi} - \delta\varphi_m)}{(1 - \bar{\varphi})} = 1 + \frac{m - 1 - \delta\varphi_m}{1 - \bar{\varphi}}, \tag{6.8}$$

probes mostly pre-recombination physics and so can be used to extract information on the amount of dark energy present before last scattering [72].

If we knew how the phase shifts depended on cosmological parameters, it would be possible to extract l_A from the measured CMB spectrum. Since any given cosmological model predicts a certain value of l_A, this is a simple way of distinguishing between different models – in particular we know from section 6.2 that different quintessence models with the same energy density and equation of state today can have significantly different values of l_A. Finally, having extracted l_A from observations, we could speed up likelihood analysis by being able to discard models not leading to the right value of the acoustic scale before a single perturbation equation has to be solved.

[4] The peaks are labeled by integer values of m and the troughs by half-integer values.

[5] There should be no confusion between the quintessence field φ, which is not explicitly used in this section and the phase shifts.

Symbol	Range
Ω_0^m	[0.2, 0.6]
$\Omega_b h^2$	[0.005, 0.04]
$\bar{\Omega}_{\rm ls}^{\varphi}$	[0, 0.23]
h	[0.55, 0.80]
n	[0.8, 1.2]

Table 6.4: Parameter ranges used in this section.

In a [75], a fitting formula for $\bar{\varphi}$ was given

$$\bar{\varphi} \approx 0.267 \left(\frac{r_\star}{0.3}\right)^{0.1}, \tag{6.9}$$

for the values $n = 1$, $\Omega_b h^2 = 0.02$. In this formula, $r_\star$ is the ratio of radiation to matter at last scattering[6]

$$r_\star = \rho_r(z_\star)/\rho_m(z_\star) = 0.042 \left(\Omega_m h^2\right)^{-1} \left(z_\star/10^3\right). \tag{6.10}$$

Equation (6.9) however, is valid only for the given values of spectral index, Hubble parameter and baryon density. It does not include the dependence of the peak location on the amount of quintessence present at last scattering, and is valid only for the first peak l_1. In the following, we give fitting formulae (see Appendix B) for the shifts of the first three peaks and the first trough and describe how one can use them to extract cosmological information from future CMB experiments.

Our first task in computing fitting formulae for the peak locations is to decide which cosmological parameters to fit to. The dependence on the baryon density and the Hubble parameter is sensitive only to the product $\Omega_b h^2$, and so we do not seek to fit for them separately. We further take $r_\star$ defined in Equation (6.10) and the spectral index n as parameters. For the quintessence dependence, we use the effective average density component before last scattering $\bar{\Omega}_{\rm ls}^{\varphi}$ defined in Equation (6.2).

We recall that the peak shifts are sensitive mainly to pre-recombination physics and so we do not need to use the value of Ω^φ today as a parameter. Of course the acoustic scale l_A does depend on today's quintessence component (see section 6.2). We will thus seek to find the dependence of $(\bar{\varphi}, \delta\varphi_m)$ on the cosmological parameter set $\left(\Omega_b h^2, r_\star, n, \bar{\Omega}_{\rm ls}^{\varphi}\right)$. In performing these calculations, we restricted each of the cosmological parameters used to lie within a certain interval, which in each case is over- rather than under-cautious. The ranges of parameter values chosen are displayed in Table 6.4. To gain intuition for the fitting formulae, we plot curves for the shift of the first and the second peak as well as the relative shifts of the first trough and the second peak in Figures 6.4 and 6.5.

[6] This relation also holds in the presence of quintessence.

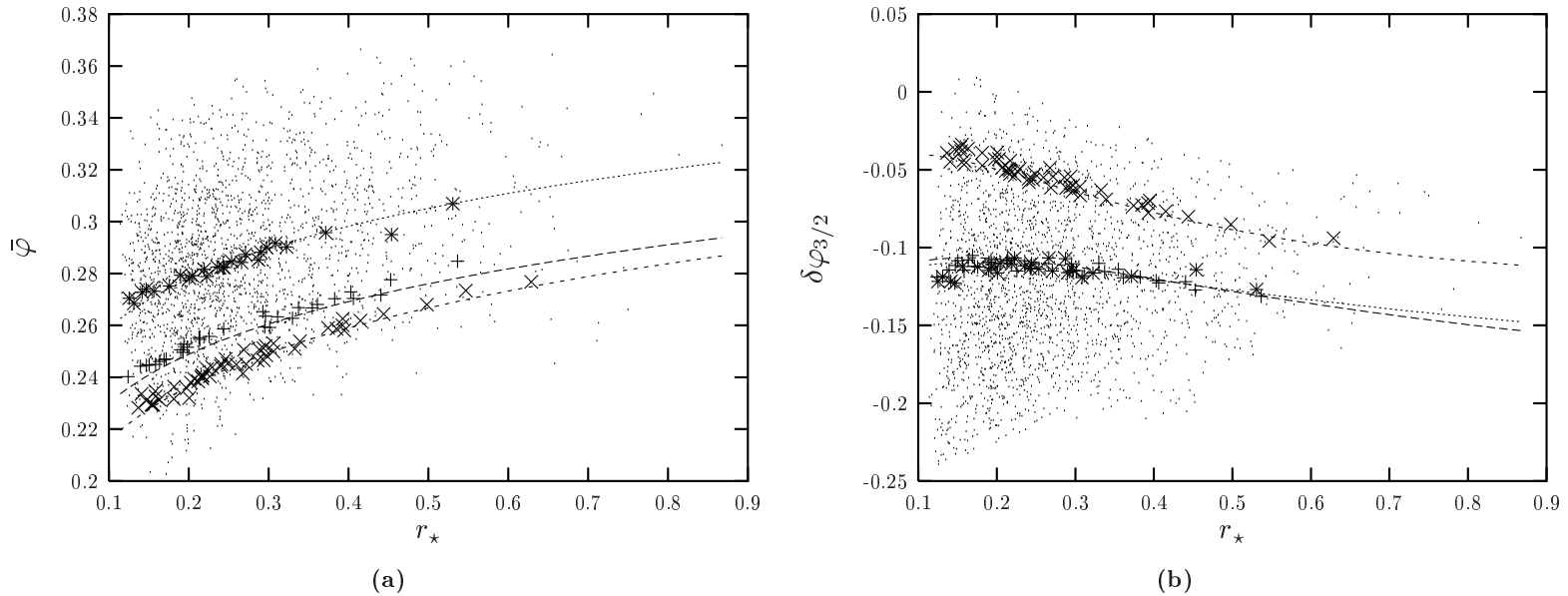

Figure 6.4: The overall shift $\bar{\varphi}$ (a) and the relative shift of the first trough (b). In both figures, the long dashed, dotted and the dashed lines represent the fitting formulae for the parameters $\left(\Omega_b h^2, r_\star, n, \bar{\Omega}_{\rm ls}^{\varphi}\right)$ = (0.02, $r_\star$, 1, 0), (0.02, $r_\star$, 1, 0.1) and (0.01, $r_\star$, 1, 0) respectively. The large symbols show the data corresponding to these curves. The errors quoted in Appendix B are calculated from the spread of these symbols relative to the curves. The sprinkled dots represent thousands of models selected at random from the parameter space given in Table 6.4, and indicate the ranges of values taken on by $\bar{\varphi}$ etc. for these models.

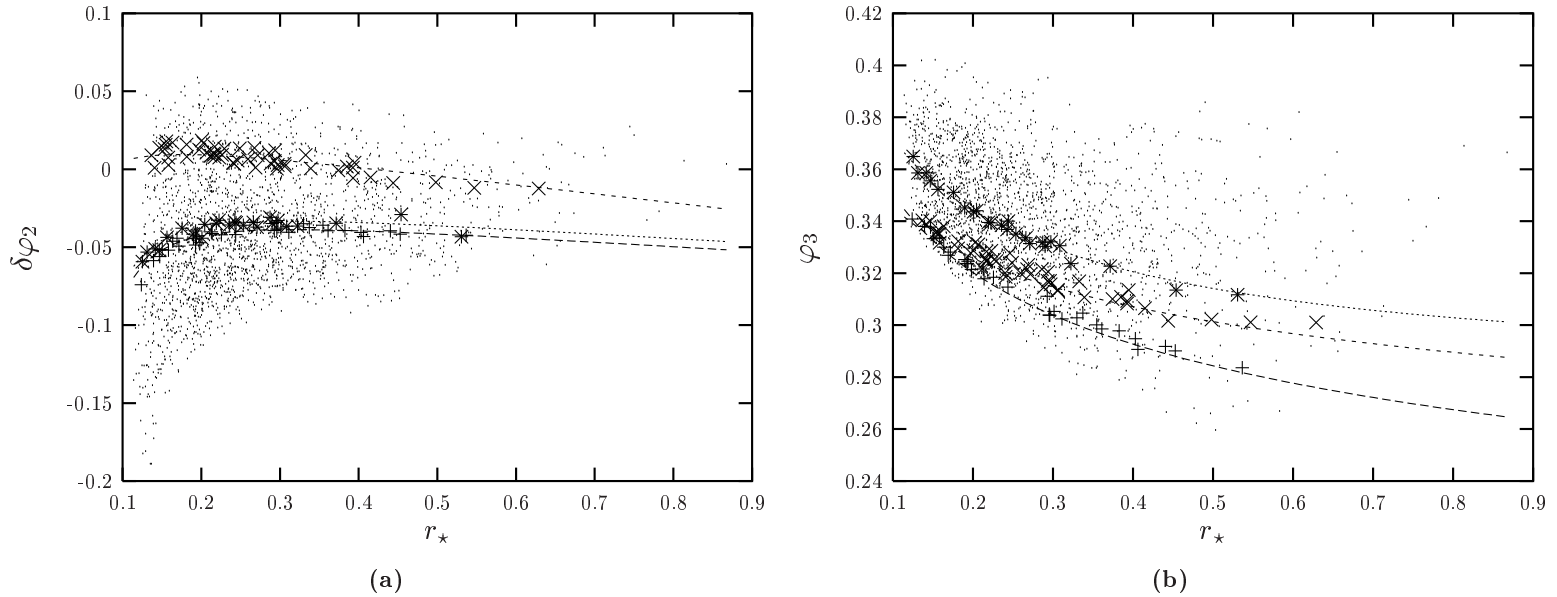

Figure 6.5: The relative shift of the second peak (a) and the overall shift of the third peak (b). In both figures, the long dashed, dotted and the dashed lines represent the fitting formulae for the parameters $\left(\Omega_b h^2, r_\star, n, \bar{\Omega}_{\rm ls}^{\varphi}\right)$ = (0.02, $r_\star$, 1, 0), (0.02, $r_\star$, 1, 0.1) and (0.01, $r_\star$, 1, 0) respectively. The large symbols show the data corresponding to these curves. The errors quoted in Appendix B are calculated from the spread of these symbols relative to the curves. The sprinkled dots represent thousands of models selected at random from the parameter space given in Table 6.4, and indicate the ranges of values taken on by $\bar{\varphi}$ etc. for these models.

In Sections 6.3.1 and 6.3.2 we describe a systematic procedure for extracting the acoustic scale l_A from the location of the first three peaks. Section 6.3.3 introduces a quantity κ which is useful as it depends only on two of our four parameters. The model (in)dependence of the fitting formulae is discussed in Section 6.3.4. Finally, our fitting formulae are given in Appendix B.

6.3.1 Retrieving the Shifts from CMB Measurements

With future high precision measurements of the *MAP*[7] and *PLANCK*[8] satellites, we expect that the position of the first three peaks and troughs will be determined to high accuracy. From these few data points, it is possible to extract valuable information on the cosmological parameters. We have observed, during our computation of CMB spectra for thousands of universes, that the overall shift of the third peak φ_3 (i.e. $\varphi_3 = \bar{\varphi} + \delta\varphi_3$) is a relatively insensitive quantity. In the parameter range we used (see Table 6.4) we found that $\varphi_3 = 0.341 \pm 0.024$.[9] In using $\varphi_3 = 0.341$ we introduce slight (at most one percent) systematic deviations in our estimate, because an increase of $\bar{\Omega}_{\rm ls}^{\varphi}$ typically increases φ_3 (see Fig. 6.5(b)). We will partially correct for these effects by improving our estimate for φ_3, via the procedure described below.

We start by extracting our first estimate of the overall phase shift, from the measured locations of the first and third peaks

$$\bar{\varphi} = 1 - (3 - \varphi_3)\frac{l_1}{l_3} \approx 1 - 2.66\frac{l_1}{l_3}. \tag{6.11}$$

Comparing this estimate with the value calculated from numerical simulations, we find $\Delta\bar{\varphi} = 0.006$. Having a handle on the overall phase shift, it is now simple to infer the relative shifts $\delta\varphi_m$ of the remaining troughs and peaks. From equation (6.8) we get the relation

$$\delta\varphi_m = (m-1) - \left(\frac{l_m}{l_1} - 1\right)(1 - \bar{\varphi}). \tag{6.12}$$

The error of this estimate is

$$\Delta\left(\delta\varphi_m\right) = \left(\frac{l_m}{l_1} - 1\right)\Delta\bar{\varphi}. \tag{6.13}$$

Having a first (and already quite accurate) estimate of the shifts, we now correct for the systematic effects described above. Taking the cosmological parameter set we wish to maximize over (i.e. Table 6.4), we calculate for each model universe the phase shifts of the first three peaks using the fitting formulae given in Appendix B. We then discard those models for which any phase shift deviates significantly

[7] http://map.gsfc.nasa.gov/

[8] http://astro.estec.esa.nl/SA-general/Projects/Planck/

[9] Here and in the following, we quote 1-σ errors. All errors follow approximately a bell curve.

$\bar{\Omega}_{\rm ls}^{\varphi}(\%)$	$\langle\varphi_3^{\rm num}\rangle$	$\langle\varphi_3^{\rm improved}\rangle$
0 - 2	0.313	0.326
10 - 12	0.340	0.337
18 - 20	0.362	0.348

Table 6.5: Binned average φ_3 of the numerical simulation and the improved deduction.

(say > 2-σ) from the data-inferred values. This leaves an improved cosmological parameter set, for which the average value of φ_3 is calculated (see Table 6.5). This improved φ_3 can then be used to re-calculate the phase shifts from Equations (6.11) and (6.12).

6.3.2 Extracting l_A from CMB Measurements

Using the improved value[10] for φ_3 from the previous section, we can extract to very good accuracy the acoustic scale l_A, provided l_3 has been measured:

$$l_A = \frac{l_3}{3 - \varphi_3} \tag{6.14}$$

In fact, the deviation of the value of l_A estimated from this formula and the numerically-obtained value is small for models within the parameter range of Table 6.4, with a 1-σ error of 0.8% (see also Table 6.6). This is a very valuable result, for the value of l_A can be simply computed for any given quintessence (or indeed any other) cosmology. In particular, different quintessence models with the same energy density and equation of state today can have significantly different values of l_A. In this way stringent bounds on cosmological models can be imposed just by comparing the l_A value of specific models.

6.3.3 Insensitive Quantities

The phase shifts depend on the cosmological parameters $\left(\Omega_b h^2, r_\star, n, \bar{\Omega}_{\rm ls}^{\varphi}\right)$. Of course, if it were possible to find a linear combination of phase shifts which is insensitive to some of these parameters and thus reduce the dimensionality of our parameter space, it would greatly help in extracting cosmological information. To this end, we note an anti-correlation between $\bar{\varphi}$ and $\delta\varphi_3$ – empirically, we have found that the quantity

$$\kappa \equiv \bar{\varphi} + \frac{2}{5}\delta\varphi_3 \tag{6.15}$$

is practically insensitive to $r_\star$ and $\Omega_b h^2$, and depends only on n and $\bar{\Omega}_{\rm ls}^{\varphi}$. In fact, it is to very good approximation given by the fit

$$\kappa = \left(0.277 + 0.284\bar{\Omega}_{\rm ls}^{\varphi}\right)(1.3 - 0.3n), \tag{6.16}$$

[10] In fact, using $\varphi_3 = 0.34$ instead of the improved value also gives reasonable results.

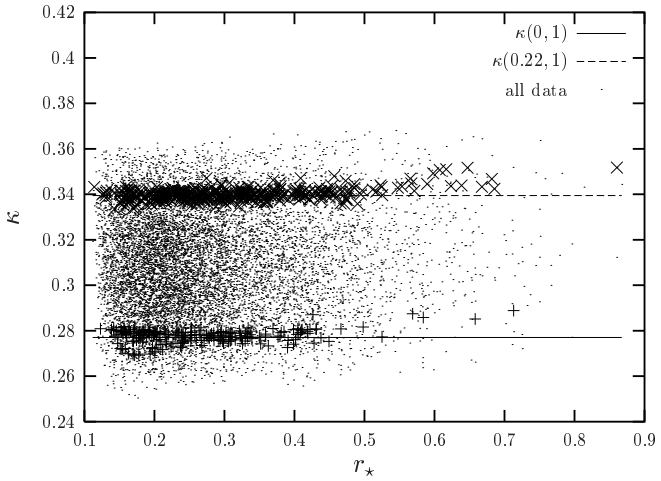

Figure 6.6: The quantity κ as a function of $r_\star$. It is practically insensitive to $r_\star$ and $\Omega_b h^2$ for most of the initial conditions considered. The dots represent fifty thousand models with parameters in the ranges given in Table 6.4 The +'s and ×'s represent models with $\bar{\Omega}_{\rm ls}^{\varphi}$= 0 and 0.22 respectively, for $n = 1$, and all values of other input parameters.

with $\Delta\kappa^{\rm fit} \approx 0.0024$ being the deviation of the fit from the numerically-simulated values (see Fig. 6.6). Following the procedure in Section 6.3.1, we can deduce κ from the measured values of the peak locations. Within our parameter range, κ is then determined with error $\Delta\kappa^{\rm deduc.} = 0.013$.

In the parameter space we have considered, the value of κ varies between 0.26 and 0.36. Hence to 1-σ confidence level, about three quarters of our two-dimensional $(n, \bar{\Omega}_{\rm ls}^{\varphi})$ parameter space can be excluded for any given κ. For instance, without quintessence, the value of κ lies between 0.26 and 0.29 for $n \in [0.8, 1.2]$. The measurement by *MAP* or *PLANCK* of a value of $\kappa > 0.29$ would therefore be a strong hint of a dark energy component playing a role at last scattering.

6.3.4 Model Dependence of the Shift Functions

The fitting formulae were obtained using a standard exponential potential [6] for the quintessence component. Because the shifts are almost independent of post recombination physics, we expect the results to be approximately correct for any realization of quintessence, i.e. all potentials. One should however be cautious with models that are qualitatively extremely different from the exponential potential before last scattering, as for example the Ratra-Peebles inverse power law [7] with substantial $\bar{\Omega}_{\rm ls}^{\varphi}$. In these models there is a sharp increase in Ω^{φ}during recombination, whereas the quintessence content for the exponential potential is fairly constant at this epoch. The inverse power law is characterized by its potential $V^{\rm IPL} = A/\varphi^{\alpha}$. Models with $\alpha \gtrapprox 2$ are phenomenologically disfavored [35]. We use these models only as cross checks for the fitting formulae. In terms of phase shifts, one finds that the sensitive relative shifts of the first trough and the second peak

$\bar{\Omega}_{\rm ls}^{\varphi}(\%)$	l_1	$l_{3/2}$	l_2	l_3	l_A	$\bar{\varphi}$	$\delta\varphi_{3/2}$	$\delta\varphi_2$	κ
Leaping kinetic term									
3	214	396	521	788	293	0.269	-0.121	-0.045	0.287
					294	0.271	-0.119	-0.041	0.292
13	210	396	522	799	301	0.301	-0.120	-0.038	0.317
					301	0.301	-0.120	-0.038	0.318
22	208	397	524	808	307	0.324	-0.116	-0.030	0.341
					305	0.320	-0.120	-0.035	0.333
Ratra Peebles inverse power law									
5×10^{-3}	199	366	480	724	269	0.259	-0.119	-0.043	0.278
					270	0.261	-0.117	-0.038	0.284
10	178	339	443	674	251	0.294	-0.140	-0.054	0.304
					253	0.298	-0.138	-0.050	0.312
22	172	338	444	683	258	0.333	-0.144	-0.057	0.340
					258	0.334	-0.145	-0.057	0.340

Table 6.6: The peak locations and the phase shifts of leaping kinetic term [32] and Ratra Peebles inverse power law [7] models for $\Omega_b h^2 = 0.021$, $\Omega_0^{\varphi} = 0.6$, $h = 0.65$, $n = 1$ and varying $\bar{\Omega}_{\rm ls}^{\varphi}$. The inverse power law models correspond to $\alpha = 6$, 22 and 40 respectively. The first row of each model gives the CMBEASY-obtained values of the locations of the peaks and the phase shifts as well as l_A and κ. The second row gives the values deduced using the method described in Section 6.3.1.

differ substantially for the two models (see Table 6.6). However, $\bar{\varphi}$ and κ are seen to be more robust and the deduced value of l_A is accurate to within one percent in every case.

In the next section, we will use this possibility of determining l_A from measurement to constrain quintessence models.

6.4 The Boomerang 2001 Data and Quintessence

The data released in spring 2001 by the BOOMERANG [14] and MAXIMA [15] team covers the multipoles up to $l \approx 1000$. It shows three peaks as distinct features, seeming to confirm beyond any reasonable doubt the inflationary picture of structure formation from predominantly adiabatic initial conditions. Here, we will use this data to extract the acoustic scale l_A. This together with bounds from structure formation will permit us to constrain inverse power law and leaping kinetic term models. We also show that the new CMB data provides strong evidence for an accelerating universe, independent of supernovae (SNe Ia) data, to which we return later. In this section, we have assumed a flat universe, with $\Omega_b h^2 = 0.022 \pm 0.003$

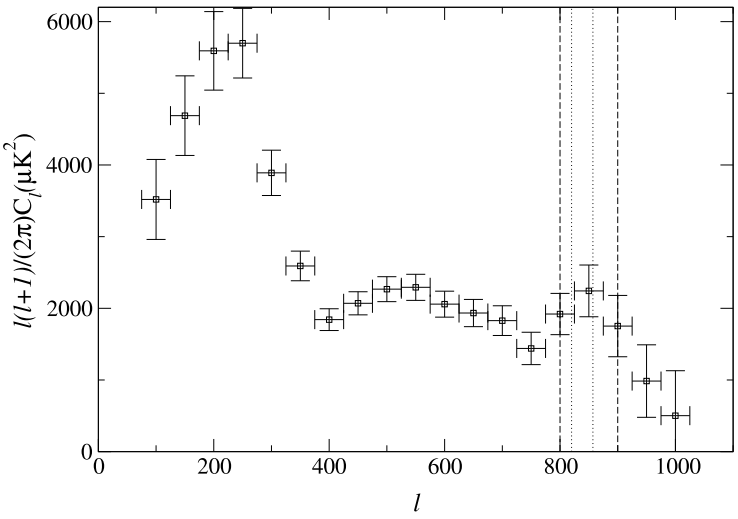

Figure 6.7: The CMB anisotropy power spectrum as measured by BOOMERANG [20]. The inner vertical lines show the region $820 < l_3 < 857$ as calculated by the BOOMERANG team [24], and the outer lines our more conservative region $800 < l_3 < 900$.

(in accordance with Big Bang Nucleosynthesis) and spectral index $n = 1$ unless otherwise stated.

We have shown in section 6.3, that the shift of the third peak, φ_3 is relatively insensitive to cosmological parameters, and that by assuming the constant value $\varphi_3 = 0.341$ we can estimate l_A to within one percent if the location of the third peak l_3 is measured, via the relation (6.14). The measurement of a third peak in the CMB spectrum by BOOMERANG [14] now allows us to extract the acoustic scale l_A and use this as a constraint on cosmological models. In an analysis of peak positions, the BOOMERANG team performed a model-independent analysis of their data [67], and found the third peak to lie in the region

$$l_3 = 845^{+12}_{-25}, \tag{6.17}$$

from which we calculate the value

$$l_A = 316 \pm 8. \tag{6.18}$$

If we instead chose the more conservative assumption that $800 < l_3 < 900$, we would get the bound

$$l_A = 319 \pm 23, \tag{6.19}$$

We will perform our analysis using both of these ranges for the location of the third peak. The two ranges are displayed, along with the BOOMERANG data, in

Fig. 6.7. Independently of [67] we have performed cubic spline fittings to the data presented in [14], as well as to the combined multiple-experiment data given in [76]. We allowed the data to vary according to the Gaussian errors given. We find for the BOOMERANG and combined data respectively:

$$l_1 = 221 \pm 14, \quad 222 \pm 14 \tag{6.20}$$

$$l_2 = 524 \pm 35, \quad 539 \pm 21 \tag{6.21}$$

$$l_3 = 850 \pm 28, \quad 851 \pm 31 \tag{6.22}$$

We applied our CMB-derived l_A constraints to two types of quintessence model: an inverse power law (IPL) potential [7] as defined in Equation (2.23) and a leaping kinetic term (LKT) model [32], as specified in Equations (2.20,2.21). Please note that the IPL model has equation of state today given by $w_0 \equiv w(\text{today}) = -2/(\alpha + 2)$. In contrast to this, w_0 for LKT depends strongly on the precise shape of $k(\varphi)$.For a steep increase in the kinetic term, one can have w_0 very close to -1 und thus mimic a cosmological constant at the present epoch (see also figure 6.12). Other models of quintessence share the effective time dependence of w [38,81]. We also applied the constraints to a cosmological constant ($\Omega_0^\varphi \equiv \Omega_\Lambda$) universe (i.e. IPL quintessence with $\alpha = 0$) for comparison.

In Figs 6.8, 6.9 we show for our chosen dark energy models the range of Ω_0^φ and h allowed by Equations (6.18) and (6.19). These ranges are similar for the cosmological constant, LKT (also for $\bar{\Omega}_{\rm ls}^\varphi = 0.2$) and IPL for small α whereas IPL with $\alpha = 2$ would be pushed to small values of h. The comparatively low values of h inferred from the BOOMERANG data can be combined with information from LSS formation. The growth of density fluctuations slows down when quintessence starts to dominate. In this way LSS can serve as a probe of quintessence at intermediate redshifts. We will come back to this in section (6.6). Meanwhile, we note that cluster abundance constraints for quintessence models with constant equation of state yield [77]

$$\sigma_8 \Omega_{\rm m}^\gamma = 0.5 - 0.1\,[(n-1) + (h - 0.65)] \tag{6.23}$$

where γ depends slightly on w, and typically $\gamma \sim 0.6$. In [77], the uncertainty for Equation (6.23) was estimated as 20% at 2-σ, and this is the constraint shown in the plots. We have chosen to shade the 2-σ LSS and conservative l_A concordance region in the Ω_0^φ-h plane, but not to impose any bounds on these parameters. Recently, however, the HST has measured $h = 72 \pm 8$ [79], and the 2dF survey $\Omega_m h = 0.20 \pm 0.03$ [80].

The current CMB and LSS data are consistent with a cosmological constant (Fig. 6.8). The LKT model with 5% quintessence at last scattering is marginally compatible for small h. If the amount of quintessence at last scattering is increased beyond 5%, the l_A bounds do not change significantly. Compatibility with LSS data would require, however, even higher h-values, at odds with the BOOMERANG data. In contrast to the CMB measurements, the determination of σ_8 by cluster abundances involves systematic uncertainties that are difficult to quantify. Furthermore, the theoretical expectation for σ_8 depends strongly on the spectral index n.

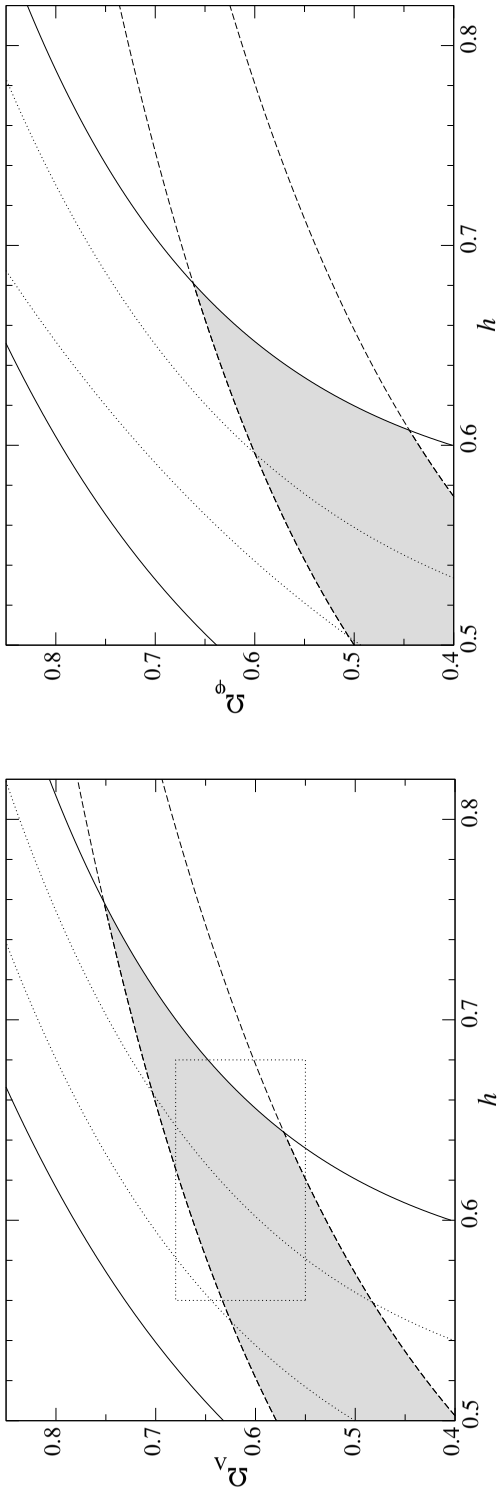

Figure 6.8: BOOMERANG (solid lines give conservative bound, dotted lines more strict bound) and LSS (dashed lines) constraints in Ω_Λ-h plane (left) and Ω_0^φ-h plane for LKT quintessence with $\bar{\Omega}_{\rm ls}^\varphi = 0.05$ (right). The dotted box indicates the 1-σ maximum likelihood ranges obtained by the BOOMERANG data analysis team with flatness and LSS priors.

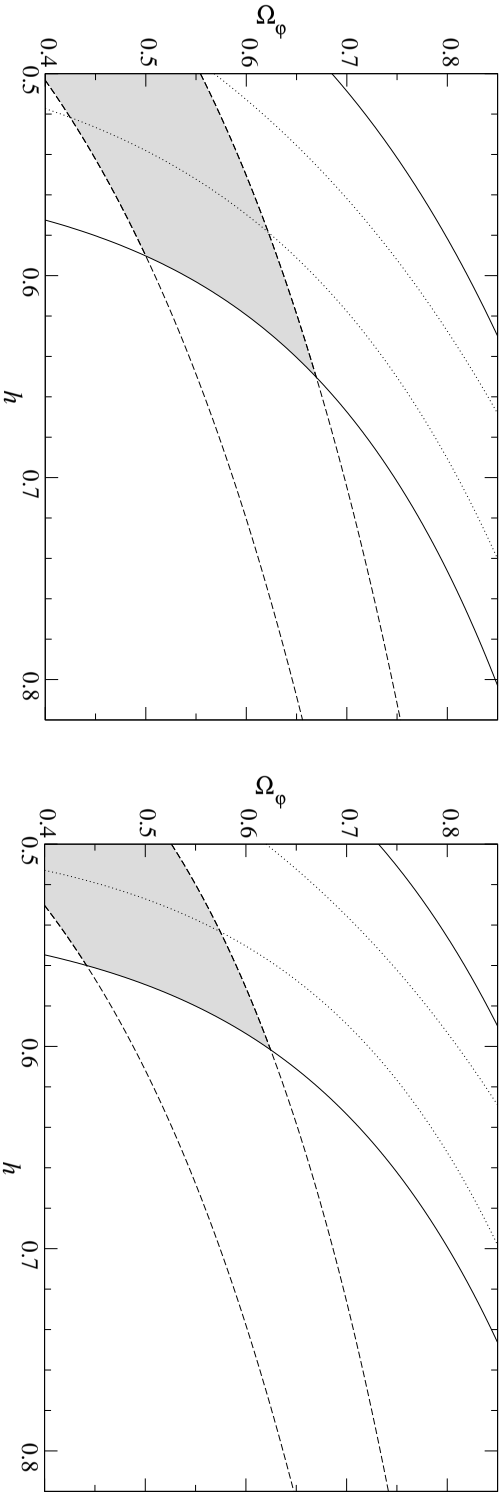

Figure 6.9: Constraints in the Ω_0^φ-h plane for IPL quintessence, from BOOMERANG and LSS , $\alpha = 1$ (left) and $\alpha = 2$ (right).

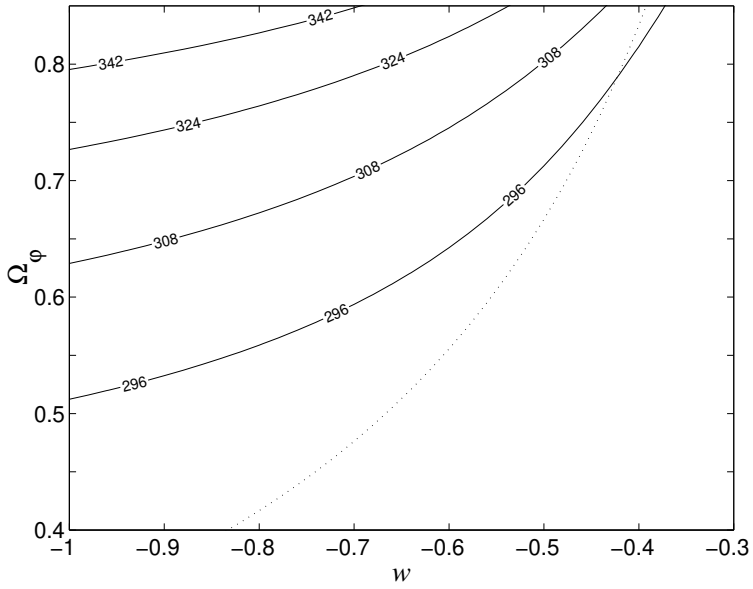

Figure 6.10: Lines of constant l_A in the Ω_0^φ-$\bar{w}_0$ plane, for $h = 0.6$. All universes to the left of the dotted line are accelerating. For larger values of h, the l_A lines are shifted north-west.

Some inflationary models indeed connect the smallness of primordial density fluctuations to $n = 1.1$–1.15 [78]. Increasing n increases the amount of dark energy allowed during structure formation. For $n = 1.1$, the LKT model with 10% quintessence at last scattering becomes feasible.

The IPL model (Fig. 6.9) with $\alpha = 2$ is disfavored, with higher values of α even worse, but $\alpha = 1$ survives. Of course IPL models with $\alpha < 1$ provide a better fit to the data, however for $\alpha \to 0$ IPL approaches the cosmological constant and the problem of naturalness becomes more and more severe (with possible exceptions [41]). Similar conclusions on the IPL model have been derived from the 1998 BOOMERANG data [35], but only for fixed $h = 0.65$. We see from our figures that the results can be very sensitive to changes in h.

A flat universe is accelerating today if the dark energy component and its equation of state satisfy

$$\Omega_0^\varphi \, w_0 < -\frac{1}{3}. \tag{6.24}$$

Assuming that there is no significant dark energy component at last scattering, we can combine our constraints on l_A with Equation (6.6). Fig 6.10 shows that provided $h > 0.6$, the CMB now gives strong evidence for an accelerating universe, independently of supernovae data.

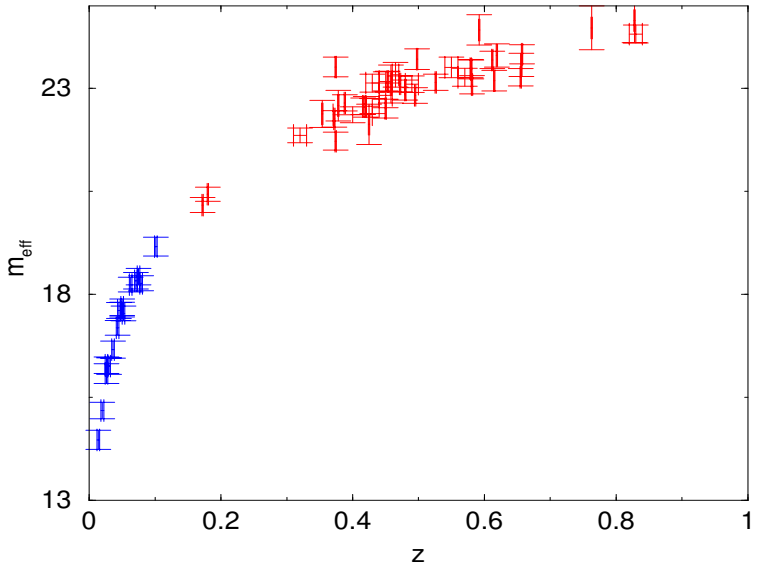

Figure 6.11: Effective magnitudes $m_{\mathrm{B}}^{\mathrm{eff}}$ of low (blue, $z < 0.18$, from [82]) and high (red, $z > 0.18$, from [84]) redshift SNe Ia as a function of z.

6.5 Supernovae Ia

Astronomers use the so called *distance ladder* to determine the distance of some far away object. If one knows by some means the distance of an object one can in principle determine the distance of any other object by measuring the flux of incoming photons, *provided* both objects are equally bright. Unfortunately, one cannot just enter some spaceship, fly to the two objects in question and measure their brightness.[11] Therefore, astronomers make the educated guess that two similar objects should be similarly bright.

When looking into the deep universe, photon fluxes get low and only bright objects can be used to calibrate distances. Among the brightest objects are supernovae, exploding stars. And among supernovae is a class called Type Ia, which look quite similar. Using an empirical correction factor, SNe Ia seem to become *standard candles*. They therefore are an ideal tool to measure redshift versus distance, provided they really are standard candles.[12]

SNe Ia data is usually quoted by the effective magnitude $m_{\mathrm{B}}^{\mathrm{eff}}$ versus redshift z (see figure 6.11). The effective magnitude can be expressed as

$$m_{\mathrm{B}}^{\mathrm{eff}} = \mathcal{M}_B + 5\mathrm{lg}\mathcal{D}_{\mathrm{L}}(\mathrm{z}), \tag{6.25}$$

[11] This, indeed would be the golden age of astronomy

[12] The universe at redshift $z \approx 1$ was much younger and there are still doubts possible whether different environmental conditions could have influenced SNe Ia such that they explode differently at low and high redshift.

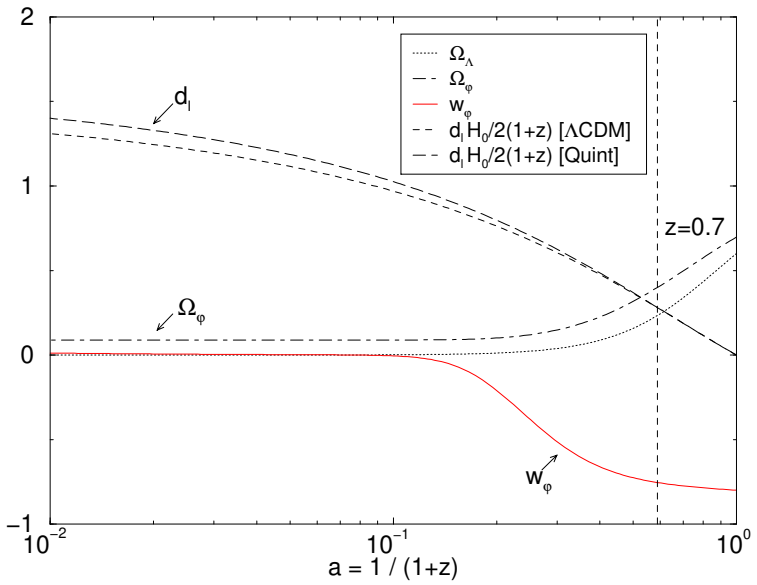

Figure 6.12: The luminosity distance $d_l(z)$ (plotted as $d_l(z)H_0/2(1+z)$) and $\Omega(z)$ for a ΛCDM and a LKT universe with $\Omega_\Lambda^0 = 0.6$ and $\Omega_0^\varphi = 0.7$ respectively. The equation of state $w_\phi(z)$ of the LKT quintessence is also given. For low redshift, the equation of state is close to -1, $w_0 = -0.8$. For $w_0 \left[\Omega_0^\varphi\right]^{1.4} = \Omega_\Lambda^0$, the luminosity distance of both LKT and ΛCDM fall on top of each other in the redshift region relevant for current SN Ia analysis (two upper most curves). Despite the similar late time behaviour, the LKT model has $\Omega^\varphi \approx 0.1$ from very early times on, whereas in the cosmological constant model, dark energy plays a role only recently.

where $\mathcal{D}_L(z)$ is just the *luminosity distance*

$$d_L(z) = (1+z)\int_0^z H^{-1}(z')\mathrm{d}z', \tag{6.26}$$

times the Hubble parameter today:

$$\mathcal{D}_L(z) = H_0 d_L(z). \tag{6.27}$$

In practice, $\mathcal{M}_B$ is calibrated by fitting $m_\mathrm{B}^\mathrm{eff}$ of some given model to the low redshift data of SNe Ia [82]. With the so fixed $\mathcal{M}_B$, one predicts $m_\mathrm{B}^\mathrm{eff}$ for the high redshift SNe Ia and determines the goodness of the fit.

Now, the universe at redshift $z = 0\ldots 2$ can be well described by a mixture of quintessence and matter. By simply using the Friedmann equation (2.7), on gets

$$\left(\frac{H}{H_0}\right)^2 = (1-\Omega_0^\varphi)a^{-3} + \Omega_0^\varphi a^{-3(1+\bar{w}_\varphi)}, \tag{6.28}$$

for an equation of state $\bar{w}_\varphi$ that has been averaged over the redshift range in question and should generically be close to $\bar{w}_0^\varphi$. Inserting Equation (6.28) in (6.26),

yields

$$\begin{aligned}(1+z)^{-1}\mathcal{D}_L &= (1+z)^{-1}H_0 d_L \\ &= \int_0^z \mathrm{d}z' \left\{(1-\Omega_0^\varphi)a^{-3} + \Omega_0^\varphi a^{-3(1+\bar{w}_\varphi)}\right\}^{-\frac{1}{2}}. \end{aligned} \tag{6.29}$$

It is hence the integral (6.29) that determines solely whether a given quintessence model fits the data or not, provided the equation of state doesn't change too drastically.[13] Unfortunately, there is no closed expression for the integral. However, $(1+z)^{-1}\mathcal{D}_L$ is to very good accuracy described by a straight line in the variable

$$x \equiv \bar{w}_\varphi \left[\Omega_0^\varphi\right]^{1.4}, \tag{6.30}$$

at fixed redshift $z \in [0.35, 0.7]$:

$$(1+z)^{-1}\mathcal{D}_L \approx g_0(z) + x g_1(z). \tag{6.31}$$

As most of the SNe Ia data is in this redshift region, one is led to conclude that dark energy models that have the same $\bar{w}_\varphi \left[\Omega_0^\varphi\right]^{1.4}$ are indistinguishable by current SNe Ia measurements. This degeneracy is the subject of many publications that try to quantify the possibilities to measure the dark energy equation of state by a future SNe Ia sattelite mission [19,58,83]. SNe Ia measurements have been extensively used to restrict dark energy models [21,40,58,59,84–87]. A cosmological constant is restricted to $\Omega_\Lambda \in [0.5, 0.9]$ at 2σ confidence level [84,85]. Using the relation (6.30) this bound on Ω_Λ can easily be translated into one on $\bar{w}_\varphi$ and Ω_0^φ.

$$-0.86\left[\Omega_0^\varphi\right]^{-1.4} < \bar{w}_\varphi < -0.38\left[\Omega_0^\varphi\right]^{-1.4}. \tag{6.32}$$

For the inverse power law model, where $\bar{w}_\varphi = -2/(\alpha+2)$, this gives $\Omega_0^\varphi > 0.3(\alpha+2)^{5/7}$, i.e. assuming that $\Omega_0^\varphi < 0.8$, we have $\alpha < 1.9$ (see also [40]). This is comparable to our CMB and LSS constraint of section 6.4. On the other hand, leaping kinetic term models can be consistent with SNe Ia and nevertheless differ substantially from cosmological constant scenarios for the CMB and LSS (see figure 6.12). For these models, the CMB+LSS and the SNe Ia constraints are not directly related and cannot easily be compared.

6.6 Structure formation

The influence of quintessence on the growth of structure has been discussed in [28, 77,89–92]. In a CDM universe without dark energy, cold dark matter perturbations are not growing[14] within the horizon during the radiation dominated regime. Only from matter-radiation equality on, cdm fluctuations within the horizon start to grow.

[13] Examples for possible pitfalls with drastically changing equations of state can be found in [88].

[14] The statements on perturbations in this section are valid in synchronous gauge.

Quintessence has roughly two main effects on this picture [91,92]: firstly, from the definition of $a_{\rm eq}$ (2.41), one sees that $a_{\rm eq}$ gets shifted. This is due to the fact that whereas in a universe without quintessence, $\Omega_0^{\rm c} \approx 0.9$, one has including quintessence $\Omega_0^{\rm c} \approx 1 - \Omega_0^{\varphi}$. Therefore, structure growth starts *later* in a universe with substantial Ω_0^{φ}. The second main effects is a decrease in the growth exponent for cdm fluctuations: the more dark energy present at some epoch, the more slowly structure grows. In [91,92] the useful formula

$$\frac{\sigma_8(\varphi)}{\sigma_8(\Lambda)} = a_{\rm eq}^{3\bar{\Omega}_{\rm sf}^{\varphi}/5} \left(1 - \Omega_0^{\Lambda}\right)^{-(1+\bar{w}^{-1})/5} \sqrt{\frac{\tau_0(\varphi)}{\tau_0(\Lambda)}}, \tag{6.33}$$

relates the rms-fluctuations on scales of $8h^{-1}\,$Mpc of any quintessence model to a model with a cosmological constant, where $\Omega_0^{\varphi} = \Omega_0^{\Lambda}$. In the above, $\bar{\Omega}_{\rm sf}$ and $\bar{w}$ are suitably defined averages [91,92]. The usefulness of Equation (6.33) lies in the fact that if one knows $\sigma_8(\Lambda)$ (say, from a data base), then one can estimate $\sigma_8(\varphi)$ from the knowledge of the background evolution only. We use this in the likelihood part of CMBEASY to give a quick (two orders of magnitude faster than normal) estimate of likelihoods.

Applying Press-Schechter Theory to quintessence scenarios, cluster abundance constraints yield the useful relation (6.23) derived in [77]. For any quintessence model, the normalization of the fluctuations via the CMB predicts a certain value of σ_8. Relation (6.23) then determines whether this value of σ_8 is compatible with cluster abundances or not.

7

Quantum Loop Corrections

The evolution of the quintessence scalar field is usually treated at the classical level. However, quantum fluctuations may alter the classical quintessence potential. We will in the following investigate one-loop contributions both from quintessence and fermion fluctuations to the effective potential. We[1] will show that in the late universe, quintessence fluctuations are harmless for most of the potentials used in the literature. For inverse power laws and SUGRA inspired models, this has already been demonstrated in [34]. Also, it has been noted in [94,95], that the mass of the quintessence field needs to be protected by some symmetry. In contrast to the rather harmless quintessence field fluctuations, fermion fluctuations severely restrict the magnitude of a possible coupling of quintessence to fermionic dark matter, as we will show.

In Euclidean conventions, the action we use for the quintessence field Φ and a fermionic species Ψ to which it may couple [4,71,101] is

$$S = \int d^4x \, \sqrt{g} \Bigg[\mathrm{M}_{\mathrm{P}}^2 R + \frac{1}{2} \partial_\mu \Phi(x) \partial^\mu \Phi(x) + V(\Phi(x)) + \bar{\Psi}(x) \left[i \not{\nabla} + \gamma^5 m_{\mathrm{f}}(\Phi) \right] \Psi(x) \Bigg], \quad (7.1)$$

with $m_{\mathrm{f}}(\Phi)$ as a Φ dependent fermion mass. This Φ dependence (if existent in a model) determines the coupling of the quintessence field to the fermions. As long as one is not interested in quantum gravitational effects, one may set $\sqrt{g} = 1$, $R = 0$ and replace $\not{\nabla} \to \not{\partial}$ in the action (7.1).

By means of a saddle point expansion [96], we arrive at the effective action $\Gamma[\Phi_{\mathrm{cl}}]$ to one loop order of the quintessence field. The equation governing the dynamics of the quintessence field is then determined by $\delta\Gamma[\Phi_{\mathrm{cl}}]_{|\Phi_{\mathrm{cl}}=\Phi_{\mathrm{cl}}^\star} = 0$. When estimating the magnitude of the loop corrections, we will assume that $\Phi_{\mathrm{cl}}^\star$ is close to the solution of the classical field equations: $\delta S = 0$. Evaluating Γ for constant fields, we can factor out the space-time volume U from $\Gamma = UV$. This gives the

[1] This chapter is based on work in collaboration with Jörg Jäckel [93].

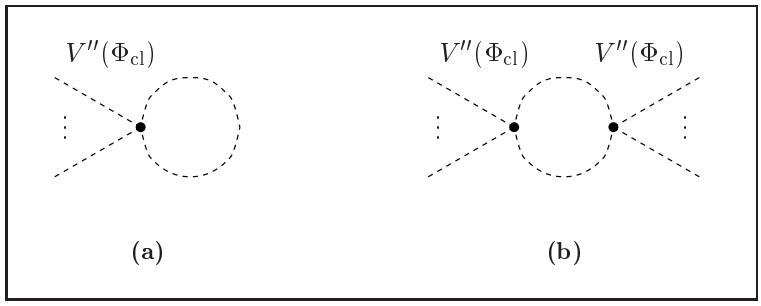

Figure 7.1: Pure quintessence fluctuations (depicted as dashed lines). The loop of the fluctuating quintessence field modifies the potential. Since the potential involves in principle arbitrary powers of Φ, we depict V'' as multiple external lines.

effective potential

$$V_{\text{1-loop}}(\Phi_{\rm cl}) = V(\Phi_{\rm cl}) + \frac{\Lambda^2}{32\pi^2}\, V''(\Phi_{\rm cl}) - \frac{\Lambda_{\rm ferm}^2}{8\pi^2}\left[m_{\rm f}(\Phi_{\rm cl})\right]^2 . \tag{7.2}$$

Here, primes denote derivatives with respect to Φ; $\Phi_{\rm cl}$ is the classical field value and Λ and $\Lambda_{\rm ferm}$ are the ultra violet cutoffs of scalar and fermion fluctuations. The second term in Equation (7.2), is the leading order scalar loop, depicted in figure 7.1(a). We neglect graphs of the order $(V''_{|\rm cl})^2$ and higher like the one in figure 7.1(b), because V and its derivatives are of the order 10^{-120} (see section 7.2). We have also ignored Φ-independent contributions, as these will not influence the quintessence dynamics.

However, the Φ-independent contributions add up to a cosmological constant of the order $\Lambda^4 \approx \mathcal{O}(\mathrm{M_P^4})$. This is the old cosmological constant problem, common to most field theories. We hope that some symmetry[2] or a more fundamental theory will force it to vanish. The same symmetries or theories could with the same right remove the loop contribution by some cancelling mechanism. After all, this mechanism must be there, for the observed cosmological constant is far less than the naively calculated $\mathcal{O}(\mathrm{M_P^4})$.

Besides, none of the potentials under investigation can be renormalized in the strict sense. However, as we will see, terms preventing renormalization may in some cases be absent to leading order in $V''_{|\rm cl}$. As the mass of the quintessence field is extremely small, one may for all practical purposes view these specific potentials (such as the exponential potential) as renormalizable.

There is also a loophole for all models that will be ruled out in the following: The potential used in a given model could be the full effective potential including all quantum fluctuations, down to macroscopic scales. For coupled quintessence models, this elegant argument is rather problematic and the loophole shrinks to a

[2]Unfortunately, SUSY is too badly broken to be this symmetry [94].

point (see section 7.2).

In the following, we apply Equation (7.2) to various quintessence models in order to check their stability against one loop corrections. We do this separately for coupled and uncoupled models. We use units in which $\mathrm{M_P} = 1$. For clarity, we restore it when appropriate.

7.1 Uncoupled Quintessence

Here, we are going to discuss inverse power law, pure and modified exponential and cosine-type potentials.

7.1.1 Inverse power law and exponential potentials

Inverse power law [7,5] and exponential potentials [6,28] and mixtures of both [38] can be treated by considering the potential (2.25). Deriving V from Equation (2.25) twice with respect to Φ, we find

$$V'' = A\Phi^{-\alpha}\exp(-\lambda\Phi^{\gamma})\Big\{\alpha(\alpha+1)\Phi^{-2} + 2\alpha\lambda\gamma\Phi^{\gamma-2} + \lambda^2\gamma^2\Phi^{2\gamma-2} - \lambda\gamma(\gamma-1)\Phi^{\gamma-2}\Big\}. \quad (7.3)$$

Inverse Power Laws

For inverse power laws, we set $\gamma = \lambda = 0$. This gives the classical potential $V_{\mathrm{cl}}^{\mathrm{IPL}} = A\Phi_{\mathrm{cl}}^{-\alpha}$ and by means of Equation (7.2) the loop corrected potential

$$V_{\text{1-loop}}^{\mathrm{IPL}} = V_{\mathrm{cl}}^{\mathrm{IPL}}\left(1 + \frac{1}{32\pi^2}\,\Lambda^2\alpha(\alpha+1)\Phi_{\mathrm{cl}}^{-2}\right). \quad (7.4)$$

The potential is form stable if $\frac{1}{32\pi^2}\,\Lambda^2\alpha(\alpha+1)\Phi^{-2} \ll 1$, which today is satisfied, as $\Phi \approx \mathrm{M_P}$ [38].

However, if the field is on its attractor today, then $\Phi \propto (1+z)^{-3/(\alpha+2)}$, where z is the redshift [38]. Using this, we have for $z \gg 1$

$$V_{\text{1-loop}}^{\mathrm{IPL}} \approx V_{\mathrm{cl}}^{\mathrm{IPL}}\left(1 + \frac{1}{32\pi^2}\,\Lambda^2\alpha(\alpha+1)z^{6/(\alpha+2)}\right). \quad (7.5)$$

Thus, the cutoff needs to satisfy $\Lambda^2 \ll \frac{32\pi^2}{\alpha(\alpha+1)} \times z^{-6/(\alpha+2)}$. From section 6.4, we know that cosmologically viable inverse power law potentials seem to be restricted to $\alpha < 2$ (see also [35,36]). Using $\alpha = 1$ and $z \approx 10^4$ for definiteness, the bound becomes $\Lambda^2 \ll 10^{-6}$.

So at equality (and even worse before that epoch), the cutoff needs to be well below 10^{12} Gev, if classical calculations are meant to be valid. In [34] it is argued that for inverse power laws, the quintessence content in the early universe is negligible and hence the fluctuation corrections are important only at an epoch

where quintessence is subdominant. As the loop corrections introduce only higher negative powers in the field, it is hoped that even though one does not know the detailed dynamics, the field will nevertheless roll down its potential (which at that time is supposed to be much steeper) and by the time it is is cosmologically relevant, the classical treatment is once again valid. Having no means of calculating the true effective potential for the inverse power law in the early universe, this view is certainly appealing.

Pure Exponential Potentials

The pure exponential potential is special because its derivatives are multiples of itself. The classical potential (with $\alpha = 0,\ \gamma = 1$) is $V_{\rm cl}^{\rm EP} = A\exp(-\lambda\Phi_{\rm cl})$ and to one loop order

$$V_{\text{1-loop}}^{\rm EP} = V_{\rm cl}^{\rm EP}\left\{1 + \frac{1}{32\pi^2}\,\Lambda^2\lambda^2\right\}. \tag{7.6}$$

It is easy to see that a rescaling of $A \to A/\left(1 + \frac{1}{32\pi^2}\,\Lambda^2\lambda^2\right)$ absorbs the loop correction, leading to a stable potential up to order $V_{\rm cl}''$. Working to next to leading order, i.e restoring terms of order $(V_{\rm cl}'')^2$ we get

$$V_{\text{1-loop, n.l.}}^{\rm EP} = \frac{1}{32\pi^2}\left(V_{\rm cl}''\right)^2 \ln\left(\frac{V_{\rm cl}''}{\Lambda^2}\right).$$

It is this term which in four dimensions spoils strict renormalizability.

7.1.2 Nambu-Goldstone Cosine Potentials

Cosine type potentials resulting from an quintessence axion have been introduced in [97,98] and their implications on the CMB have been studied in [99]. They take on the classical potential $V_{\rm cl}^{\rm NG} = A\left[1 - \cos\left(\Phi_{\rm cl}/f_Q\right)\right]$ and including loop corrections

$$V_{\text{1-loop}}^{\rm AS} = A\left[1 - \left\{1 - \frac{1}{32\pi^2}\,\frac{\Lambda^2}{f_Q^2}\right\}\cos\left(\frac{\Phi_{\rm cl}}{f_Q}\right)\right].$$

Upon a redefinition $A \to A/\left\{1 - \frac{1}{32\pi^2}\,\frac{\Lambda^2}{f_Q^2}\right\}$ and recalling that the loop correction is only defined up to a constant, one arrives at the same functional form as the classical potential.

7.1.3 Modified Exponentials

In the model proposed by Albrecht and Skordis [33], the classical potential is $V_{\rm cl}^{\rm AS} = V_p\exp(-\lambda\Phi_{\rm cl})$, where V_p is a polynomial in the field. To one loop order, this leads to

$$V_{\text{1-loop}}^{\rm AS} = V_{\rm cl}^{\rm AS}\left\{1 + \frac{1}{32\pi^2}\,\Lambda^2\left(\frac{V_p''}{V_p} - 2\lambda\,\frac{V_p'}{V_p} + \lambda^2\right)\right\}. \tag{7.7}$$

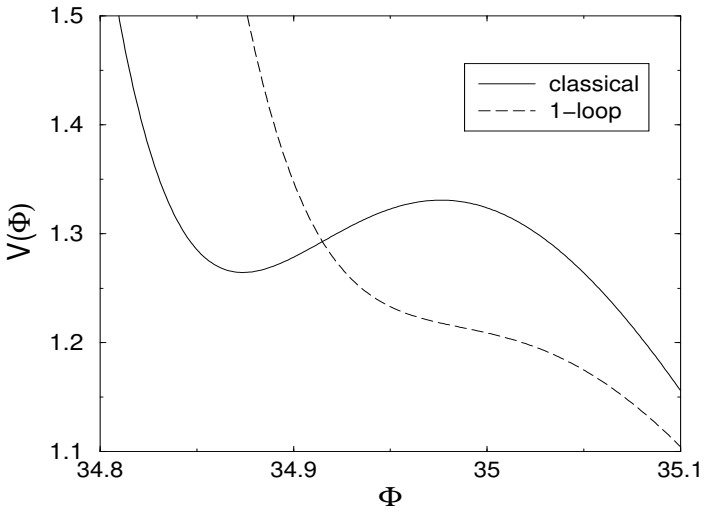

Figure 7.2: Classical and 1-loop corrected potential [in $10^{-123}\mathrm{M_P^4}$] for $V_{\mathrm{cl}}^{\mathrm{AS}} = \left[(\Phi - B)^2 + C\right] \exp(-\lambda\Phi_{\mathrm{cl}})$ with $B = 34.8$, $C = 0.013$, $\Lambda = 1.2$. The classical potential has a local minimum, which is absent for the loop corrected one. This is a hand-picked example and in most cases, the bump will not vanish but move and change its form.

Let us for definiteness discuss the example given in [33], where the authors chose $V_p(\Phi) = (\Phi - B)^2 + C$. With this choice, we have

$$V_{\text{1-loop}}^{\text{AS, EXMPL}} = V_{\mathrm{cl}}^{\text{AS, EXMPL}} \times \left\{1 + \frac{1}{32\pi^2}\,\Lambda^2 \Big(\frac{1}{V_p}\left[2 - 4\lambda(\Phi_{\mathrm{cl}} - B)\right] + \lambda^2 \Big) \right\}. \quad (7.8)$$

Now consider field values close to the minimum of V_p, i.e. let the absolute value of $\xi \equiv \Phi_{\mathrm{cl}} - B$ be small compared to $\sqrt{C}$. Then

$$V_{\text{1-loop}}^{\text{AS, EXMPL}} = V_{\mathrm{cl}}^{\text{AS, EXMPL}} \left\{1 + \frac{\Lambda^2}{32\pi^2} \left(\frac{2 - 4\lambda\xi}{C + \xi^2} + \lambda^2 \right) \right\}, \quad (7.9)$$

and to leading order in ξ

$$V_{\text{1-loop}}^{\text{AS, EXMPL}} \approx V_{\mathrm{cl}}^{\text{AS, EXMPL}} \left\{1 + \frac{\Lambda^2}{32\pi^2} \left(\frac{1}{C}\left[2 - 4\lambda\xi\right] + \lambda^2 \right) \right\}. \quad (7.10)$$

Now consider, as has been the case in the example given in [33], $C = 0.01$ for definiteness. If we assume the cutoff Λ and the Plank mass of approximately the same order, we get

$$V_{\text{1-loop}}^{\text{AS, EXMPL}} \approx V_{\mathrm{cl}}^{\text{AS, EXMPL}} \left\{1 + \frac{1}{32\pi^2} \left(100\left[2 - 4\lambda\xi\right] + \lambda^2 \right) \right\}. \quad (7.11)$$

The ξ (and hence $\Phi_{\rm cl}$) dependent contribution in the curly bracket of Equation (7.11) is $-25/(2\pi^2)\lambda\xi$ which for the value $\lambda = 8$ chosen in the example gives $-200/(2\pi^2)\xi \approx -10\xi$.

If we now look at the behaviour of the loop correction as a function of $\Phi_{\rm cl}$ and hence ξ in the vicinity of the minimum of this example polynomial, we see that for e.g. $\xi = 0.01$, the one loop contribution dominates the classical potential giving rise to a linear term in $\Phi_{\rm cl}$ unaccounted for in the classical treatment. For many values of the parameters B and C, this just changes the form and location of the bump in the potential. In principle, however the loop correction can remove the local minimum altogether (see figure 7.2).

Needless to say that this finding depends crucially on the cutoff. If it is chosen small enough, the conclusion is circumvented. In addition, only the specific choice of V_p above has been shown to be potentially unstable. The space of polynomials is certainly large enough to provide numerous stable potentials of the Albrecht and Skordis form.

7.2 Coupled Quintessence

Various models featuring a coupling of quintessence to some form of dark matter have been proposed [11,30,71,100,101]. From the action Equation (7.1), we see that the mass of the fermions could be Φ dependent: $m_{\rm f} = m_{\rm f}(\Phi_{\rm cl})$ (see also Figure 7.3). Two possible realization of this mass dependence are for instance $m_{\rm f} = m_{\rm f}^0 \exp(-\beta\Phi_{\rm cl})$ and $m_{\rm f} = m_{\rm f}^0 + c(\Phi_{\rm cl})$, where in the second case, we may have a large field independent part together with small couplings to quintessence.[3] For the model discussed in [71], the coupling is of the first form, whereas in [101], the coupling is realized by multiplying the cold dark matter Lagrangian by a factor $f(\Phi)$. This factor is usually taken of the form $f(\Phi) = 1 + \alpha(\Phi - \Phi_0)^\beta$. Hence, the coupling is $m_{\rm f}(\Phi) = f(\Phi)\, m_{\rm f}^0$, if we assume that dark matter is fermionic. If it were bosonic, the following arguments would be similar.

We will first discuss general bounds on the coupling and in a second step check whether these bounds are broken via an effective gravitational coupling.

7.2.1 General Bounds on a Coupling

We will only discuss the new effects coming from the coupling and set

$$V_{\text{1-loop}} = V_{\rm cl} - \Delta V, \tag{7.12}$$

where $\Delta V = \Lambda_{\rm ferm}^2 \left[m_{\rm f}(\Phi_{\rm cl})\right]^2 / \left(8\pi^2\right)$. If we assume that the potential energy of the quintessence field constitutes a considerable part of the energy density of the universe today, i.e. $\rho_{\rm q} \sim \rho_{\rm critical}$, we see from the Friedman equation

$$3H^2 = \rho_{\rm critical}, \tag{7.13}$$

[3] The constant $m_{\rm f}^0$ is *not* the fermion mass today, which would rather be $m_{\rm today} = m_{\rm f}(\Phi_{\rm cl}(\text{today}))$.

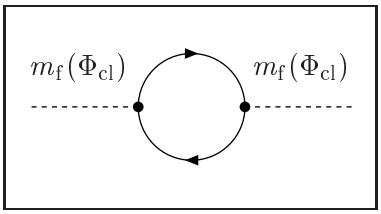

Figure 7.3: Correction to the quintessence potential due to fermion fluctuations. Fermion lines are solid, quintessence lines dashed. Shown is the case where $m_f(\Phi)$ gives a Yukawa coupling, i.e. $c(\Phi) = \beta\Phi$, corresponding to one quintessence line. Of course, for more complicated $m_f(\Phi)$ such as $m_f(\Phi_{cl}) = m_f^0 \exp(-\beta\Phi_{cl})$, several external lines like in figure 7.1 would appear.

that $V_{cl} \sim H^2$. With todays Hubble parameter $H = 8.9 \times 10^{-61}\, h$ ($h = 0.5 \ldots 0.9$), we have

$$V_{cl} \sim 7.9 \times 10^{-121}\, h^2. \tag{7.14}$$

The ratio of the 'correction' to the classical potential is

$$\frac{\Delta V}{V_{cl}} = \frac{1}{8\pi^2} \frac{\Lambda_{ferm}^2 \left[m_f(\Phi_{cl})\right]^2}{V_{cl}}\,. \tag{7.15}$$

Let us first consider the case that all of the fermion mass is field dependent, i.e. we consider cases like $m_f = m_f^0 \exp(-\beta\Phi_{cl})$. As an example, we choose a fermion cutoff at the GUT scale $\Lambda_{ferm} = 10^{-3}$, and a fermion mass, $m_f(\Phi_{cl})$ of the order of $100\,\mathrm{Gev} = 10^{-16}\mathrm{M_P}$. Then Equation (7.15) gives the overwhelmingly large ratio

$$\frac{\Delta V}{V_{cl}} \approx 10^{80}. \tag{7.16}$$

Thus, the classical potential is negligible relative to the correction induced by the fermion fluctuations.

Having made this estimate, it is clear that the fermion loop corrections are only harmless, if the square of the coupling takes on *exactly* the same form as the classical potential itself. If, for example we have an exponential potential $V_{cl} = A \exp(-\lambda\Phi_{cl})$ together with a coupling $m_f(\Phi_{cl}) = m_f^0 \exp(-\beta\Phi_{cl})$, then this coupling can only be tolerated, if $2\beta = \lambda$.[4] Taken at face value, this finding restricts models with these types of coupling. It is however interesting to note that for the exponential coupling, the case $2\beta = \lambda$ is not ruled out by cosmological observations [30].

Turning to the possibility of a fermion mass that consists of a field independent part and a coupling, i.e. $m_f = m_f^0 + c(\Phi_{cl})$, Equation (7.15) becomes

$$\frac{\Delta V}{V_{cl}} = \frac{1}{8\pi^2} \frac{\Lambda_{ferm}^2 \left[2m_f^0 c(\Phi_{cl}) + c(\Phi_{cl})^2\right]}{V_{cl}}\,, \tag{7.17}$$

[4] Of course, sufficiently small β, will lead to a more or less constant contribution, where $m_f(\Phi_{cl}) \approx m_f^0 - \beta\Phi_{cl}$.

where we have ignored a quintessence field independent contribution proportional to $(m_{\mathrm{f}}^0)^2$. Assuming $c(\Phi_{\mathrm{cl}}) \ll m_{\mathrm{f}}^0$, and demanding that the loop corrections should be small compared to the classical potential, Equation (7.17) yields the bound

$$c(\Phi_{\mathrm{cl}}) \ll \frac{4\pi^2\, V_{\mathrm{cl}}}{\Lambda_{\mathrm{ferm}}^2 m_{\mathrm{f}}^0}\,. \tag{7.18}$$

If, as above, we assume $\Lambda_{\mathrm{ferm}} = 10^{-3}\mathrm{M_P}$, $m_{\mathrm{f}}^0 = 10^{-16}\mathrm{M_P}$ and V_{cl} from Equation (7.14), this gives

$$c(\Phi_{\mathrm{cl}}) \ll 3 \times 10^{-97}, \tag{7.19}$$

in units of the Planck mass. Once again, the bound from Equation (7.18) only applies if the functional form of the loop correction differs from the classical potential. Assuming a Yukawa type coupling $c(\Phi_{\mathrm{cl}}) = \beta\Phi_{\mathrm{cl}}$ and field values of at least the order of a Plank mass, we get $\beta \ll 10^{-97}$.

For the coupling $c(\Phi) = m_{\mathrm{f}}^0\alpha(\Phi-\Phi_0)^\beta$ with the values $\alpha = 50$, $\beta = 8$, $\Phi_0 = 32.5$ given in [101], $c(\Phi)$ is usually larger than m_{f}^0. Therefore we take $m_{\mathrm{f}}(\Phi_{\mathrm{cl}}) \approx c(\Phi_{\mathrm{cl}})$. With $m_{\mathrm{f}}(\Phi_{\mathrm{cl}}) = 10^{-16}$ as before, we get the same result as in (7.16).

The coupled models share one property: the loop contribution from the coupling is by far larger than the classical potential. At first sight, the golden way out of this seems to view the potential as already effective: all fluctuations would be included from the start. However, there is no particular reason, why *any* coupling of quintessence to dark matter should produce just exactly *the* effective potential used in a particular model: there is a relation between a coupling and the effective potential generated. Put another way, *if* the effective potential is of an elegant form and we have a given coupling, then it seems unlikely that the *classical* potential could itself be elegant or natural.

7.2.2 Effective gravitational Fermion Quintessence Coupling

The bound in Equation (7.18) is so severe that the question arises whether gravitational coupling between fermions and the quintessence field violates it. To give an estimate, we calculate two simple processes depicted in figure 7.4. We evaluate the diagrams for vanishing external momenta. This is consistent with our derivation of the fermion loop correction Equation (7.2), in which we have assumed momentum independent couplings. The effective coupling due to the graviton exchange contributes to the fermion mass, which becomes Φ_{cl} dependent. We assume that this coupling is small compared to the fermion mass and write $m_{\mathrm{f}}(\Phi_{\mathrm{cl}}) = m_{\mathrm{f}}^0 + c(\Phi_{\mathrm{cl}})$.

Fermions in general relativity are usually treated within the tetrad formalism. The γ matrices become space-time dependent: $\gamma^\mu(x) \equiv \gamma^a e_a^\mu(x)$. Together with the spin connection ω, one uses (see e.g. [102], [103]):

$$\not{\nabla} = e_a^\mu(x)\gamma^a \left(\partial_\mu + \frac{i}{4}\,\sigma_{bc}\omega_\mu^{bc}\right). \tag{7.20}$$

The action (7.1) can then be expanded in small fluctuations around flat space: $g_{\mu\nu} = \delta_{\mu\nu} + h_{\mu\nu}/\mathrm{M_P}$.

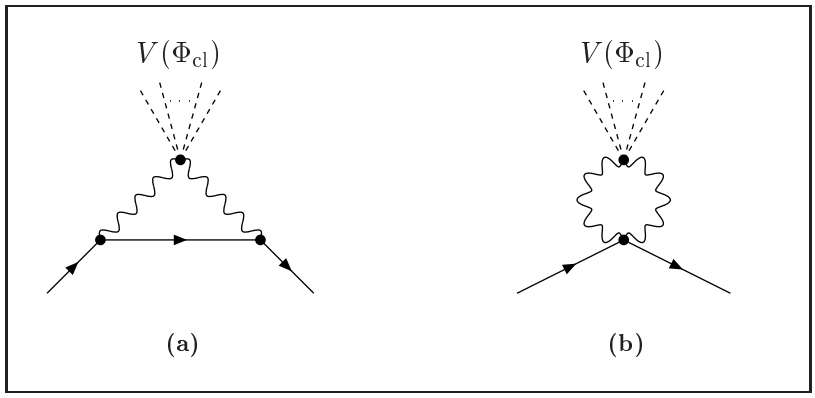

Figure 7.4: Effective fermion-quintessence coupling via graviton exchange. The fermions (solid lines) emit gravitons (wiggled lines) which are caught by the quintessence field (dashed lines). As the graphs involve couplings of the gravitons to the classical quintessence potential, the generated coupling is proportional to the classical potential. Since the potential involves arbitrary powers of Φ, we depict it as several Φ-lines. A Yukawa type coupling, corresponding to just one line, is then generated by power expanding $V(\Phi) = V(\Phi_{\rm cl}) + V'_{|{\rm cl}}(\Phi - \Phi_{\rm cl})$ in the fluctuating field.

Using the gauge fixing term $-\frac{1}{2}(\partial^\nu h_{\mu\nu} - \frac{1}{2}\partial_\mu h^\nu_\nu)^2$ and expanding the action to second order in h, we find the propagator [103]:

$$P^{-1}_{\rm grav}(k) = \frac{\delta_{\mu\alpha}\delta_{\nu\beta} + \delta_{\mu\beta}\delta_{\nu\alpha} - \delta_{\mu\nu}\delta_{\alpha\beta}}{k^2}\,. \tag{7.21}$$

The diagrams in figure 7.4 are generated by the expansion of $\sqrt{g} = 1 + \frac{1}{2}h^{\mu\mu} - \frac{1}{4}(h^{\mu\nu})^2 + \frac{1}{8}(h^{\mu\mu})^2$ multiplying the matter Lagrangian. Additional (and more complicated) vertices originate from the spin connection and the tetrad.

However, we don't consider external graviton lines, which would only give corrections to the couplings and wave function renormalization of the gravitons. Therefore only internal gravitons appear. In order to contribute a quintessence dependent part to the fermion mass, the gravitons starting from the fermion-graviton vertices (complicated as they may be) have to touch quintessence-graviton vertices. As these quintessence vertices are proportional to $V(\Phi_{\rm cl})$, all diagrams to lowest order in $V(\Phi_{\rm cl})$ will only produce mass contributions proportional to $V(\Phi_{\rm cl})$.

Evaluating the diagrams in figure 7.4 for vanishing external momenta we get from the first diagram, figure 7.4(a)

$$c(\Phi_{\rm cl}) = \frac{1}{8\pi^2}\, m_{\rm f}^0 V(\Phi_{\rm cl}) \left[\ln\left(\frac{\Lambda^2}{\Lambda^2 + \left[m_{\rm f}^0\right]^2}\right) - \ln\left(\frac{\lambda^2}{\lambda^2 + \left[m_{\rm f}^0\right]^2}\right)\right], \tag{7.22}$$

whereas 7.4(b) gives

$$c(\Phi_{\rm cl}) = \frac{5}{8\pi^2}\, m_{\rm f}^0 V(\Phi_{\rm cl}) \ln\left(\frac{\Lambda}{\lambda}\right). \tag{7.23}$$

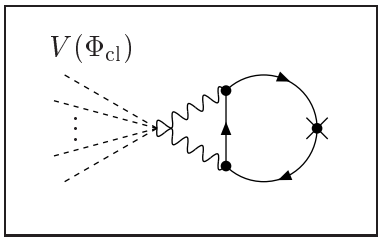

Figure 7.5: Fermion loop contribution to the quintessence potential involving the effective coupling figure 7.4(a). The cross in the fermion line depicts the field independent fermion mass m_{f}^0.

Here, we have introduced infrared and ultraviolet cutoffs λ and Λ for the graviton momenta. We assume Λ to be of the order $\mathrm{M_P}$ and λ about the inverse size of the horizon. Since the results depend only logarithmically on the cutoffs, this choice is not critical and in addition $\ln(\mathrm{M_P}/H) \approx 140$, which is small. From Equation (7.17, 7.22, 7.23), we see that in leading order, the change in the quintessence potential due to this effective fermion coupling would be proportional to $V(\Phi_{\mathrm{cl}})$ and could hence be absorbed upon redefining the pre-factor of the potential (see also figure 7.5). In next to leading order, the contribution is proportional to $V(\Phi_{\mathrm{cl}})^2$ which is negligible.

From Equation (7.20) it is clear that there are processes where the vertices are more complicated. However, to this order all diagrams are proportional to $V(\Phi_{\mathrm{cl}})$. Thus, they can be absorbed just like the two processes presented above.

7.3 Weyl-transformed Fields

So far, we have assumed a constant Planck mass together with a field independent cutoff. We could however, assume that the Planck mass is not constant, but rather given by the expectation value of a scalar field χ. We will call the frame resulting from this Weyl scaling Weyl frame, opposed to the frame with constant Plank mass which we will call Einstein frame. From the classical point of view, both frames are equivalent. On calculating quantum corrections, we have to evaluate a functional integral. Usually, the functional measure in the Einstein frame is set to unity. In principle, the variable change associated with the Weyl scaling leads to a non-trivial Jacobian and therefore a different functional measure. Taking on the position that the Weyl frame is fundamental, this measure could with the same right be set to unity in the Weyl frame. Therefore, it is a priori unclear whether the loop corrected potential in the Weyl frame, when transformed back into the Einstein frame, will be the same as the one from Equation (7.2).

As the cutoff in the Einstein frame is a constant mass scale and hence proportional to the Plank mass, it seems natural to assume that the cutoff in the Weyl frame is proportional to χ. We restrict our discussion to this case. For other choices

of the χ-dependence of the cutoff, the results may differ.

The Weyl transformation is achieved by scaling the metric, the curvature scalar, all fields and the tetrad by appropriate powers of $\chi/\mathrm{M_P}$ (see table 7.1) [6,11]:

$$\tilde{S} = \int d^4x \sqrt{\tilde{g}} \Bigg[\chi^2 \tilde{R} + \frac{z}{2}\, \partial_\mu \chi \partial^\mu \chi + W(\chi) + \bar{\tilde{\psi}} \left(i\, \tilde{\gamma}^\mu(x) \nabla_\mu + \chi\, \frac{m_\mathrm{f}(\Phi_\mathrm{cl})}{\mathrm{M_P}}\, \gamma^5 - \frac{3}{2}\, i \tilde{\gamma}^\mu(x) \ln \chi_{,\mu} \right) \tilde{\psi} \Bigg], \quad (7.24)$$

where $\Phi = (12+z)^{1/2} \mathrm{M_P} \ln(\chi/\mathrm{M_P})$ and

$$W(\chi) \equiv \left(\frac{\chi}{\mathrm{M_P}} \right)^4 V(\Phi(\chi)). \quad (7.25)$$

The term proportional to $\ln \chi_{,\mu}$ in Equation (7.24) is somewhat inconvenient. Adopting the position that the Weyl frame is fundamental, this term is unnatural. Instead, one would formulate the theory with canonical couplings for the fermions. Dropping this term,

$$\tilde{S}_\mathrm{can.} = \int d^4x \sqrt{\tilde{g}} \Bigg[\chi^2 \tilde{R} + \frac{z}{2}\, \partial_\mu \chi \partial^\mu \chi + W(\chi) + \bar{\tilde{\Psi}} \left(i\, \tilde{\gamma}^\mu(x) \nabla_\mu + \frac{\chi}{\mathrm{M_P}}\, m_\mathrm{f}(\Phi(\chi))\, \gamma^5 \right) \tilde{\Psi} \Bigg], \quad (7.26)$$

we observe by going back to the usual action $\tilde{S}_\mathrm{can.} \to S$

$$S = \int d^4x\, \sqrt{g} \Bigg[\frac{1}{2}\, \partial_\mu \Phi(x) \partial^\mu \Phi(x) + V(\Phi(x)) + \bar{\Psi}(x) \left(i \not{\nabla} + \gamma^5 m_\mathrm{f}(\Phi) + \frac{3}{2\mathrm{M_P}}\, i\, \gamma^\mu(x) \phi_{,\mu} \right) \Psi(x) \Bigg], \quad (7.27)$$

that the canonical form of the action in the Weyl frame gives rise to a derivative coupling of the quintessence field to the fermions in the Einstein frame, which we can safely ignore.[5]

Working with Equation (7.26), we get the loop correction in the Weyl frame by replacing $V \to W$ and $\Phi \to \chi$ in Equation (7.2). In addition, the constant cutoffs Λ and Λ_ferm are replaced by $const \cdot \chi$:

$$W_\text{1-loop} = W(\chi) + \frac{(\mathcal{C}\chi)^2}{32\pi^2\, z^2}\, W''(\chi) - \frac{(\mathcal{C}_\mathrm{f}\chi)^2}{8\pi^2} \left[\frac{\chi}{\mathrm{M_P}}\, m_\mathrm{f}(\chi) \right]^2. \quad (7.28)$$

[5] Actually, this coupling is non-renormalizable in the strict sense. Since the theory is non-renormalizable anyhow, this is not of great concern. In addition, if one believes that the Weyl frame is fundamental, there is no need in going back to the Einstein frame and hence no need to face this nuisance.

$$
\begin{aligned}
g_{\mu\nu} &\to (\chi/\mathrm{M_P})^2\, \tilde{g}_{\mu\nu} \\
g^{\mu\nu} &\to (\chi/\mathrm{M_P})^{-2}\, \tilde{g}^{\mu\nu} \\
\sqrt{g} &\to (\chi/\mathrm{M_P})^4\, \sqrt{\tilde{g}} \\
R &\to (\chi/\mathrm{M_P})^{-2} \left(\tilde{R} - 6\tilde{g}^{\mu\nu}\sigma_{;\mu\nu} - 6\tilde{g}^{\mu\nu}\sigma_{,\mu}\sigma_{,\nu} \right) \\
e^{\mu}_{a}(x) &\to (\chi/\mathrm{M_P})^{-1}\, \tilde{e}^{\mu}_{a}(x) \\
\Psi &\to (\chi/\mathrm{M_P})^{-3/2}\, \tilde{\Psi}
\end{aligned}
$$

Table 7.1: Weyl scaling of various quantities. The transformation of the curvature scalar R follows from the scaling of the metric. This scaling, in turn, originates from the condition that instead of the Plank mass squared multiplying R in the action in the Einstein frame, a factor χ^2 should appear. Here, we have set $\sigma = \ln(\chi/\mathrm{M_P})$.

Transforming $W_{\text{1-loop}}$ back into the Einstein frame, the potential V is modified by

$$
\begin{aligned}
V_{\text{1-loop}} = V(\Phi_{\mathrm{cl}}) + \frac{(\mathcal{C}_{\mathrm{f}}\mathrm{M_P})^2}{8\pi^2}\left[m_{\mathrm{f}}(\Phi_{\mathrm{cl}})\right]^2 + \frac{(\mathcal{C}\mathrm{M_P})^2}{32\pi^2\, z^2} \\
\times \left[12\,\frac{V(\Phi_{\mathrm{cl}})}{\mathrm{M_P^2}} + 7\sqrt{12+z}\,\frac{V'(\Phi_{\mathrm{cl}})}{\mathrm{M_P}} + (12+z)V''(\Phi_{\mathrm{cl}})\right]. \quad (7.29)
\end{aligned}
$$

As an example, lets calculate the correction to the pure exponential potential $V_{\mathrm{cl}}^{\mathrm{EP}} = A\exp(-\lambda\Phi_{\mathrm{cl}})$, once again setting $\mathrm{M_P} = 1$. The Weyl frame potential is

$$
W(\chi) = A\chi^4 \exp(-\lambda\Phi_{\mathrm{cl}}(\chi)) = A\chi^{(4-\lambda\sqrt{12+z})}. \quad (7.30)
$$

Neglecting fermion fluctuations and choosing $z = 1$,

$$
W_{1-\mathrm{loop}} = \left[1 + \frac{\mathcal{C}^2}{32\pi^2\, z^2}\,(4-\lambda\sqrt{13})(3-\lambda\sqrt{13})\right] W(\chi). \quad (7.31)
$$

Again (and not surprisingly) we can absorb the square bracket in a redefinition of the pre-factor A. In the case of the inverse power law, the term proportional to V' in Equation (7.29) leads to a slightly different contribution compared to Equation (7.4) (a term $\propto \Phi_{\mathrm{cl}}^{-\alpha-1}$ arises). For the modified exponential potentials the expressions corresponding to V' in Equation (7.29) make no structural difference.

8

CMBEASY

In chapter 2, 4 and 5, we have reviewed cosmological perturbation theory and the physics of CMB anisotropies. Having all necessary equations at hand[1] , we can thus set out to calculate the CMB spectrum for any cosmological model. Since 1996, the CMBFAST computer code implementing the fast *line of sight* integration method is publicly available. It can calculate spectra for open, closed and flat universes containing massless and massive neutrinos, baryons, cold dark matter and a cosmological constant. It is a very well tested program that has enabled many cosmologists to test their model of the universe against CMB data.

However, from the point of view of code design, there is maybe no program that could not be improved. This is also true for CMBFAST: it is a rather monolithic code that is quite difficult to oversee and modify.

In order to address these shortcomings and simplify modifications of the code – in our case the implementation of quintessence models and gauge invariant variables – we have ported the CMBFAST package to the C++ programming language. The C++ language is *object* oriented and it turns out that to think in objects (more of this soon), is very advantageous in cosmology. The program has not been rewritten from scratch, but redesigned step by step. Some people may argue that it is hence not *independent*, i.e. some unknown errors and limitations in CMBFAST could be present in the new code. The object oriented modular design, however, ensures that each part of the code is independently testable. If, for instance, one does not trust the integrator, one can use another one to check it, without changing anything else in the package. Also, practically all lines in the code *have* been rewritten, to benefit from the redesign.

There are roughly three main steps needed to calculate the CMB anisotropy spectrum,

- solving the expansion and thermal background evolution,
- calculating the perturbation equations in Fourier space,
- mapping the calculations onto the sky today.

[1] The full set of equations used is summarized in Appendix C

Before we present the implementation we chose for this task, let us briefly review the concept of object oriented programming.

8.1 Objects

Quite often, some data and functions acting on the data are so tightly connected, that it is sensible to think of them as one object. As an example, let us discuss splines. Given a discrete set of n points x_i with $x_{i+1} < x_i$ and corresponding $f(x_i) = y_i$, a spline can smoothly interpolate, i.e. give $f(x)$ for any $x \in [x_0, x_n]$. For as long as the sampling is dense enough, arbitrary functions may be described by a spline for all practical purposes. This is widely used in CMBFAST. Even the C_l's are calculated only every 50 l-value for $l > 200$. As the spectrum is very smooth, this still gives a precise result.

Now, a function like the visibility that is calculated in the thermal history part of the code, can be used to define a spline. Without object orientation, one would need to keep track of various variables, most notably arrays for the x, y data and derivatives needed for spline interpolation. Also, in order to assure quick access within the spline data table, one either needs to know the precise layout of the data arrays (CMBFAST does this), or even more variables (storing for instance the last interpolation x value) would be necessary. In total, this sums up to a lot of bookkeeping for a conceptually simple entity like a spline.

Alternatively, one may define a *class* holding all necessary variables a spline needs together with *definitions* of an interface with which other parts of the program can access and manipulate the spline data. An object behaves as described by the corresponding class. There can be an arbitrary number of objects of a certain class (just like there is one floating point type `float`, but many variables of *type* `float` in a program).[2] The class (in our case) called Spline, can hence be viewed as yet another data type, with no more bookkeeping needed than say for a floating point number. To illustrate this, let us discuss the visibility function $g \equiv \dot{\kappa} \exp(\kappa(\tau) - \kappa(\tau_0))$. Its typical shape is depicted in Figure 4.5. As mentioned in Section 4.5, its peak defines the epoch of last scattering. As soon as the Spline called **visibility** has been given the data, its maximum can be determined by a single line of code:

```
tau_ls = visibility.getMaximum();        get τ of last scattering
z_ls = cosmos.tau2z(tau_ls);             convert to redshift
```

Here, the second line asks the **cosmos** object to convert[3] conformal time to red-

[2] We usually denote here (and in the code) classes with capital first letter. In some cases where there is only one object of a class used in the code, we denote the object with the same name as the class, but with lower case initial letter. Hence, the line

```
Cosmos cosmos;
```

creates an object 'cosmos' of the class 'Cosmos'.

[3] Many of these 'convenience' functions are defined in the `Cosmos` class and moving from a to

shift. As the expansion history has been calculated before the thermal history, this is accurately possible. The important point to notice is that *all* functions defined in the Spline class are immediately available to everyone who uses Splines. So, whenever one needs to find the maximum, integrate a spline, calculate the convolution of two Splines etc, this can be done in very few lines of code: the functionality is fully encapsulated in the implementation of the Spline class. Any increase in performance or sophistication of the Spline class immediately translates over to all Splines used in the program.

8.1.1 Inheritance

Tightly connected to the fact that data and methods are combined within one object, the concept of *inheritance* proofs very powerful in cosmology. A class can inherit from another class (in this context called base class). All variables and the full functionality the base class implements is instantly available to the inheriting class,[4] called sub-class. The sub-class can then re-implement functions of the base class to provide a different functionality, or add new functions and variables. The important point to note is that *all* classes deriving from the same base class necessarily need to provide *all* functions the base class provides. Hence, for as long as other parts of the code use the base class, one can substitute any of the inheriting classes for the base class *without* changing a single line of code in the part that uses the bases class. As an illustration, let us look at the `Perturbation` class of CMBEASY. It is designed to evolve the perturbation equations for one k-mode through conformal time and calculate the temperature perturbation. It defines functions to do this that other parts of the program can be sure to find implemented in all sub-classes. In practice, there are four classes that inherit from it, for perturbations in gauge-invariant variables and in synchronous gauge both with and without quintessence (see also Figure 8.3). From the point of view of the rest of the program, all of them are equally well suited.[5]

8.2 Design

A hierarchy overview of the main classes of CMBEASY is given in Figure 8.3. Maybe the most central part of the package is the `CmbCalc` class. It provides functions to prepare and execute the perturbation evolution in k space and the integration of the C_l's. During the preparation, it also calls the `Cosmos` class which calculates the expansion and thermal background evolution. The `Cosmos` class is the

z to τ to t is easily possible. All conversion functions have the syntax $y = X2Y(x)$, where the number 2 should be spelled as 'to'.

[4] This is as if a child was born with the whole knowledge of its parents. No training and learning would be necessary. It could instantly go and increase its capabilities starting from the level of its parents.

[5] Except for the fact that if one wants quintessence, the perturbation class should of course support it.

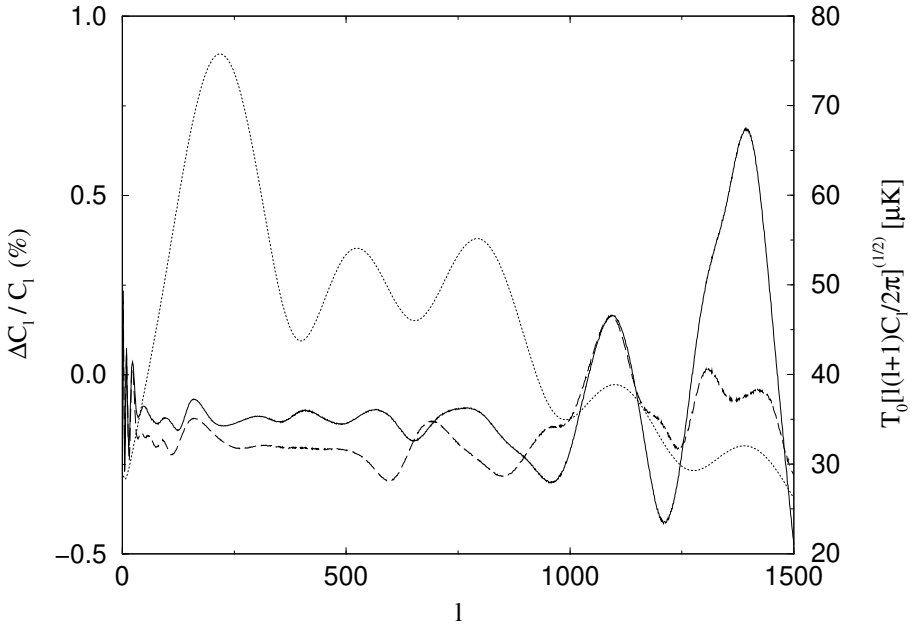

Figure 8.1: Temperature anisotropy spectrum for $h = 0.65$, $\Omega_0^\Lambda = 0.6$, $\Omega_0^{\rm b} h^2 = 0.02$, $\Omega_0^{\rm c} = 1 - \Omega_0^\Lambda - \Omega_0^{\rm b}$ obtained from CMBFAST. The relative deviation $\Delta C_l / C_l$ of CMBEASY's synchronous (long dashed line) and gauge invariant (solid line) solution with respect to the original CMBFAST spectrum are also given. The accordance of all spectra is always better than 1%. In the gauge invariant case, both the background and perturbation evolution as well as the C_l integration are entirely independent of the CMBFAST code. However, they use the same thermal history algorithm that should in principle be independently implemented for cross checks.

central instance providing background quantities like $\bar{\rho}(\tau)$ of all species etc. Already the centralization of the background evolution within the `Cosmos` class facilitates the modification of the code greatly. A different background cosmology (such as quintessence) can be implemented by just inheriting from `Cosmos` and re-implementing the expansion history part of the code.[6] As already mentioned, the `Perturbation` class and its subclasses propagate the perturbation variables for one k-mode through conformal time. Finally, the `Integrator` subclasses perform the convolution of the sources with the Bessel functions, (4.68), as well as the final k-integration of Equation (4.15).

8.2.1 Quintessence Implementation

The different background evolution of quintessence scenarios is implemented using the `QuintCosmos` and the `Quintessence` class. Each subclass of `Quintessence`

[6] All in all 800 lines of a total of 2500 lines of `Cosmos`.

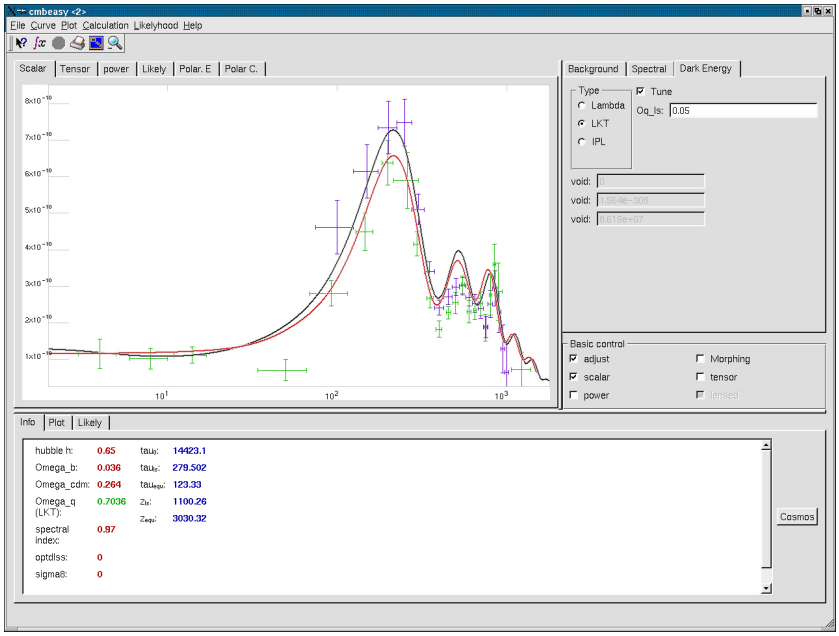

Figure 8.2: Graphical user interface (GUI) for CMBEASY.

corresponds to a certain model, such as EP, IPL, LKT etc. Certainly, a more monolithic design with the quintessence models implemented in the `QuintCosmos` class would have been possible. However, we believe that the *details* of the models are best kept to a class of its own. For instance tuning model parameters in order to get the right amount of Ω_0^φ etc. is different for each model and a monolithic design would have to call *differently named* functions for *different* models. Using subclassing, `QuintCosmos` (and `Perturbation`) always call functions with the same argument and name for all models. Yet, as the object implementing the function differs for each model, the code executed by calling the function can be totally different. Thus, a new quintessence model can be implemented by simply subclassing `Quintessence` and implementing a minimal set of functions, such as one for the potential etc.

8.3 Graphical User Interface

For educational purposes and also to simplify the parameter input and subsequent visualization of results, a graphical user interface (GUI) is of great value. Luckily, there is the very sophisticated and publicly available 'Qt' library[104] with which the creation of a GUI is facilitated. Its object oriented C++ design is a perfect match for the CMBEASY package. There is therefore an executable program called 'cmbeasy' giving interactive access to almost the full capabilities of the package, including quintessence. As is seen from Figure 8.2, the spectra are visualized in

separate plots arranged in a so called Tab-Widget.[7] One can for instance zoom in, select and save curves or print the plot. In addition, a likelihood analysis, using SNe Ia data, peak locations and cluster abundance constraints is available. Its aim is rapid calculation and visualization and hence it only uses the background evolution, estimating peak locations via the peak shift formulas of appendix B and σ_8 from Equation (6.33) and a library of pre-calculated ΛCDM models.

8.4 Documentation

Using the DOXYGEN program, the documentation is automatically generated from the source code of the CMBEASY package. In its HTML version, it is interactively navigable and includes the full source code. Due to the automatic generation, the documentation and the code are naturally synchronized. A postscript version of the documentation is also generated. Depending on the depth of information requested, it easily exceeds several hundred pages, making it less accessible than its HTML counterpart.

[7] A widget is a part of a user interface that can interact. Examples are buttons, sliders, etc.

Figure 8.3: Hierarchy of the main classes of the CMBEASY package. All classes dealing with mathematics inherit from MathObject for technical reasons. The Cosmos class calculates the background evolution and can be extended using subclasses such as QuintCosmos for quintessence. The perturbation equations are encapsulated in the Perturbation class. Implementing different gauges as subclasses is therefore unproblematic. The central instance invoking Cosmos, the Perturbations and Integrators is the CmbCalc class. Not shown are several (sometimes small) classes, e.g. the ControlPanel, which holds commonly used settings, or e.g. the MiscMath class providing low-level mathematical functions.

9

Conclusions

We have started this work by describing the effects of dark energy on the expansion history of the universe. Depending on its effective equation of state $\overline{w}_0$, the age of the universe ranges from $\tau \approx 9000\,\mathrm{Mpc}$ ($\overline{w}_0 = 0$) to approximately $14000\,\mathrm{Mpc}$ in the case of a cosmological constant. The Perturbations to homogenous background quantities have been introduced using gauge-invariant variables. The gauge invariant scalar quintessence fluctuation X is identical to the fluctuation in longitudinal gauge. This makes the longitudinal gauge the ideal tool to derive quintessence related perturbation equations. We have then reviewed the gauge-invariant formulation of CMB anisotropies along the lines of [18]. In order to benefit from the numerically fast line of sight method [16], we have formulated it using gauge invariant variables.

To set the numerical calculation up, one needs initial conditions. For this purpose, the equation of motion of the field fluctuation X has been solved analytically in the case of tracking quintessence. As most scalar quintessence models are in such an attractor solution at early times, this result is widely applicable. The fluctuation X follows a simple power-law in conformal time with exponent $(1 - 3w^{\varphi})/2$. As it turns out, this solution for X is identical to the solution for X following from adiabatic initial conditions. Like all perturbations, the metric potential Φ needs to be determined consistently at initial time. The existing literature assumes that Φ is given by the same relation as in the case without quintessence. This is certainly true if quintessence is subdominant at early times. More importantly, we have shown that this also holds whenever the quintessence model resembles an exponential potential model at the time of interest. In most practical situation, Φ is therefore indeed given by the same relation as without quintessence.

For tracking quintessence, the gauge-invariant energy density perturbation D_g^{φ} remains constant on scales outside the horizon. As quintessence is in principle very versatile, we can't prove this intuitively expected result for arbitrary realizations.

Moving towards observational tests for dark energy, we have calculated the acoustic scale l_A. The acoustic scale determines the inter-peak spacing in the CMB multipole spectrum. The influence of quintessence on l_A has been expressed by the three parameters $\overline{w}_0$, $\bar{\Omega}_{\mathrm{ls}}^{\varphi}$ and Ω_0^{φ}. Unfortunately, the effects of dark energy can be

mimicked by the Hubble parameter. An independent determination of the Hubble parameter is therefore mandatory if l_A is used to restrict quintessence models. The acoustic scale is still found in the literature as an estimate for the location of the first peak despite the fact that this introduces large errors [69,75]. In addition, the relation between Ω_0 and the position of the first peak noted in [73] is based on numerical simulations. These simulations did not take dark energy into account. In order to accurately connect the acoustic scale and CMB peak positions, we have parameterised the peak positions with peak shifts φ_m. For these shifts, we devised fitting formulae that are applicable over a wide range of parameters. As the shifts are influenced mostly by pre-recombination physics, dark energy before last scattering (quantified by $\bar{\Omega}^{\varphi}_{\rm ls}$) has been an important parameter in our analysis. The independence from post-recombination effects means that the shift formulae are also applicable to non-flat universes. During these numerical simulations, the shift of the third peak φ_3 proved rather insensitive to the cosmological model. As both the Boomerang and the Maxima experiments released data covering three peaks in spring 2001, we used this insensitivity to extract the acoustic scale from the measurements. The value we find is $l_A = 319 \pm 23$. As the acoustic scale is easily calculable from background physics only, this provides a quick way to estimate whether a model is possibly in agreement with the CMB data or not. Combining this bound on l_A with cluster abundance constraints, we find that inverse power law models with exponent $\alpha > 2$ are disfavoured. This is both in agreement with SNe Ia constraints, as well as with the result of [35]. In addition, the amount of dark energy during recombination is restricted to $\bar{\Omega}^{\varphi}_{\rm ls} \lessapprox 0.15$. Yet, for a spectral index slightly greater than one, a small contribution at the 5% level is favoured. In order to *detect* quintessence via the CMB, a more precise measurement of the location of the first peak may be necessary. From this and l_A, one would be able to extract the quantity κ that could give hints to the amount of quintessence present at recombination. Using the value of l_A, we find that the expansion of the universe is most likely accelerating. This result is entirely independent of SNe Ia observations.

In order to implement quintessence models numerically, we chose to modify the CMBFAST computer code. We have ported the package to the object oriented C++ programming language. The code has been re-designed and grouped in classes. As all functionality is cleanly encapsulated in these classes, the code is easier to overview. This facilitates bug-finding and leads to more confidence in the numerical results. By inheriting from existing classes, the implementation of different models, cosmologies or gauges is greatly simplified. In addition, a powerful graphical user interface is available for the modified code. This will make the CMB accessible to non-experts also, increasing intuition for the effect of different parameters on the spectrum. Besides, it can be used for educational purposes.

Turning to SNe Ia observations, we have shown that dark energy models with the same value of $\bar{w}_{\varphi}\,[\Omega^{\varphi}_0]^{1.4}$ are indistinguishable by current SNe Ia-data. This in principle well known degeneracy has to our knowledge not been cast in such a simple relation before.

Leaving the observational side, we have calculated one-loop quantum correc-

tions to quintessence potentials. In the late universe, most potentials are stable with respect to scalar quintessence fluctuations. The pure exponential and Nambu-Goldstone type potentials are form invariant up to order V'', yet terms of the order $(V'')^2$ prevent them from being renormalizable in the strict sense. For the modified exponential potential introduced by Albrecht and Skordis, stability depends on the specific form of the polynomial factor V_p in the potential. In some cases the local minimum in the potential can even be removed by the loop. An explicit coupling of the quintessence field to fermions (or similarly to dark matter bosons) seems to be severely restricted. The effective potential to one loop level would be completely dominated by the contribution from the fermion fluctuations. All models in the literature share this fate. One way around this conclusion could be to view these potentials as already effective. They must, however, not only be effective in the sense of an effective quantum field theory originating as a low-energy limit of an underlying theory, but also include all fluctuations from this effective QFT. In this case, there is a strong connection between coupling and potential and it is rather unlikely that the *correct* pair can be guessed. The bound on the coupling is so severe that for consistency, we have calculated an effective coupling due to graviton exchange. To lowest order in $V(\Phi)$, this coupling leads to a fermion contribution which can be absorbed by redefining the pre-factor of the potential.

Surely, the one-loop calculation does not give the true effective potential. Symmetries or more fundamental theories that make the cosmological constant small as it is, could force loop contributions to cancel. In addition, the back-reaction of the changing effective potential on the fluctuations remains unclear in the one loop calculation. A renormalization group treatment would therefore be of great value.

In the last years, cosmology became more and more quantitative. With the high precision data of the MAP satellite, the cosmic microwave background will soon restrict many cosmological parameters to breath taking accuracy. However, the CMB spectrum is degenerate in several parameters. The same is true for SNe Ia observations. In fact, practically all observations are plagued by such degeneracies. It is only the combination of several tests – each of high precision – that can fix the parameters of the cosmological model. If the standard Λ-CDM model is well describing the soon available data, high energy physicists may need to find a reason for a non-vanishing and yet incredibly small vacuum energy.

However, it may well be that Λ-CDM runs into difficulties. Given the fact that it seemingly involves so much fine-tuning, it it rather unlikely the correct model. Taken together all the soon available precision data, this should manifest itself in an observational mismatch. It is well possible that a quintessence model will be favoured by the experiments. But as quintessence is so versatile, it is hard to imagine that only one quintessence scenario will be matching observations. To single out *the* quintessence model, a deeper understanding of the fundamental physics leading to the effective scalar theory is needed. If one day this theory is found, we shouldn't wonder if it involves a light scalar field which funny enough tricked scientists at the beginning of the 21st century into believing that there is a cosmological constant.

A

Christoffel Symbols

The Christoffel symbols

$$\Gamma^{\mu}_{\alpha\beta} = \frac{1}{2} g^{\mu\sigma} \left(g_{\sigma\beta,\mu} + g_{\alpha\sigma,\beta} - g_{\alpha\beta,\sigma} \right) \tag{A.1}$$

for the Robertson Walker metric (2.2) are in the unperturbed case

$$\Gamma^{0}_{00} = \frac{\dot{a}}{a} \tag{A.2}$$

$$\Gamma^{0}_{ij} = \frac{\dot{a}}{a} \delta_{ij} \tag{A.3}$$

$$\Gamma^{i}_{0j} = \frac{\dot{a}}{a} \delta^{i}_{j} \tag{A.4}$$

$$\Gamma^{i}_{jl} = \Gamma^{0}_{i0} = 0 \tag{A.5}$$

Using the scalar longitudinal gauge metric (3.26), the first order perturbations become

$$\delta\Gamma^{0}_{00} = \dot{\Psi} Q \tag{A.6}$$

$$\delta\Gamma^{0}_{i0} = -k Q_i \Psi \tag{A.7}$$

$$\delta\Gamma^{0}_{ij} = 2 \left(\frac{\dot{a}}{a} \left[\Phi - \Psi \right] + \dot{\Phi} \right) Q \, \delta_{ij} \tag{A.8}$$

$$\delta\Gamma^{i}_{00} = -k Q^i \Psi \tag{A.9}$$

$$\delta\Gamma^{i}_{j0} = \dot{\Phi} \, Q \, \delta^{i}_{j} \tag{A.10}$$

$$\delta\Gamma^{i}_{jl} = k \, \Phi \left(Q^i \delta_{jl} - Q_j \delta^{i}_{l} - Q_l \delta^{i}_{j} \right) \tag{A.11}$$

B

Fitting formulas for the peak shifts

We present here our fitting formulae for the overall phase shift $\bar{\varphi}$, followed by the relative shifts of the first trough ($\delta\varphi_{3/2}$) and the second ($\delta\varphi_2$) and third ($\delta\varphi_3$) peaks.[1] In each case we also give an estimate of the accuracy of the formulae.

Overall phase shift $\bar{\varphi}$

For the overall phase shift $\bar{\varphi}$ (i.e. the phase shift of the first peak) we find the formula

$$\bar{\varphi} = (1.466 - 0.466n)\left[a_1 r_\star^{a_2} + 0.291\bar{\Omega}_{\rm ls}^{\varphi}\right], \tag{B.1}$$

where a_1 and a_2 are given by

$$a_1 = 0.286 + 0.626\left(\Omega_b h^2\right) \tag{B.2}$$

$$a_2 = 0.1786 - 6.308\,\Omega_b h^2 + 174.9\left(\Omega_b h^2\right)^2 \tag{B.3}$$

$$-1168\left(\Omega_b h^2\right)^3. \tag{B.4}$$

It contains the main dependence of any shift φ_m on $\bar{\Omega}_{\rm ls}^{\varphi}$. The 1-$\sigma$ error for $\bar{\varphi}$ is

$$\Delta\bar{\varphi} = 0.0031 \tag{B.5}$$

Relative shift of first trough $\delta\varphi_{3/2}$

The relative shift of the first trough is a very sensitive quantity spanning a wide range of values. It can very well be used to restrict the allowed parameter space for cosmological models. We have

$$\delta\varphi_{3/2} = b_0 + b_1 r_\star^{1/3}\exp(b_2 r_\star) + 0.158\,(n-1), \tag{B.6}$$

[1] A small c++ package providing functions for the shifts is available at http://www.thphys.uni-heidelberg.de/~doran/peak.html

with

$$\begin{aligned} b_0 &= -0.086 - 0.079\,\bar{\Omega}_{\rm ls}^{\varphi} - \left(2.22 - 18.1\bar{\Omega}_{\rm ls}^{\varphi}\right)\Omega_b h^2 \\ &\quad - \left[140 + 403\bar{\Omega}_{\rm ls}^{\varphi}\right]\left(\Omega_b h^2\right)^2 \qquad \text{(B.7)} \\ b_1 &= 0.39 - 0.98\,\bar{\Omega}_{\rm ls}^{\varphi} - \left(18.1 - 29.2\bar{\Omega}_{\rm ls}^{\varphi}\right)\Omega_b h^2 \qquad \text{(B.8)} \\ &\quad +440\left(\Omega_b h^2\right)^2 \qquad \text{(B.9)} \\ b_2 &= -0.57 - 3.8\exp\left\{-2365.0\left(\Omega_b h^2\right)^2\right\}. \qquad \text{(B.10)} \end{aligned}$$

For the one standard-deviation error we have

$$\Delta\delta\varphi_{3/2} = 0.0039. \qquad \text{(B.11)}$$

Relative shift of second peak $\delta\varphi_2$

The relative shift of the second peak is a very sensitive quantity. It is thus not surprising to find a strong dependence of $\delta\varphi_2$ on the parameters. We have

$$\delta\varphi_2 = c_0 - c_1 r_\star - c_2 r_\star^{-c_3} + 0.05\,(n-1), \qquad \text{(B.12)}$$

with

$$\begin{aligned} c_0 &= -0.1 + \left(0.213 - 0.123\,\bar{\Omega}_{\rm ls}^{\varphi}\right) \qquad \text{(B.13)} \\ &\quad \times\exp\left\{-\left(52 - 63.6\,\bar{\Omega}_{\rm ls}^{\varphi}\right)\Omega_b h^2\right\} \qquad \text{(B.14)} \\ c_1 &= 0.063\,\exp\left\{-3500\left(\Omega_b h^2\right)^2\right\} + 0.015 \qquad \text{(B.15)} \\ c_2 &= 6\times10^{-6} + 0.137\left(\Omega_b h^2 - 0.07\right)^2 \qquad \text{(B.16)} \\ c_3 &= 0.8 + 2.3\,\bar{\Omega}_{\rm ls}^{\varphi} + \left(70 - 126\,\bar{\Omega}_{\rm ls}^{\varphi}\right)\Omega_b h^2. \qquad \text{(B.17)} \end{aligned}$$

The error of this approximation is

$$\Delta\delta\varphi_2 = 0.0044. \qquad \text{(B.18)}$$

Relative shift of third peak $\delta\varphi_3$

For the third peak, we find

$$\delta\varphi_3 = 10 - d_1 r_\star^{d_2} + 0.08\,(n-1), \qquad \text{(B.19)}$$

with

$$\begin{aligned} d_1 &= 9.97 + \left(3.3 - 3\Omega_{ls}^{\phi}\right)\Omega_b h^2 \qquad \text{(B.20)} \\ d_2 &= 0.0016 - 0.0067\,\Omega_{ls}^{\phi} + \left(0.196 - 0.22\,\Omega_{ls}^{\phi}\right)\Omega_b h^2 \\ &\quad + \frac{(2.25 + 2.77\,\Omega_{ls}^{\phi})\times10^{-5}}{\Omega_b h^2}\,, \qquad \text{(B.21)} \end{aligned}$$

and error given by

$$\Delta\delta\varphi_3 = 0.0052. \tag{B.22}$$

Overall shift of third peak φ_3

For completeness, we give a fit for φ_3 which in principle could be obtained by adding $\bar{\varphi}$ and $\delta\varphi_3$. However, a one-step-fit yields better errors here. Our formula is

$$\varphi_3 = e_1\,(1 + e_3 r_\star)\, r_\star^{e_2} + e_4 - 0.037\,(n-1), \tag{B.23}$$

with

$$\begin{aligned}
e_1 &= 0.302 - 2.112\,\Omega_b h^2 + 0.15\exp\left\{-384\Omega_b h^2\right\} && \text{(B.24)}\\
e_2 &= -0.04 - 4.5\,\Omega_b h^2 && \text{(B.25)}\\
e_3 &= \left(-0.118 + 44.7\,\Omega_b h^2\right)\bar{\Omega}_{\rm ls}^{\varphi} && \text{(B.26)}\\
e_4 &= \left(0.214\exp\left\{-48\Omega_b h^2\right\} + 0.106\right)\bar{\Omega}_{\rm ls}^{\varphi}, && \text{(B.27)}
\end{aligned}$$

and error

$$\Delta\varphi_3 = 0.0017. \tag{B.28}$$

C

Full set of Perturbation Equations

In this appendix, we summarize the formulae needed to evolve the gauge-invariant perturbation variables listed in Table C.1.

The Metric Potentials Φ and Ψ

In order to solve Einstein's equations, we first use Equation (3.55) in the form

$$-\Psi = \Phi + \mathrm{M_P^{-2}}\, k^{-2} a^2 \bar{p}\, \bar{\Pi}, \tag{C.1}$$

where $\bar{p}\bar{\Pi} \equiv \bar{p}_\gamma \Pi_\gamma + \bar{p}_\nu \Pi_\nu$. With this, we get from Equations (3.72) and (3.45)

$$\begin{aligned} a^2 \bar{\rho}_\varphi D_\varphi &= a^2 \bar{\rho}_\varphi D_g^\varphi - 3a^2(\bar{\rho}_\varphi + \bar{p}_\varphi)\Phi + 3a^2(\bar{\rho}_\varphi + \bar{p}_\varphi)\,\frac{\dot{a}}{a}\,\frac{V_\varphi}{k} \\ &= \dot{\bar{\varphi}}\left[\dot{X} + \mathrm{M_P^{-2}}\, k^{-2} a^2 \bar{p}\, \bar{\Pi}\right] + a^2 V'(\varphi) X \\ &\qquad + a^2(\bar{\rho}_\varphi + \bar{p}_\varphi)\Phi + 3a^2(\bar{\rho}_\varphi + \bar{p}_\varphi)\,\frac{\dot{a}}{a}\,\frac{V_\varphi}{k}\,, \end{aligned} \tag{C.2}$$

which is of the form $a^2 \bar{\rho}_\varphi D_\varphi = A_\varphi - B_\varphi \Phi$. For the other species, things are more simple

$$a^2 \bar{\rho}_i D_i = a^2 \bar{\rho}_i D_g^i - 3\bar{\rho}_i a^2 (1 + w_i)\Phi, \tag{C.3}$$

which is also of the form $a^2 \bar{\rho}_i D_i = A_i + B_i \Phi$. Therefore, Equation (3.53) yields

$$\Phi = \frac{\sum A_i}{2\mathrm{M_P^2} k^2 + \sum B_i} \tag{C.4}$$

where the summation runs over all species, including quintessence and A_i and B_i can be read off Equations (C.2) and (C.3) respectively. This fixes Φ, because the right hand side of Equation (C.4) contains only known variables. The gravitational potential Ψ follows then immediately from Equation (C.1).

Symbol	Meaning
$\mathcal{M}_l$	Photon multipole, $l = 0 \dots 7$
E_l	Photon polarization multipole, $l = 2 \dots 7$
$\mathcal{N}_l$	Neutrino multipole, $l = 0 \dots 9$
X	Quintessence field fluctuation
$\dot{X}$	$\mathrm{d}X/\mathrm{d}\tau$ (because e.o.m. is second order)
D_g^b	Density perturbation for baryons
D_g^c	Density perturbation for cold dark matter
V_b	Velocity of baryons
V_c	Velocity of cold dark matter
D_g^γ	Density perturbation for photons (from $\mathcal{M}_0$)
D_g^ν	Density perturbation for massless neutrinos (from $\mathcal{N}_0$)
V_γ	Velocity of photons (from $\mathcal{M}_1$)
V_ν	Velocity of neutrinos (from $\mathcal{N}_1$)
V_φ	Quintessence velocity (from $\dot{X}$)
Π_γ	Photon shear (from $\mathcal{M}_2$)
Π_ν	Neutrino shear (from $\mathcal{N}_2$)

Table C.1: Perturbations propagated through conformal time (upper half). Quantities that are not propagated themselves, but derived algebraically from quantities propagated are grouped in the lower half.

Cold dark matter, Baryons and Photons

For cold dark matter, we use Equations (5.13) and (5.14). As far as photons and baryons are concerned, one distinguishes between the tight-coupling and the 'no-tight-coupling' regime:

(I) Tight coupling:

In tight coupling, one combines the Equations (C.8) governing the velocity evolution for baryons and photons (4.49) into one single Equation along the lines of Section 5.1

$$\dot{V} = k\Psi + \left[Rk\left(\frac{1}{4}D_g^\gamma - \frac{1}{6}\Pi_\gamma\right) + kc_s^2 D_g^b - \frac{\dot{a}}{a}V(1-3c_s^2) - k\Phi(R+3c_s^2)\right](R+1)^{-1}, \quad \text{(C.5)}$$

where c_s^2 is the baryon sound speed,[1] V is the common velocity of baryons and photons and $R = 4\rho_\gamma/(3\rho_b)$. The monopoles evolve according to

$$\dot{D}_g^b = -kV_b - 3c_s^2 D_g^b \frac{\dot{a}}{a}, \tag{C.6}$$

and

$$\dot{\mathcal{M}}_0 = -\frac{k}{3} V. \tag{C.7}$$

All higher moments of $\mathcal{M}$ as well as the polarization terms E_l are set to zero.

(II) No Tight coupling:

Without tight coupling, baryons obey

$$\dot{V}_b = k(\Psi - 3c_s^2\Phi) + kc_s^2 D_g^b + \frac{\dot{a}}{a}\left(3c_s^2 - 1\right) V_b + \dot{\kappa}R(V_\gamma - V_b), \tag{C.8}$$

where c_s is still the baryon sound speed. For the photon velocity, one uses Equation (4.49). The densities D_g for photons and baryons evolve as in the tight coupling regime. Multipoles $l > 1$ for photons are calculated using Equations (4.49, 4.50). The multipole expansion is truncated at some $l < 10$ for sufficient precision. In order to avoid truncation effects as good as possible, one uses [27] the recursion relation for spherical Bessel functions

$$\dot{\mathcal{M}}_{l_{\max}} = \frac{2l_{\max}+1}{2l_{\max}-1}\, k\, \mathcal{M}_{l_{\max}-1} - \mathcal{M}_{l_{\max}} \left(\frac{l_{\max}+1}{\tau} + \dot{\kappa}\right) \tag{C.9}$$

The polarization E is propagated using Equations (4.52,4.53), and the recursion relation

$$\dot{E}_{l_{\max}} = \frac{2l_{\max}+1}{2l_{\max}-1}\, kE_{l_{\max}-1} - E_{l_{\max}} \left(\frac{l_{\max}+1}{\tau} + \dot{\kappa}\right), \tag{C.10}$$

for truncation.

Massless Neutrinos

Massless neutrinos evolve according to Equations (4.54-4.56). The hierarchy is truncated using

$$\dot{N}_{l_{\max}} = \frac{2l_{\max}+1}{2l_{\max}-1}\, kN_{l_{\max}-1} - N_{l_{\max}} \frac{l_{\max}+1}{\tau}. \tag{C.11}$$

Quintessence

The scalar field fluctuation is propagated using a first order formulation of Equation (3.73), i.e. $\mathrm{d}X/\mathrm{d}\tau = \dot{X}$ and $\mathrm{d}(\dot{X})/\mathrm{d}\tau$ is then given by $\ddot{X}$ of (3.73).

[1] This is practically vanishing for most of the time, thus setting $c_s^2 = 0$ in this Equation is still quite accurate.

D

Conventions, Symbols and Conversion Factors

- ⋆ We take the metric with signature $(-,+,+,+)$.
- ⋆ Greek indices run from $0\ldots3$ and are raised and lowered by the metric $g_{\mu\nu}$.
- ⋆ Latin indices run from $1\ldots3$ and are raised and lowered by δ_{ij}.
- ⋆ The partial derivative of a tensor $\partial_\mu T$ is abbreviated by $T_{,\mu}$.
- ⋆ The co-variant derivative of a tensor $\nabla_\mu T$ is abbreviated by $T_{;\mu}$.
- ⋆ Perturbations in a certain gauge are denoted by lower case letters: $\delta,\ v,\ \chi\ldots$
- ⋆ Gauge-invariant variables are denoted by capital letters: $D_g,\ \Pi,\ X\ldots$
- ⋆ Three-vectors are denoted by bold letters and their scalar product is given by $\boldsymbol{a}\cdot\boldsymbol{b}=a^i\,b^j\,\delta_{ij}$.
- ⋆ The Christoffel symbols are

$$\Gamma^\mu_{\alpha\beta}=\frac{1}{2}\,g^{\mu\sigma}\left(g_{\sigma\beta,\mu}+g_{\alpha\sigma,\beta}-g_{\alpha\beta,\sigma}\right),$$

while the Riemann tensor is

$$R^\mu{}_{\nu\alpha\beta}=\partial_\alpha\Gamma^\mu_{\nu\beta}-\partial_\beta\Gamma^\mu_{\nu\alpha}+\Gamma^\sigma_{\nu\beta}\Gamma^\mu_{\sigma\alpha}-\Gamma^\sigma_{\nu\alpha}\Gamma^\mu_{\sigma\beta}.$$

One Mpc is ...
1.5637×10^{38} Gev^{-1}
3.0856×10^{22} m
1.0292×10^{14} s
3.264×10^{6} years
One Mpc^{-1} is ...
6.3952×10^{-39} Gev
3.2408×10^{-23} m^{-1}
9.7163×10^{-15} s^{-1}
In terms of Mpc is ...
$\mathrm{M_P} = 3.753 \times 10^{-56}$ Mpc^{-1}
$H = 3.34 \times 10^{-6}\, h$ Mpc^{-1}
One Mpc^{-4} is ...
1.673×10^{-153}Gev

Table D.1: Conversion of Mpc to various units.

Symbol	Meaning
t	time
τ	conformal time
a	scale factor, normalized $a(\text{today}) = 1$
z	redshift $z = (1-a)/a$
$\dot{y}$	conformal time derivative $\frac{\mathrm{d}}{\mathrm{d}\tau} y$
V'	derivative with respect to the field φ
y_{eq}	Quantity y at matter radiation equality
y_{ls}	Quantity y at last scattering
y_0	Quantity y today
$\mathrm{M_P}$	Reduced Plank mass $\mathrm{M_P} = (8\pi G)^{-1/2}$.
H	Hubble parameter $H = (\mathrm{d}a/\mathrm{d}t)/a$
h	defined via $H = 100\,h\,\mathrm{km\,s^{-1}Mpc^{-1}}$
$\bar{\rho}_y$	Background energy density of y
$\bar{p}_y$	Background pressure of y
w_y	Equation of state $w = \bar{p}/\bar{\rho}$ of species y
c_s	Sound speed (of some species) see (3.42)
Ω^y	Fraction of energy $\bar{\rho}_y/\rho_{\mathrm{total}}$.
Ω_0^y	$\Omega^y(\text{today})$.
$\bar{\varphi}$	Background quintessence field
φ	Quintessence field
φ_m	Shift of peak m
D_g^y	Density perturbation of species y
V_y	Velocity perturbation of species y.
Π_y	Shear of species y.
X	Gauge invariant quintessence field fluctuation
$\mathcal{M}_l$	Photon multipole
E_l	Photon polarization multipole
$\mathcal{N}_l$	Neutrino multipole
Q	Scalar perturbation basis function
Q_i	Scalar basis function for vector fields
Q_{ij}	Scalar basis function for tensor fields

continued on next page ...

	continued ...
n_e	Number density of free electrons
σ_T	Thomson scattering cross-section
$\dot{\kappa}$	Differential optical depth $\dot{\kappa} = a n_e \sigma_T$.
n	spectral index of initial fluctuations
l_A	Acoustic scale
$\overline{w}_0$	Average equation of state (2.44)
$\bar{\Omega}^{\varphi}_{\mathrm{ls}}$	Average Ω^{φ} until last scattering
σ_8	RMS cold dark matter fluctuations on scales of $8h^{-1}$ Mpc.

Table D.2: Frequently used symbols, continued from page before.

Bibliography

[1] D. Adams, The Hitchhiker's guide to the Galaxy, Random House, New York (1979)

[2] A. G. Riess *et al.*, Astron. J. **116** (1998) 1009 [astro-ph/9805201].

[3] R. R. Caldwell, R. Dave and P. J. Steinhardt, Phys. Rev. Lett. **80** (1998) 1582 [astro-ph/9708069].

[4] C. Wetterich, Nucl. Phys. B **302** (1988) 645.

[5] B. Ratra and P. J. Peebles, Phys. Rev. D **37** (1988) 3406.

[6] C. Wetterich, Nucl. Phys. B **302** (1988) 668.

[7] P. J. Peebles and B. Ratra, Astrophys. J. **325** (1988) L17.

[8] J. A. Frieman, C. T. Hill, A. Stebbins and I. Waga, Phys. Rev. Lett. **75** (1995) 2077 [arXiv:astro-ph/9505060].

[9] Ya. B. Zeldovich, Pis'ma Zh. Eksp. Teor. Fiz. **6** (1967) 883 [JETP Lett. **6** (1967) 316].

[10] S. Weinberg, Rev. Mod. Phys. **61** (1989) 1.

[11] C. Wetterich, Astron. Astrophys. **301** (1995) 321 [hep-th/9408025].

[12] P. J. Steinhardt, L. Wang and I. Zlatev, Phys. Rev. D **59** (1999) 123504 [astro-ph/9812313].

[13] E. J. Copeland, A. R. Liddle and D. Wands, Phys. Rev. D **57** (1998) 4686 [gr-qc/9711068].

[14] C. B. Netterfield *et al.*, astro-ph/0104460.

[15] A. T. Lee *et al.*, Astrophys. J. **561** (2001) L1 [astro-ph/0104459].

[16] U. Seljak and M. Zaldarriaga, Astrophys. J. **469** (1996) 437 [arXiv:astro-ph/9603033].

[17] M. Doran, XXXVII Recontres de Moriond, *The cosmological model* (2002)

[18] R. Durrer, J. Phys. Stud. **5** (2001) 177 [arXiv:astro-ph/0109522].

[19] J. Weller and A. Albrecht, arXiv:astro-ph/0106079.

[20] E. W. Kolb and M. S. Turner, *Redwood City, USA: Addison-Wesley (1990) 547 p. (Frontiers in physics, 69).*

[21] S. Perlmutter, M. S. Turner and M. J. White, Phys. Rev. Lett. **83** (1999) 670 [astro-ph/9901052].

[22] R. d'Inverno, *Oxford, UK: Clarendon (1992).*

[23] R. M. Wald, *General Relativity*, University of Chicago Press, Chicago (1984)

[24] J.W. York, J. Math. Phys. 14 (1973) 456

[25] J. M. Bardeen, Phys. Rev. D **22** (1980) 1882.

[26] H. Kodama and M. Sasaki, Prog. Theor. Phys. Suppl. **78** (1984) 1.

[27] C. P. Ma and E. Bertschinger, Astrophys. J. **455** (1995) 7 [arXiv:astro-ph/9506072].

[28] P. G. Ferreira and M. Joyce, Phys. Rev. D **58** (1998) 023503 [astro-ph/9711102].

[29] L. Amendola, Lecture given at Dartmouth college (1996)

[30] D. Tocchini-Valentini and L. Amendola, [astro-ph/0108143].

[31] R. Bean, Phys. Rev. D **64** (2001) 123516 [astro-ph/0104464].

[32] Hebecker, A., Wetterich, C., 2001, Phys. Lett. B, 497, 281 [hep-ph/0008205]

[33] A. Albrecht and C. Skordis, Phys. Rev. Lett. **84** (2000) 2076 [astro-ph/9908085].

[34] P. Brax and J. Martin, Phys. Rev. D **61**, 103502 (2000) [astro-ph/9912046].

[35] A. Balbi, C. Baccigalupi, S. Matarrese, F. Perrotta and N. Vittorio, Astrophys. J. **547** (2001) L89

[36] M. Doran, M. Lilley and C. Wetterich, Phys. Lett. B **528** (2002) 175 [astro-ph/0105457].

[37] A. d. Macorra and G. German, arXiv:astro-ph/0203094.

[38] P. Brax and J. Martin, Phys. Lett. B **468** (1999) 40 [astro-ph/9905040].

[39] Brax, P., Martin, J., Riazuelo, A., 2000, Phys. Rev. D, 62, 103505 [astro-ph/0005428]

[40] P. S. Corasaniti and E. J. Copeland, Phys. Rev. D **65** (2002) 043004 [astro-ph/0107378].

[41] A. de la Macorra and C. Stephan-Otto, astro-ph/0106316.

[42] A. A. Penzias and R. W. Wilson, Astrophys. J. **142** (1965) 419.

[43] P.J.E. Peebles, *Principles of Cosmology*, Princeton University Press, Princeton (1993)

[44] Hu, W., Sugiyama, N., 1995, ApJ, 444, 489

[45] Hu, W., Sugiyama, N., Silk, J., 1997, Nat, 386, 37 [astro-ph/9604166]

[46] C.W. Misner, K.S. Thorn, J. A. Wheeler, *Gravitation*, Freeman, San Francisco (1973)

[47] R.W. Lindquist, Ann. of Phys., **37**, 487-518 (1966)

[48] R. Durrer, Fund.Cosmic Phys. **15**, 209 (1994)

[49] W. Hu and M. J. White, Phys. Rev. D **56** (1997) 596 [arXiv:astro-ph/9702170].

[50] E. Newman and R. Penrose, J. Math. Phys. **7**, 863 (1966).

[51] K. S. Thorne, Rev. Mod. Phys. **52** (1980) 299.

[52] W. Hu, U. Seljak, M. J. White and M. Zaldarriaga, Phys. Rev. D **57** (1998) 3290 [arXiv:astro-ph/9709066].

[53] Seljak, U., Apj., **482**, 6 (1997)

[54] R. K. Sachs and A. M. Wolfe, Astrophys. J. **147** (1967) 73.

[55] F. Perrotta and C. Baccigalupi, Phys. Rev. D **59** (1999) 123508 [arXiv:astro-ph/9811156].

[56] R. Trotta, private communication.

[57] A. R. Cooray and D. Huterer, Astrophys. J. **513** (1999) L95 [arXiv:astro-ph/9901097].

[58] D. Huterer and M. S. Turner, Phys. Rev. D **64** (2001) 123527 [astro-ph/0012510].

[59] R. Bean and A. Melchiorri, astro-ph/0110472.

[60] J. Kujat, A. M. Linn, R. J. Scherrer and D. H. Weinberg, arXiv:astro-ph/0112221.

[61] R. Durrer, B. Novosyadlyj and S. Apunevych astro-ph/0111594

[62] Ferreira, P. G., & Joyce, M., Phys. Rev. Lett., **79**, 4740 (1997)

[63] Coble, K., Dodelson, S., Frieman, J. A., 1997, Phys. Rev. D, 55, 1851 [astro-ph/9608122].

[64] L. Amendola, Mon. Not. Roy. Astron. Soc. **312** (2000) 521 [arXiv:astro-ph/9906073].

[65] G. Efstathiou, arXiv:astro-ph/9904356.

[66] Bond, J. R. et al. 2000, preprint (astro-ph/0011379)

[67] P. de Bernardis *et al.*, astro-ph/0105296.

[68] Hanany, S. et al. ApJ. Lett., 545, L5 (2000)

[69] Hu, W., White, M., 1996, in Proceedings of 31st Rencontres de Moriond: Microwave Background Anisotropies, Les Arcs, France, 16-23 March 1996 (Editions Frontieres) [astro-ph/9606140]

[70] Huey, G., Wang, L., Dave, R., Caldwell, R. R., Steinhardt, P. J., 1999, Phys. Rev. D, 59, 063005 [astro-ph/9804285]

[71] Amendola, L., 2000, Phys. Rev. D, 62, 043511 [astro-ph/9908023]

[72] Doran, M., Lilley, M. J., Schwindt. J., Wetterich, C., 2000, ApJ in press [astro-ph/0012139].

[73] Kamionkowski, M., Spergel, D. N., Sugiyama, N., 1994, ApJ, 426, L57 [astro-ph/9401003]

[74] Weinberg, S., 2000, Phys. Rev. D, 62, 127302 [astro-ph/0006276]

[75] Hu, W., Fukugita, M., Zaldarriaga, M., Tegmark, M., 2000, astro-ph/0006436

[76] X. Wang, M. Tegmark and M. Zaldarriaga, astro-ph/0105091.

[77] L. Wang and P. J. Steinhardt, Astrophys. J. **508** (1998) 483 [astro-ph/9804015].

[78] C. Wetterich, Nucl. Phys. B **324** (1989) 141.

[79] W. L. Freedman *et al.*, astro-ph/0012376.

[80] W. J. Percival *et al.*, astro-ph/0105252.

[81] P. Brax, J. Martin and A. Riazuelo, Phys. Rev. D **64** (2001) 083505 [hep-ph/0104240].

[82] Hamuy, M., et al., AJ, **106**, 2392 (1993)

[83] Y. Wang and G. Lovelace, Astrophys. J. **562** (2001) L115 [arXiv:astro-ph/0109233].

[84] S. Perlmutter *et al.*, Astrophys. J. **517** (1999) 565 [astro-ph/9812133].

[85] G. Efstathiou, S. L. Bridle, A. N. Lasenby, M. P. Hobson and R. S. Ellis, [astro-ph/9812226].

[86] A. de la Macorra and C. Stephan-Otto, astro-ph/0110460.

[87] Y. Wang and P. M. Garnavich, Astrophys. J. **552** (2001) 445 [astro-ph/0101040].

[88] I. Maor, R. Brustein, J. McMahon and P. J. Steinhardt, arXiv:astro-ph/0112526.

[89] C. Skordis and A. Albrecht, arXiv:astro-ph/0012195.

[90] K. Benabed and F. Bernardeau, Phys. Rev. D **64** (2001) 083501 [arXiv:astro-ph/0104371].

[91] J. Schwindt, Diploma Thesis, University of Heidelberg, 2001

[92] M. Doran, J. M. Schwindt and C. Wetterich, Phys. Rev. D **64** (2001) 123520 [arXiv:astro-ph/0107525].

[93] M. Doran and J. Jackel, arXiv:astro-ph/0203018.

[94] C. F. Kolda and D. H. Lyth, Phys. Lett. B **458** (1999) 197 [arXiv:hep-ph/9811375].

[95] R. D. Peccei, arXiv:hep-ph/0009030.

[96] M. E. Peskin and D. V. Schroeder, Perseus Books, Cambridge MA, 1995

[97] J. E. Kim, JHEP **9905** (1999) 022 [hep-ph/9811509].

[98] Y. Nomura, T. Watari and T. Yanagida, Phys. Lett. B **484** (2000) 103 [hep-ph/0004182].

[99] M. Kawasaki, T. Moroi and T. Takahashi, Phys. Rev. D **64**, 083009 (2001) [astro-ph/0105161].

[100] O. Bertolami and P. J. Martins, Phys. Rev. D **61** (2000) 064007 [arXiv:gr-qc/9910056].

[101] R. Bean and J. Magueijo, Phys. Lett. B **517** (2001) 177 [astro-ph/0007199].

[102] J. Zinn-Justin, *Quantum Field Theory and Critical Phenomena*, Oxford Science Publications, USA (1995)

[103] M.J.G Veltman, in Les Houches, Session XXVIII - *Méthodes en théories des champs* (1975)

[104] Qt-library, Trolltech, Oslo, www.trolltech.com

Acknowledgments

I would like to thank Christof Wetterich for a supervision leaving room for my own ideas, while still answering many tricky question when they arose.

I am also indebted to my second supervisor, Michael G. Schmidt for giving advice and reading this thesis (and of course for the oral exam).

I am very grateful to Gert Aarts, Jürgen Berges and Matthew Lilley. Firstly, because Post-Docs are *so* intelligent. And secondly, because Gert taught me how to say 'Dooooeeee' in Dutch and Matt must have been one of the most relaxed people on planet earth. In short: it has been fun.

For kicking the whole CMB calculation and CMBEASY project off, and for many more things (like for instance: giving advice, having a nice research group, having a nice observatory in a nice city,...), I would like to thank Luca Amendola

For talking me into incorporating gauge invariant variables in my research, and subsequent extensive support, I am greatly indebted to Ruth Durrer.

I'd like to say thanks to Uros Seljak and Matias Zaldarriga for the permission to distribute CMBEASY under its new name and their generous donation of the original CMBFAST code to the public domain.

The same is true for the hundreds of developers of the Linux and KDE projects. And of course, the TROLLTECH company for giving away the marvelous Qt-library free of charge.

For many discussions on physics and the world, and a lot of fun, I would like to thank Tobias Baier, Dietrich Foethke, Jörg Jäckel, Christian Mathias Müller, Volker Schatz, Frank Daniel Steffen, Jan Schwindt, Claus Zahlten and many more not named here.

Work would certainly have not been fun without my love, Christiane, who endured my chaotic room during the final stages of this thesis (well, it *may* have been chaotic before :-).

Finally, I would like to thank my family for their love and support.